# *A Study of Elementary Reactions of Isocyanate Production*

*Ph.D. Dissertation*


***Renáta Zsanett Boros***

***Supervisors:***
***Prof. Dr. Béla Viskolcz***
***Dr. Milán Szőri***

***University of Miskolc***

***Antal Kerpely Doctoral School of Materials Science & Technology***

***Institute of Chemistry***


***Miskolc 2019.***

*"Principles for the Development of a Complete Mind: Study the science of art. Study the art of science. Develop your senses - especially learn how to see. Realize that everything connects to everything else."*

***Leonardo da Vinci***

# Content

# INTRODUCTION

## 1.1 Polyurethanes (PURs)

Comfortable and durable mattresses, convenient seats, effective practical thermal insulation materials used in industrial buildings, sealants and adhesives, sport items such as shoe soles, sport equipment and many of the clothes are only a few examples of polyurethane application[1]. These polymeric materials appear in an astonishing variety of forms making them the most versatile plastics with several advantages such as diverse mechanical properties (flexibility, high resistance, wide range of hardness, different electrical properties etc.)[2]. The discovery of first polyurethane was made by Otto Bayer and his co-workers[3] in 1937, however, the reaction of an isocyanate (ethyl-isocyanate) with an alcohol (ethyl-alcohol) was firstly explored by Wurtz in 1849[4]. Since the first polyurethane synthesis in 1934 has been discovered, nowadays several non-isocyanate routes of polyurethane production became more and more attractive due to the scientific results. The focus of the novel polyurethane syntheses became the greener polymerization. Numerous non-isocyanate methods were established[5]. Due to the toxicity of some intermediates the most promising pathway to polyurethanes are the transurethanization polycondensation between bis-carbamates and diols[6–8] and the polyaddition between cyclic carbonates and amines[9,10]. The industrial application of these methods has not reported yet so that the emphasis of this research is concentrated on the classical polyurethane synthesis.

Classical polyurethanes are formed from the reaction between molecules containing two or more isocyanate groups with polyol molecules containing two or more hydroxyl groups forming urethane linkage (*Scheme 1*)[1].

The characteristics of polyurethanes are greatly influenced by the types of diisocyanates and polyols used.

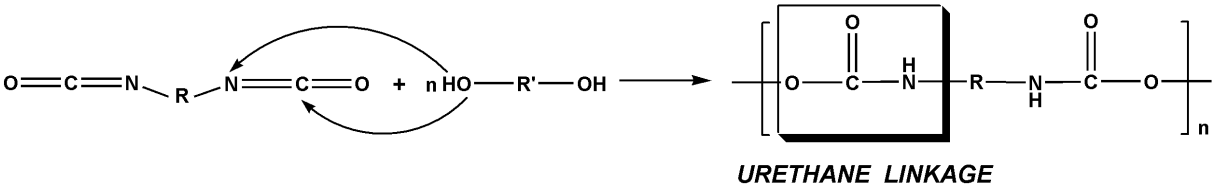


**Scheme 1**: Polyurethane formation in the reaction of diisocyanate and diol.

Polyols are reactive substances containing at least two reactive isocyanate groups attached to a single molecule. There are four classes of polyols applied in the current

chemical industry such as polyether polyols, amine-terminates polyethers, polyester polyols, polycarbonates[11].

The other important raw materials of polyurethanes are the isocyanates, especially the aromatic diisocyanates. Numerous studies were conducted about the organic isocyanates by chemists including A. W. von Hofmann[12], however industrial isocyanate synthesis was based on the discovery of Hentschel who reacted phosgene with salt of a primary amine[13]. Several diisocyanates are used nowadays but only toluene diisocyanate (TDI) and methylene diphenyl diisocyanate (MDI) are commercially the most important ones[14]. The schematic production routes towards polyurethanes are represented in *Figure 1.*

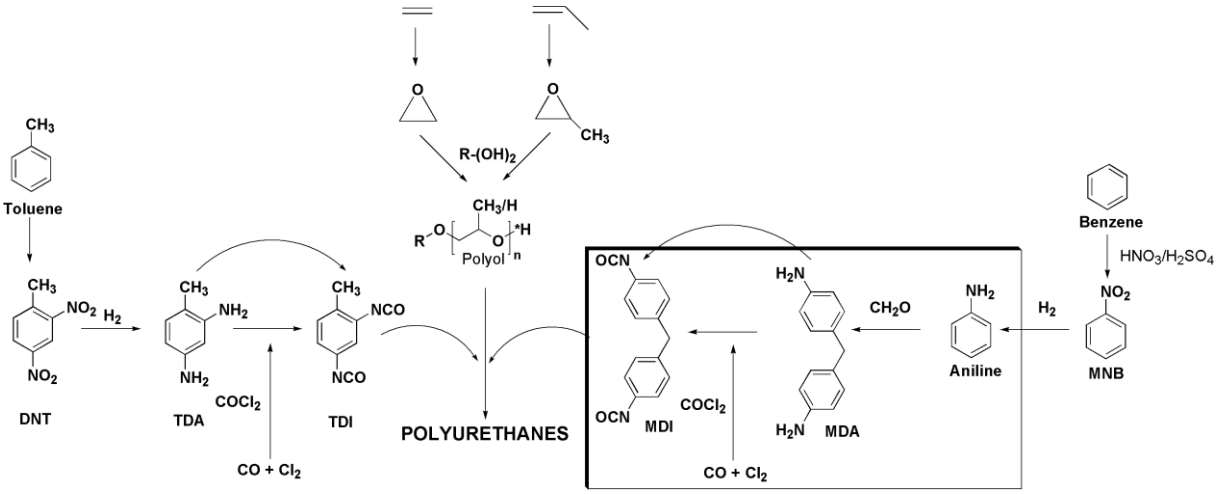


**Figure 1**: Synthetic routes to polyurethanes from the most commonly used diisocyanates[15].

The MDI market was expected to reach 6.7 Mt in 2018 and is predicted to achieve 8.7 Mt by 2023 according to the latest market report[16]. MDI is mainly produced by the reaction of 4,4′-methylenedianiline (MDA) and phosgene ($COCl_2$) in continuous operation[17]. MDA is formed reacting aniline with formalin in the presence of hydrochloric-acid solution. The aniline feedstock is produced sequentially from the nitration of benzene followed by reduction to aniline by hydrogenation[11]. The MDI product consists of a mixture of isomers (2,2-; 2,4- and 4,4'-MDI) and oligomers. The unpurified stream can be sold as polymeric MDI. The isomers are mostly separated by distillation. The main product is the 'pure' MDI containing only 4,4'-MDI isomers[2]. 'Pure' 4,4'-MDI is light yellow to white solid MDI with melting point of 38-40°C, boiling point of 300°C and flash point of 212-214°C[18]. It is an odorless material which is soluble in acetone, benzene, kerosene, and nitrobenzene[19]. MDI

can undergo slow cyclodimerization on storage so that it is transferred and stored under refrigeration or under heating[20].

The focus of this research is the examination of the main reaction steps of MDI synthesis and to examine one possible side reaction: the dimerization. As *Figure 2* illustrated firstly aniline is reacted with formaldehyde using hydrochloric-acid catalyst. Afterwards, the phosgenation of the appropriate amine, MDA, exists. Based on the reactivity of the free isocyanate groups dimers can be formed establishing a four-membered ring.

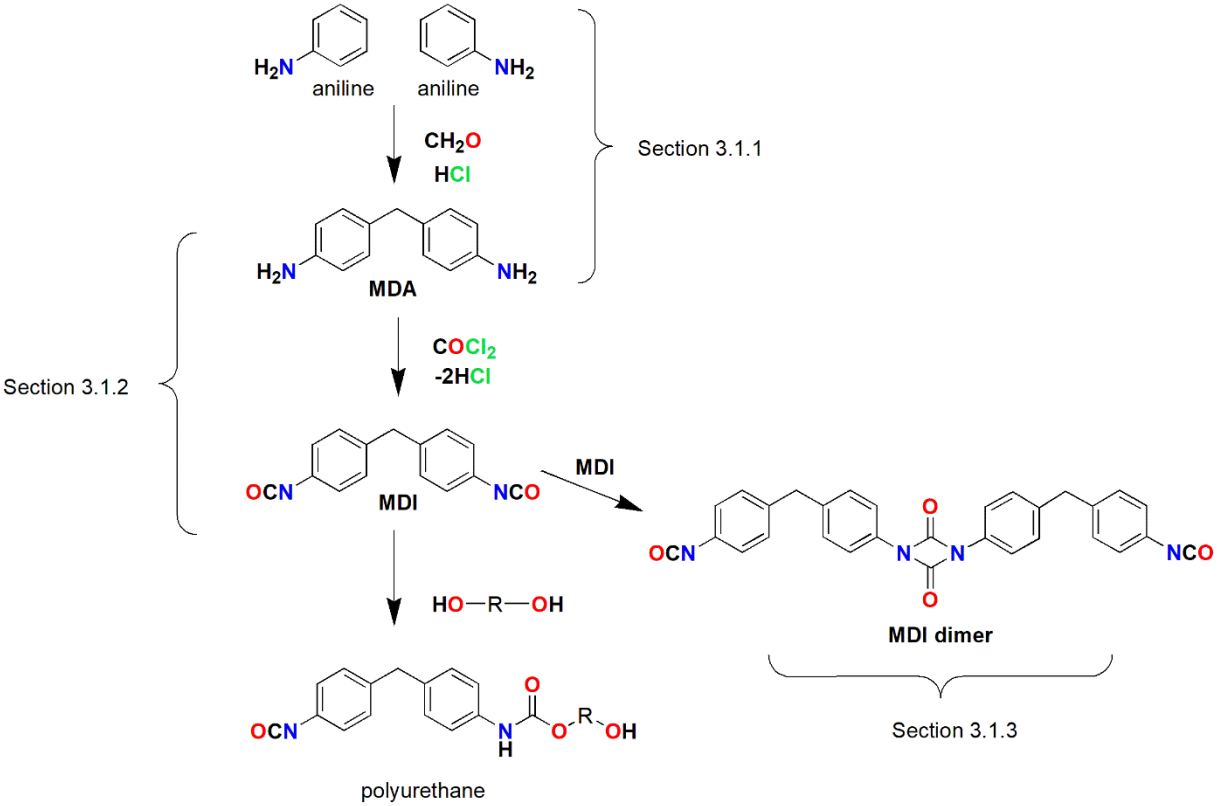


**Figure 2**: Reaction steps of MDI synthesis and the route towards the polyurethane synthesis and one possible side reaction.

## 1.2 Methylene diphenyl diamine (MDA) formation

The MDI production is mostly based on methylene diphenyl diamine (methylenedianiline, MDA). MDA can be also applied as ingredient of epoxy resins, intermediate for pigments, organic dyes, coatings, plastic fibers, insulation materials[21] making it an important synthetic agent. In chemical industry the most commonly applied MDA synthesis is the reaction of aniline with formalin in the presence of hydrochloric acid under mild (60°C-110°C) reaction conditions[22]. To avoid the use of corrosive hydrochloric acid and the formation of large amount of NaCl solution as waste, several attempts[15,23–29] had been

made to replace the current technology with catalytic process using solid acids, zeolites, delaminated materials, ionic liquids or ion exchange resins as catalysts. However, either of the catalytic MDA production never gone beyond the laboratory stage. Although proposed reaction mechanism for current MDA synthesis is presented in the study published in Kirk-Othmer Encyclopedia of Chemical Technology[17] (*Figure 3*), it has not been clarified entirely. According to this mechanism aniline (A) is reacted with formaldehyde (F) producing N-hydroxymethyl aniline as the initial reaction step. In acidic medium this product loses water rapidly to form N-methylidene anilinium (IM2) which reacts with aniline to form N (p-aminobenzyl)aniline (PABA). PABA is then decomposed to 4-aminobenzylium and aniline. In the last step of this rearrangement 4,4'-methylene diphenyl diamine (4,4'-MDA) is formed as final product.

In an alternative mechanism, reaction of N-methylenebenzeneaminium (IM2) and aniline (A) gives N,N'-diphenylmethylenediamine first (so-called aminal noted as AM in *Figure 3)* before the formation of PABA. Due to the protonation of one of the secondary amine group in AM ($AMH^+$), the C-N bond is activated for the rearrangement making protonated PABA (noted as $IM4H^+$ latter). Same is supposed to happen to the other secondary amine group to form MDA: PABA is got protonated ($PABAH^+$) which then initiates aniline rearrangement.

*Wang et al*. found some evidences to support the latter mechanism by isolation and identification of aminal using the combination of isotope labeling and HPLC-MS[30] albeit other intermediates has not been characterized at all. In the same study by-products including oligomers of MDA (e.g. 3- and 4-ring MDA) were also suggested. As a continuation of this work stabilities, potential protonation sites and structural characterization of these MDA oligomers were determined using ion mobility-mass spectrometry (IM-MS) and tandem mass spectrometry (MS/MS) techniques[31]. Although, the MDA synthesis is essential to MDI production, the thermochemical properties of the participated species are also poorly characterized. To the best of our knowledge, only the standard reaction enthalpy of formation for MDA, PABA and AM is estimated using Benson group additivity method[32].

Only the heat of formation of 4,4'-MDA had been reported very recently using G3MP2B3 quantum chemistry protocol and group additivity increments for NCO and NHCOCl groups has been recommended[33] as it was mentioned earlier[34,35].

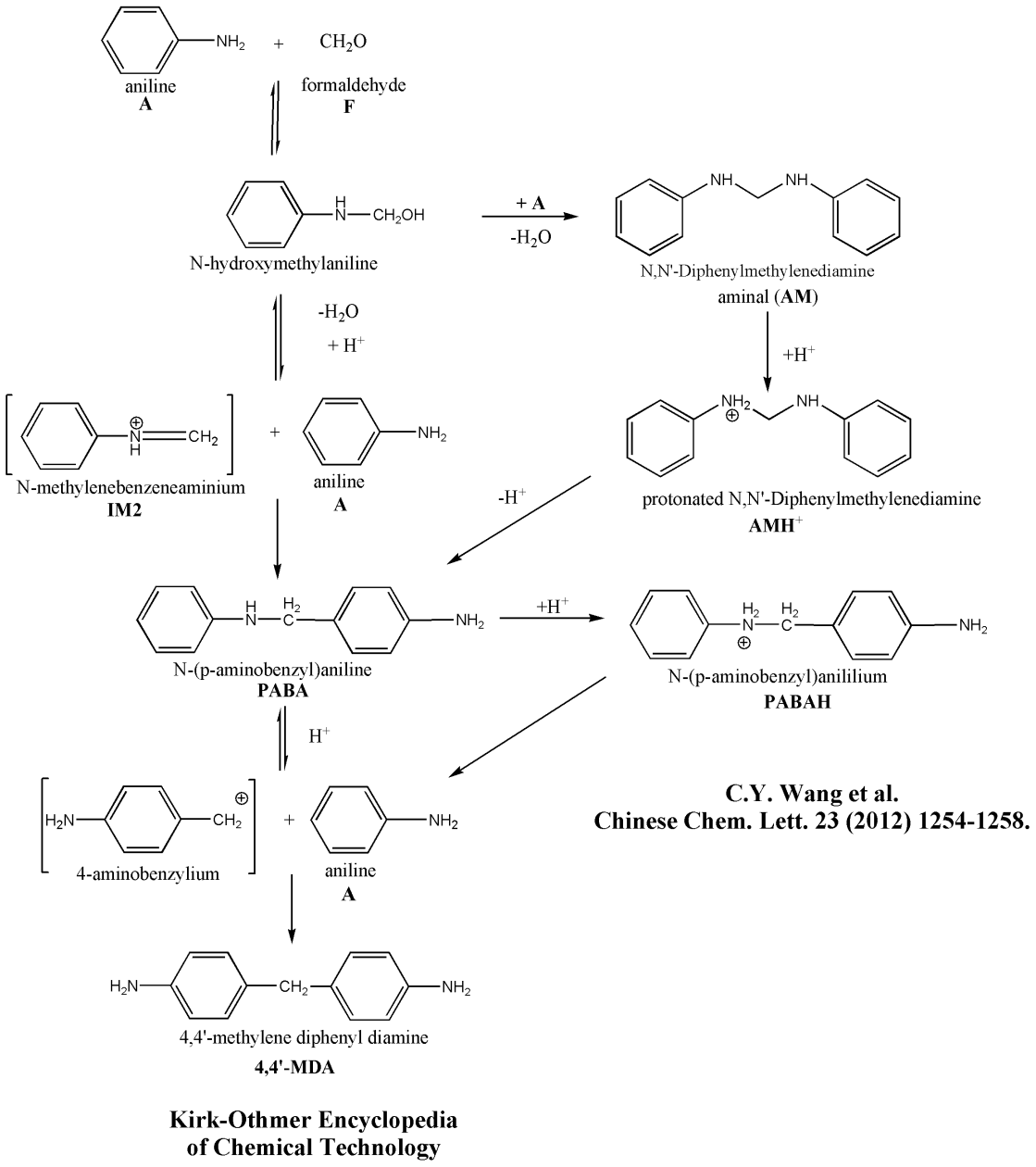


**Figure 3:** Overall reaction mechanism for MDA synthesis according Kirk-Othmer Encyclopedia of Chemical Technology and a possible side reaction according to Wang et al[17].

## 1.3 Phosgenation of MDA

The second step of MDI synthesis is the phosgenation of MDA which in the chemical industry is carried out in a suitable inert solvent such as toluene, xylene and chlorinated aromatic hydrocarbon at temperatures between 50°C and 250°C, while pressures ranging from ambient pressure up to 50 bar[36]. When ortho-dichlorobenzene (ODCB) used as solvent, mild operating condition (90-150°C and 6-11 bar pressure)[37] can be applied which is mainly due to the boiling point of the ODCB ($T_b$=180.5°C)[38]. The excess phosgene, which is necessary to obtain the appropriate isocyanate yield, and the by-product

hydrochloric acid is stripped by a nitrogen stream at higher temperature. The solvent is removed from the product by distillation. The unreacted phosgene and hydrochloric acid are recycled and utilize in the technology of MDI production[18]. As it was shown above, the chemical industry uses the phosgenation of amide in large scale, although its reaction mechanism and the corresponding energy profile is less known. The isomer and ring distribution of the product MDI could not be influenced by this phosgenation step; however, this process is very important from the view of industrial MDI production.

Phosgenation of an amine is an addition-elimination type mechanism via a chlorinated amide intermediate resulted in the release of 2 HCl molecules[39]. About the whole reaction mechanism of MDA phosgenation the number of the published results is very poor. Based on our assumption, in principle, the phosgenation of diamines such as MDA can occur via two mechanisms (*Figure 4).* In the first case both amino groups are converted to carbamoyl chloride and then two consecutive HCl-elimination steps occur (shown in *Figure 4* as 'Phosgenations first'). Alternatively, transformation of MDA into MDI consists of two consecutive addition-elimination steps (shown in *Figure 4 a*s 'Stepwise phosgenations'). At some condition, to the N-substituted carbamoyl chloride intermediate is detected according to Sonnenshcein et al[2]. At higher temperature (80 - 100°C) this intermediate can be dehydrochlorinated to form MDI[11]. Despites the importance of the above mentioned phosgenation, the thermochemical properties of the participated species are poorly characterized. For example, while the heat of formation value ($\Delta_{f,298.15K}H°$) for MDA is scarce, only one published value (165.6 kJ/mol) can be found without reported uncertainty[40] (other group additivity-based value obtained using online NIST estimator), the standard enthalpy of formation of the MDI ($\Delta_{f,298.15K}H°$)(MDI)=189±21 kJ/mol) is known with relatively large uncertainty from static bomb calorimetric study of Zhuravlev et al[41] but to the best of our knowledge, there is no thermodynamic information about the intermediates of the phosgenation of MDA.

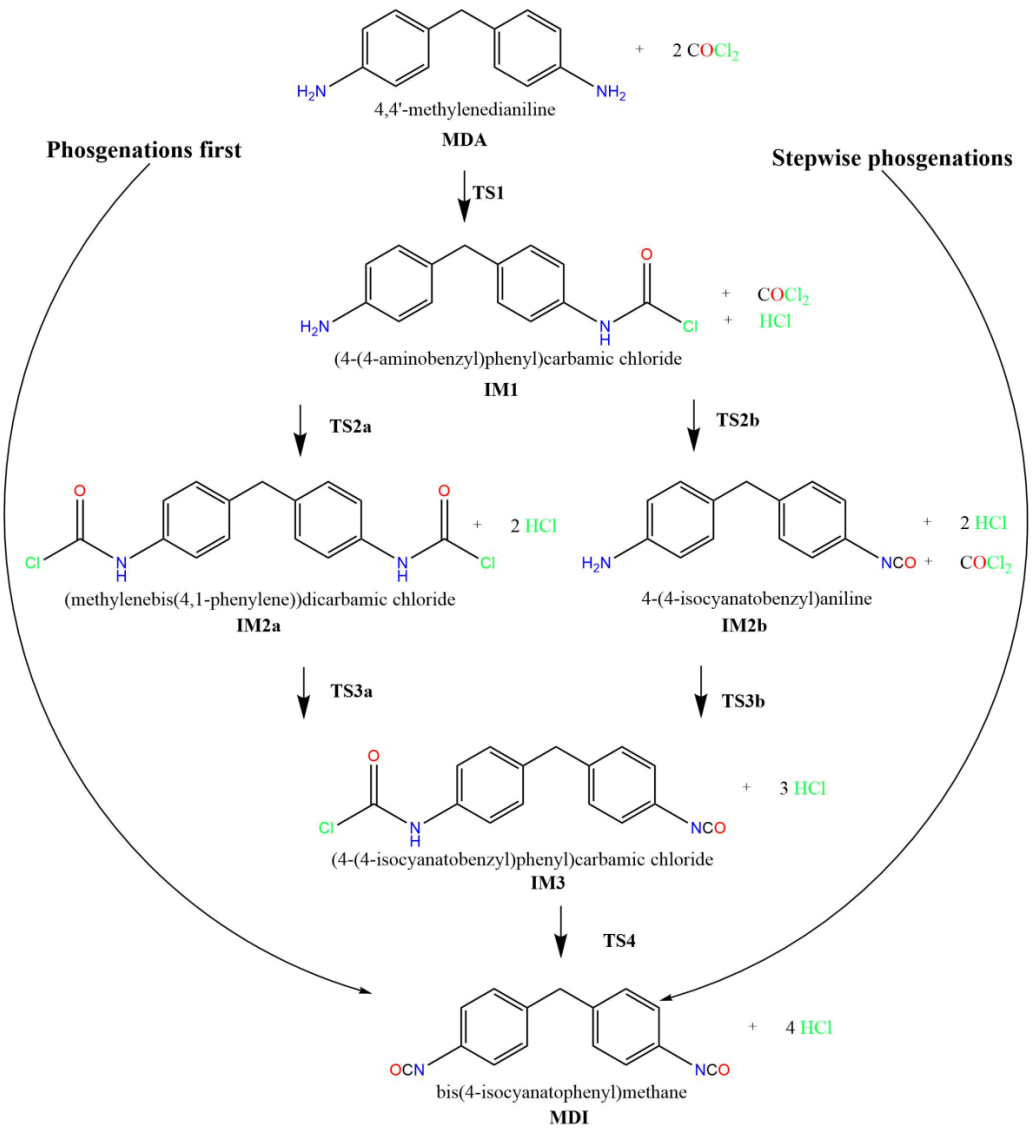


**Figure 4:** Proposed reaction mechanism of MDA phosgenation.

In the phosgenation step unwanted by-products can be also formed in side reactions causing impurities during the MDI synthesis[42,43]. For example, one of the products of the reaction, that is HCl, can possibly form a by-product with one of the giving amine hydrochlorides which are insoluble in chlorinated solvents causing several problems in the production[44]. Gibson et al. studied the stability and the structure of these compounds in chlorobenzene by FTIR, NMR and X-ray diffraction[45]. The further possible side reaction is the urea formation between the isocyanate and amine[46] which is reduced by using excess amount of phosgene in the industry[20] Besides the liquid phase phosgenation, the gas phase phosgenation of the amines seems to be relevant since it can be an economical and environmentally friendly alternative to isocyanate production due to reduced solvent and energy consumption[47]. In the first step of this procedure, amines and phosgene are

vaporized separately and could be diluted in inert gas and then reacted[48]. Despites the above-mentioned advances, the phosgenation in gas phase still suffers from technological difficulties such as evaporation of the amines may initiate side reactions and formation of deposit in the apparatus[49,50] therefore the understanding of the ongoing elementary reactions is essential to improve the applied chemical technology. On the other hand, the mechanisms of these reactions are also interesting from theoretical points of view, since the existence of different reaction intermediates and channels can extend our current knowledge as work of Fiser et al. did for the Baldwin's rules[51].

### 1.4 Dimerization of MDI – an undesired side reaction

Product MDI can undergo a dimerization process in the case of not appropriate handling (storage and transport). MDI dimers cause issue in control of the quality for MDI products. The dimerization of MDI has a negative effect on its applicability. In the case where dimerization occurs, the isocyanate becomes two-phased, causing turbidity. In addition, the melting points of solid MDI and its dimer are different. The MDI dimers are highly stable and can only decompose at high temperature; thus, at the melting point of the MDI they are not able to dissolve, which causes difficulty. The rate of dimerization is lowest at 43°C[52] (*Figure 5*) while has maximums around 38 and 62°C.

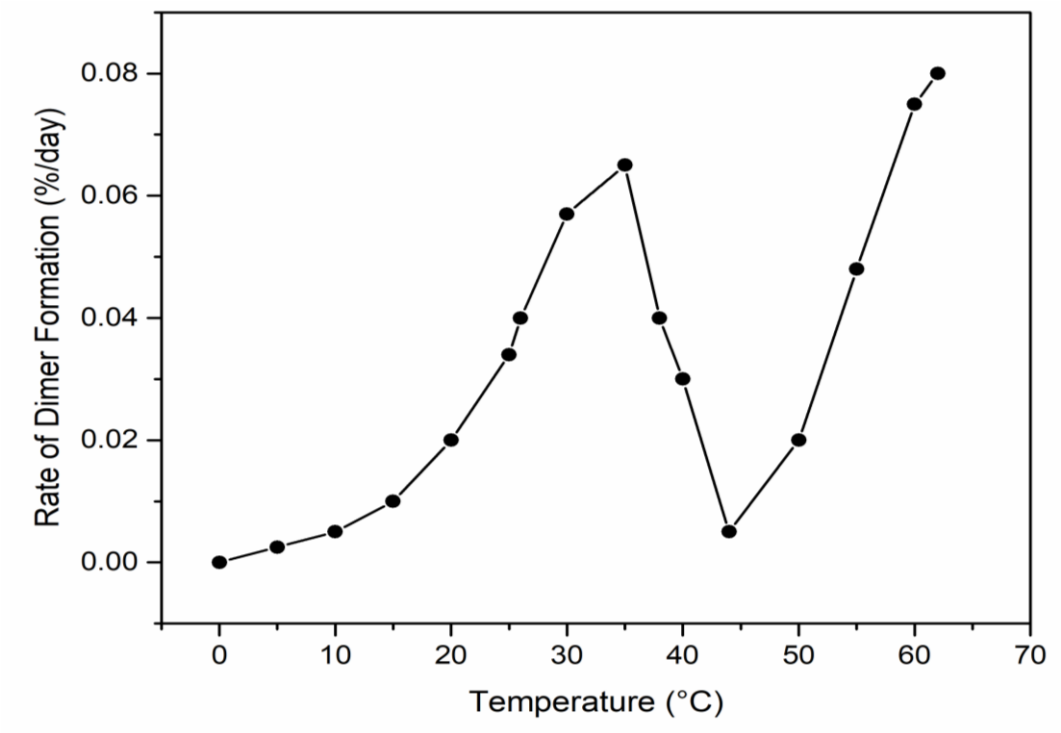


**Figure 5**: Rate of dimer formation as a function of temperature measured by BASF[52].

During the dimerization process, the 4,4′ monomer undergoes a slow, reversible and facile dimerization reaction to form the uretidione(*Figure 6*)[11]. The maximum in the conversion rate is unfortunately around ambient storage temperatures.

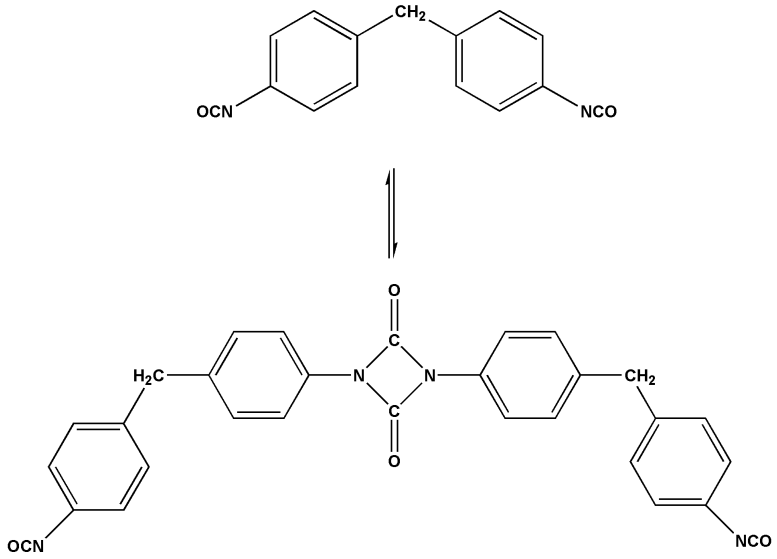


**Figure 6:** Uretidione formation from monomer MDI.

This reaction is intrinsic to the reactivity of isocyanate functionality and the packing of 4,4′ MDI in its crystal state[53]. The reaction of uretidione cross-linked isocyanates with alcohols occurred via an allophanate structure[54] which is then converted into urethane. Uretidione structures serve as a protected isocyanate group in a manner, their industrial use was found within urethane powder coatings[55,56] but is otherwise most notable as a problem related to MDI storage.

Several computational studies have been conducted to study dimerization processes. First principles calculations[57] were used to investigate the effect of epoxy monomers on dimerization. Structural and spectral characteristics of dimethylformamide (DMF) monomers and dimers were calculated[58].

**Figure 7**: MDI dimer formed during inappropriate storage.

### 1.5 A new aspect of chemical industrial production study

Production of isocyanates is a complex process requiring appropriate adjustment of reaction conditions. Knowing the elementary reaction steps of a product synthesis might facilitate the product optimization, support the solution of technological problems and even promote the new developments. Computational chemistry provides the possibility to examine industrial syntheses determining reaction mechanism considering side-reactions and by-products. Nowadays, more and more experimental developments are accompanied by theoretical calculations demonstrating proof of benefits that computational calculations provide[59]. This field has grown extremely rapidly, especially in the case of pharmaceutical industrial application[60], however more and more application can be found in the chemical industry[61] especially for examining chemical reactivity and catalysis or used as an analytical technique for structure characterization.

The novelty of this study is that computational calculations were used for determining the reaction mechanism of an industrial process, the MDI synthesis. Moreover, this technique was applied for structure characterization of MDI dimers. The achieved results and the main conclusions are described in the following sections presenting valuable insights into understanding of industrial reactions on molecular level.

## 2 METHODS

### 2.1 Computational chemistry

The basics of quantum chemistry are practically used in form of computational calculations which can predict molecular properties for comparison with experiment, to elucidate ambiguous or unclear experimental data and to model short-lived, unstable intermediates and transition states[62]. Using the adiabatic and Born-Oppenheimer approximations, potential energy can be defined by the position of nuclei in space (nuclei are considered as classical particle) and the electrons are treated as quantum particles and their description can be obtained by an approximated solution of the electronic Schrödinger equation (e.g. at certain level of theory). Obviously, the classical approach of nuclei is biased but can be corrected back via rigid rotor harmonic oscillator treatment of the kinetic energy term of nuclei in order to get the solution for the molecular Schrödinger equation.

A potential energy surface (PES) is a mathematical function that gives the total energy of a molecule as a function of its geometry (*Figure 8*). That is potential energy of a set of reactants is plotted as a function of the coordinates representing the molecular geometries of the system[63].

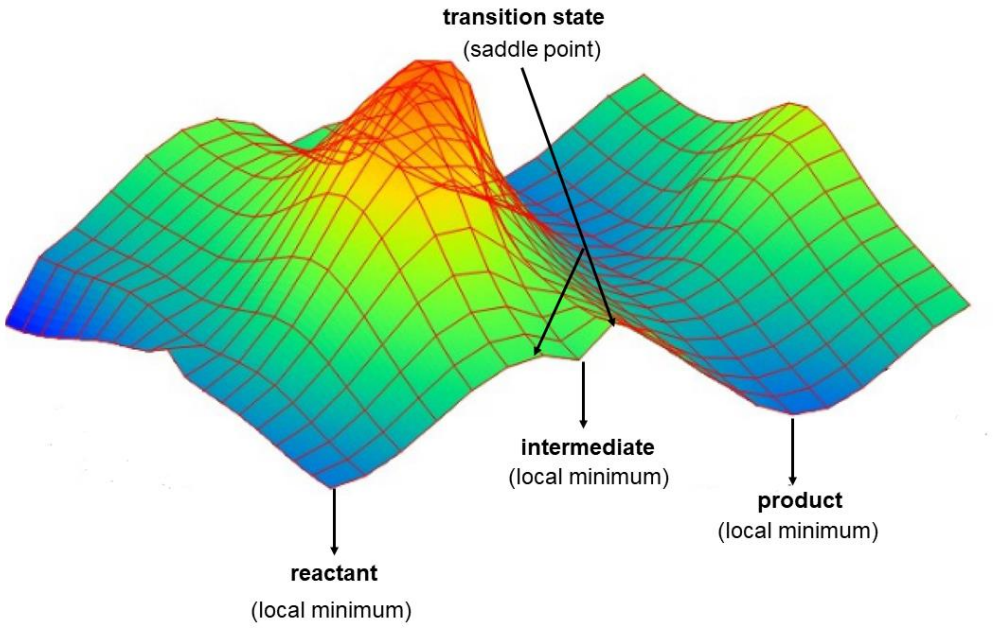


**Figure 8**: Schematic representation of a potential energy surface.

According to IUPAC, molecules are defined as an electrically neutral entity consisting of more than one atom (n>1). Rigorously, a molecule, in which n>1 must correspond to a depression on the potential energy surface (PES) that is deep enough to confine at least one vibrational state.

In order to explore elementary steps of a reaction (reaction mechanism), reactants and products (molecules) as well as a representative transient structure of a reaction pathway has to be determinate. Minimum of the PES can be a local minimum which represents the lowest energy point of some limited region of PES or can be global minimum considering as the lowest energy point on the potential surface. Reactants (R), products (P) and intermediates (IM) are the structures existing in the local minima. The first critical step in the quantum chemical calculation is the choice of the initial structure which must be close to a local minimum. This can be aided by structural parameters from general force-field and the local minimum can be determined by changing the nuclei coordinates (R) and calculating the corresponding electronic energy and nuclei-nuclei repulsion energy (their sum is the so-called total energy, $E_{tot}$ (R). The *minimum energy*

*structure* is formed when all the convergence criteria were fulfilled. The attempt of finding the coordinates belong to a local minimum or saddle point known as **geometry optimization**. Each iteration of the geometry optimization the maximum remaining force on an atom in the system as well as the average mass weighted force constant force on all atoms together has to be checked and their valves must be smaller than the corresponding threshold value. The third and fourth convergence criteria are the maximum displacement, that is, the maximum structural change of one coordinate as well as the average (RMS) change over all structural parameters in the last two iterations. Once the current values of all four criteria fall below the threshold, the optimization is considered as complete numerical criterium of the local minimum. When the optimization had completed, we have to ensure that the predicted structure is in fact a minimum by **frequency calculation** at the optimized geometry. Frequency calculations consider the nuclear vibration in molecular systems in their equilibrium states. If the geometry is optimized into a minimum, the gradient is zero, and the force constant matrix completely determines the behavior of the system under small displacements. Tightening up the convergence criteria is useful for getting a couple of extra digits of precision in the symmetric stretch frequency (which manifested in better approximation of entropy).
In the case of the transition state structure - found in the first order saddle point of the PES - the first derivative of the potential with respect to any nuclear coordinate is zero, and the second derivative is positive for all but one coordinate (that is called reaction coordinate). Thus, such a point looks like a minimum on the potential energy surface in every direction except one in which it is a maximum that defines the reaction coordinate at the transition state.

In the following sections, the calculations of the potential energy including solvent effect as well as derivation of the rotational constant ($B_0$) and harmonic vibrational wavenumbers ($\upsilon_i$) will be shown. By means of these calculated molecular properties vibrational wavenumbers and rotational constants, the partition functions (q(V,T)) can be obtained which encode how the probabilities are partitioned among the different microstates (transition, rotation, vibration, electronic state) from which the thermodynamic functions (G(T,p), $E_0$, S(T,p), H(T) can be derived (*Figure 9*). The experimentally most important macroscopic properties, such as the reaction heat ($\Delta_rH°$), heat of formation ($\Delta_fH°$), heat capacity ($C_v$), Gibbs free energy ($\Delta_rG°$), entropy (S) and acid

dissociation constant ($pK_a$) are calculated using thermodynamic functions. By means of the macroscopic properties of the molecules, the reaction mechanism can be predicted, the by-products and side reactions can be assumed.

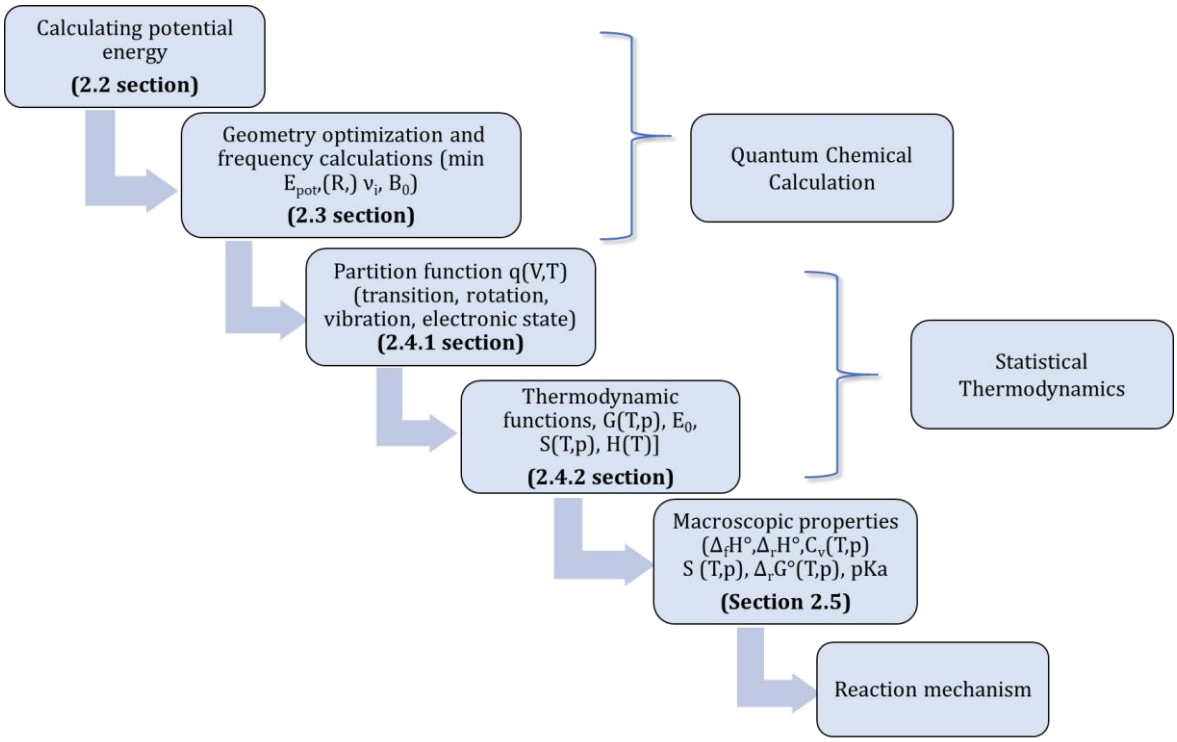


**Figure 9**: A flowchart from determining the potential energy to macroscopic properties.

## 2.2 Level of theory - computation of potential

Different theoretical methods - *referred to as levels of theory* - correspond to various approximations to the electronic Schrödinger equation with a certain accuracy.

One of the widely used approximation method in quantum chemistry is the Hartree-Fock (HF) method[64,65] which is the basis of the molecular orbital theory. It assumed that the multielectron wavefunction of the system can be approximated by a single Slater determinant which is made up of one spin orbital per electron[66]. This ab initio method requires low computational time, but it does not include the electron correlation leading to imprecise results meaning the calculated HF energy is higher than the exact energy. Only for the hydrogen atom (or other one-electron systems, such as He) are orbitals exact eigenfunctions of the full electronic Hamiltonian.

Several methods improve the treatment of electron correlation over the Hartree-Fock method to achieve better accuracy. Such post-Hartree-Fock ab initio method is the Møller–Plesset perturbation theory (MP)[67]. Calculated energy may be lower than exact

ground state energy. This method is appropriate if the level of the electron correlation is reatively low where a significant amount of correlation energy is given back at low computational cost.

The Møller-Plesset expansion is truncated at second (MP2)[68] third (MP3) or fourth (MP4) order providing higher order perturbation methods. Several important molecular properties calculated at MP3 and MP4 level are not better than their MP2 counterparts, even for small molecules. MP2 usually overestimates bond energies. Other post-Hartree-Fock methods are the configuration interaction methods (CI) and its correction called quadratic configuration interaction singles and doubles:(QCISD)[69]. These methods are used because by coupled cluster methods more accurate results can be achieved requiring the same computational capacity. Coupled cluster methods (CC)[70] are used for describing many-body systems constructing multi-electron wavefunctions employing the exponential cluster operator to account for electron correlation. These methods apply series expansion which resulted in the formation of determinants from the reference Slater-determinant like wavefunction where one or more electrons are transferred to the unoccupied orbitals in the reference. A drawback of the method is that it is not variational. The CCSD[71] (coupled cluster singles and doubles) method contains single and double excitations, while the CCSD(T) additionally includes the perturbative approximation of triple excitations. Currently, the CCSD(T) is the most precious electron-structure method still applicable for small systems.

The most popular quantum chemical approaches are the hybrid density functional theories (DFT)[72]used to determine the electronic structure of the molecules. DFT methods are based on determination of the *electron density* of the molecule calculating energy by the use of an exchange-correction functional. This exact exchange energy functional is expressed in terms of the Kohn–Sham orbitals[73] rather than the density. A large number of different functional are parameterized by experimental or highly accurate ab initio data. Practically, these functionals are implemented iteratively. DFT calculation adds an additional step to each major phase of a Hartree-Fock calculation. This step is a numerical integration of the functional (or various derivatives of the functional). However, DFT methods have deficiency of density functionals and the appropriate description of dispersion interactions. They are also lack of long-term exchange term[74]. Currently, several DFT methods are available where the London dispersion correction has been

already considered[74]. Possible solution could be to apply functionals which parameters have been optimized via data groups.

DFT of electronic structure has seen significant theoretical and formal advances. This method can predict the relative and activation energies and the structures commensurate with the high performance and costly post-SCF.

M06-2X[75] is global hybrid functional with 54% HF exchange from the group of Minesota functions parametrized only for non-metals. The M06-2X functional contains 35 fine-tuned parameters which were previously optimized on data groups[74]. This method does not contain a direct member for the dispersion correction, but via its parameters it can be related as a dispersion-corrected DFT method. This functional performed well in the case of activation energies and transition states[76–78].

The B3LYP (Becke, 3-parameter, Lee-Yang-Parr)[79,80] is a fairly robust hybrid DFT method. This functional[81] employs three empiricals[82,83]. This semiempirical exchange-correlation functional was tested on 56 atomization energies, 42 ionization potentials, 8 proton affinities, and 10 total atomic energies of first- and second-row systems and it was found that this functional fit experimental atomization energies with an impressively small average absolute· deviation of 2.4 kcal/mol[84]. B3LYP is generally faster than most of the post Hartree-Fock method and usually yields comparable results which is especially hold for geometry. On a more fundamental level, it is not as heavily parameterized as other hybrid functionals, having only 3 where as some have up to 35 such as the M06-2X. The ab initio methods discussed so far it could be said that the HF, MP2 and DFT methods provide acceptable accurate geometry, but the energy calculations are not adequate. However, the higher-level calculations such as CCSD, QCISD, CCSD(T), QCISD(T) serve the equilibrium of geometry and the frequency calculations essential for the thermochemical calculations, only for very high 'price' and for long calculation time. Other disadvantages of these methods are that only numerical derivatives are determined for harmonic frequency calculations[85].

Reasonable tradeoff is composite methods. They developed to afford quite accurate frequencies using scale factor and geometry carrying out energy calculations on it applying systematic combinations of different bases and methods. Nowadays, the CBS (Complete Basis Set) and Gaussian-n (n≤4) family CBS-4M, CBS-APNO, and the G3, G3MP2, G3MP2B3 composite methods are applied in most cases[85].

In this study the G3MP2B3[86,87] was applied most of the case therefore it is presented in detail. In the case of this method the geometries and zero-point energies are obtained from B3LYP/6-31G(d) density functional with scaled frequency of 0.96 instead of geometries from second-order perturbation theory [MP2/(FU)6-31G(d)] and zero-point energies from Hartree–Fock theory [HF/6-31G(d)]. This variation has an average absolute deviation of 1.25 kcal/mol. High accuracy of this method is obtained by determining (experimentally and theoretically) a higher-level correction E(HLC) based on calculations for the hydrogen atom and hydrogen molecule. The basis of this calculation is that the energies from a lower level calculation (MP2) is added to a higher-level correction (HLC) calculation (QCISD(T)). In the case of the atoms spin-spin correction (E(SO) was also considered, assessed it on 299 energies (enthalpies of formation, ionization potentials, electron affinities, proton affinities) from the G2/97 test set[87] Compound models performs a series of less expensive calculations providing very high accurate results for thermochemical predictions. Such model includes G4MP2[88], G4[89], CBS-QB3[90].

All of the previously mentioned electronic-structure methods require to give a basis set function (base). A basis set is a collection of mathematical functions used to build up the quantum mechanical wave function for a molecular system. In principle higher, the number of the mathematical function used the more accurate the description of the electronic structure. The drawback is the higher computing demand. Hundreds of basis sets composed of atomic centered Gaussian-type orbitals (GTOs)[91] Several basis sets are known, the so-called diffuse bases also contain Gauss functions which spatial running is slowly promoting the appropriate description of the high-distanced interactions. Pople basis sets are one of the most used basis sets. It consists of the STO-G set (where n value represents the number of Gaussian primitive functions fitted to a Slater orbital). There is one basis function for the core and two or more for the valence. When the core orbital is made of 6 Gaussians and the valence is described by 2 orbitals (first is derives from 3 Gaussians and the second from 1) the basis set is called: 6-31G. When a d polarization function is added the non-hydrogen, atoms are polarized. For the polarization of the hydrogen atoms a plus p polarization function[92].

*Solvation model*[93]

Most of the reactions relevant for industrial application are taken place in solvent. The energetics of the reaction can be significantly modified if the components can form interactions with the solvent molecules. The electronic structure problem for a molecule in a liquid is reduced to the size of the solute of interest by continuum solvation models (sometimes called implicit solvation or implicit solvent models) representing a solvated molecule surrounded by a dielectric medium that represents the solvent. In this study, SMD implicit model was used to mimic the surrounding. The SMD continuum solvation model, where the "D" stands for "density" to denote that the full solute electron density is used without defining partial atomic charges, is based on the quantum mechanical charge density of a solute molecule interacting with a continuum description of the solvent. In this model the solvent is not represented explicitly but rather as a dielectric medium with surface tension at the solute-solvent boundary. In this model the quantum mechanical charge density of a solute molecule interacting with a continuum description of the solvent. surface tension, and acidity and basicity parameters). A training set of 2821 solvation data were used for parametrization of SMD model. This solvation model achieves mean unsigned errors of 0.6-1.0 kcal/mol in the solvation free energies of tested neutrals and mean unsigned errors of 4.0 kcal/mol on average for ions.

## 2.3 Vibrational analysis[94]

The molecular geometry used for vibrational analysis must be optimized at the same level of theory and with the same basis set which the second derivatives were generated with. Vibrational analysis contains several steps that are introduced in this section. Firstly, mass weighted second derivative matrix (Hessian) is calculated converting force constants to mass weighted cartesian coordinates. Afterwards, determination of the moments and products of inertia is proceeding, deciding the principal axes of inertia, where the target is to find the matrix that diagonalizes the moment of inertia tensor. However, the mass weighted cartesian coordinates are formed, it is necessary to transform where rotation and translation of the molecule are separated out by creating coordinates in the rotating and translating frame. Then the Hessian need to be converted to internal coordinates and diagonalize. To obtain the frequencies the eigenvalues need to be converted to frequencies, first from frequencies to wavenumber. Finally, the reduce

mass, force constants and cartesian displacements are calculated which are all internally consistent.

As example determination of vibration frequency and bond length for $HCl^{95}$ - *which has* an *important role in MDI synthesis* - is presented here. As it was introduced above firstly the wavenumber is determined and the reduced mass, afterwards the force constant and bond length. The relation between these parameters is explained as follows. The vibration energy of HCl molecule uses the harmonic oscillator approximation, while the rotational energy applies the rigid rotor approximation. The vibration energy ($E_\upsilon$) can be expressed in terms of force constant (k) according to *Equation 1*, however the rotational constant $\widetilde{B}_0$ highly depends on bond length ($R_0$) (*Equation 2)*.

**Table 1**: Calculation of vibrational and rotational energy.

| Vibrational energy | Rotational energy |
|---|---|
| (1) $E_\upsilon = hc\tilde{\upsilon}_K(\upsilon + \frac{1}{2})$ | (2) $E_J = \widetilde{B}_0\ hc\ J\ (J+1)$ |
| $\tilde{\upsilon}_K$ = vibrational wavenumber | $\widetilde{B}_0$ = rotational constant |
| (3) $\tilde{\upsilon}_K = \frac{1}{2\pi c}\sqrt{\frac{k}{\mu}}$ | (4) $\widetilde{B}_0 = \frac{h}{4\pi\mu R_0{}^2 c}$ |
| k = force constant | $R_0$ = bond length |

Considering the *Equation 3* the υ represents the quantum number for the vibration, while the μ is the reduced mass calculating from the masses such as $\mu = \frac{m_1 m_2}{m_1 + m_2}$. The Planck constant is indicated with h ($h = 6.62 \cdot 10^{-34}$ J·s), while c represents the speed of light ($c=2.99 \cdot 10^8$ m/s). The quantum number for vibration is sign as υ, while in the rotational energy it is labelled as J. The first molecular energy level can be obtained as a sum of the total energy ($E_{tot}$ that is the sum of electronic and nuclei-nuclei repulsion energy and zero-point energy) and zero-point energy.

The latter is defined as

$$(5) \qquad \mathrm{ZPVE} = \sum_K \mathrm{hc}\frac{\tilde{\upsilon}_K}{2}$$

since HCl only one vibrational degree of freedom that is $hc\frac{\tilde{\upsilon}}{2}$ in this case. The fundamental vibration frequencies, moments of inertia, reduced masses and bond lengths are determined by this way. These microscopical parameters are contributed to the molecular properties with the help of statistical thermodynamics *(Figure 9).*

## 2.4 Statistical thermodynamics

Many important macroscopic parameters of the system resulted from knowledge of its microscopic constituents. In the case of the microscopic properties the system's atomic dimensions are considered, specified by the number of particles in each energy state. This approach is known as **statistical thermodynamics** which act as a bridge between the molecular properties and macroscopic thermodynamic properties such as the state functions[96].

### *2.4.1* Partition function

In the thermodynamic equilibrium energy distribution of the molecules can be described by the *Boltzmann distribution*, while the **partition function** (q(V,T)) encodes how the probabilities are partitioned among the different microstates, based on their individual energies. The total energy of the microstate of a molecule can be assumed as a sum of energies in the various degrees of freedom of the molecule.

$$(6) \qquad \varepsilon = \varepsilon_{tr} + \varepsilon_{rot} + \varepsilon_{vib} + \varepsilon_{elec}$$

The translational energy ($\varepsilon_{tr}$) is resulting from the movement (translation) of the molecular mass; the rotational energy ($\varepsilon_{rot}$) derives from the rotational degrees of freedom while the vibrational energy ($\varepsilon_{vib}$) includes the contribution from vibrational degree. In practice the vibrational frequencies need adjustment (general scale factor) to better match experimental vibrational frequencies. The electric state is usually considered as multiplicity chosen and its deviation became important for having low-lying excitations.

Similar to molecular partition function (q) can also be factorized into contributions from each mode of motion and establish the formulas for the partition functions for translational, rotational, and vibrational modes of motion and the contribution of

electronic excitation. The following equation introduces the molecular partition functions and sources of components for thermodynamic quantities.

$$q = q_{tr} \cdot q_{rot} \cdot q_{vib} \cdot q_{elec} \quad (7)$$

This factorization means that we can investigate each contribution separately.

### *2.4.2 Thermodynamic state functions*

*Table 2* summarized state functions play essential role in physical chemistry since they provide information about the spontaneous processes at different conditions.

**Table 2**: Criterion of equilibrium and the direction of the spontaneous processes in closed system (n = constant).

| Potential function | Conditions | Direction of change in spontaneous process | Criterion of equilibrium |
|---|---|---|---|
| G (Gibbs free energy) (P, T, n) | p and T are constant | decrease | minimum |
| H (enthalpy) (S, p, n) | S and p are constant | decrease | minimum |
| S (entropy) (U, V, n) | E and V are constant | increase | maximum |
| E (internal energy) (S, V, n) | S and V are constant | decrease | minimum |

Gibbs free energy (G), enthalpy (H), entropy (S), internal energy (E) derived from the partition function can describe quantitatively an equilibrium state of a thermodynamic system, irrespective of how the system arrived in that state.

The Gibbs free energy G(T,p) can be used to calculate the maximum or reversible work that may be performed by a thermodynamic system at a constant temperature (T) and pressure (p). It is defined as:

$$G(T,p) = H(T) - TS(T,p) \quad (8)$$

where *S* refers to the entropy of the *system*. Since *H*, *T* and *S* are all state functions, so is *G*. Enthalpy (H) is a measurement of the energy in a thermodynamic system. It is equivalent with the total heat content of the system. It is equal to the internal energy of the system plus the product of pressure and volume.

$$H(T) = E(T) + pV \quad (9)$$

Enthalpy (H) is defined as a state function that depends only on the prevailing equilibrium state identified by the variables internal energy, pressure, and volume.

Entropy (S) state function originally introduced to explain why part of total energy is unavailable to do useful work[97].

*2.4.2.1* Calculations of state functions

In the awareness of the partition function (q) and temperature (T) the previously mentioned state functions can be calculated. The basic calculations are introduced in this section.

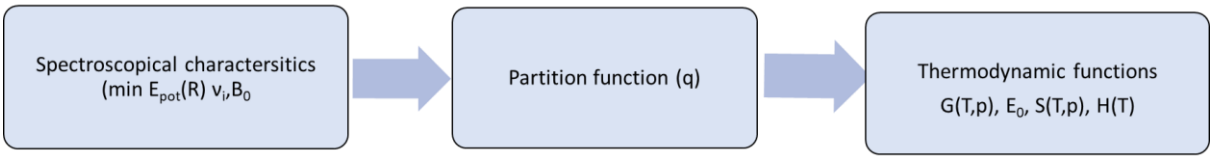


***Figure 10**: From spectroscopic characteristics to state functions.*

The partition function from any component can be used to determine the entropy contribution S from that component, using the relation:

$$S = Nk_B + Nk_B \ln\left(\frac{q(V,T)}{N}\right) + Nk_B T\left(\frac{\partial \ln q}{\partial T}\right)_V \quad (10)$$

where N represents the particle number of molecules as a dimensionless quantity.

The internal thermal energy U can be obtained from the partition function according to the followings:

$$E = Nk_B T^2 \left(\frac{\partial \ln q}{\partial T}\right)_V \quad (11)$$

Heat capacity can be calculated by using the energy:

$$C_V = \left(\frac{\partial U}{\partial T}\right)_{N,V} \quad (12)$$

The enthalpy of any substance in term of partition function can be calculated as follows:

$$H - H(0) = \left(\frac{\partial \ln Q}{\partial \beta}\right)_V + kTV\left(\frac{\partial \ln Q}{\partial V}\right)_T \quad (13)$$

$$H - H(0) = -5/2\ nRT \text{ (for atoms)} \quad (14)$$

Q represents the partition function of the system, while q is the molecular partition function. Expressing the Gibbs free energy from the partition function according to the following equation:

$$(15) \qquad G - G(0) = -nRT\ln\frac{q}{N}$$

Gibbs energy is proportional to the logarithm of the average number of thermally accessible states per molecule.

To simplify the expression of the rotational and vibrational partition function and contributions to thermodynamic properties a *characteristic temperature* ($\theta_{r,x}$ or $\theta_{v,K}$) is used in statistical thermodynamics[98]. The characteristic temperature ($\theta$) are also an estimate of the temperature at which thermal energy (of the order of $k_BT$, where $k_B$ is the Boltzmann constant) is comparable to the spacing between rotational or vibrational energy levels. At about this temperature the population of excited rotational or vibrational levels becomes important.

Thus, partition functions have a central role in statistical thermodynamics because once therefore it is known as a function of the variables on which it depends, all thermodynamic quantities may be calculated from it directly.

**Table 3**: Contribution of translation, electronic, rotational and vibrational motions to the partition and state functions.

| | Contributions from | | | |
|---|---|---|---|---|
| | Translation motion | Electronic motion | Rotational motion | Vibrational motion |
| | m: molecular mass | $\omega_0$: multiplicity | $\widetilde{B}_{0,x}$ : rotational constant in x irection | $\tilde{\upsilon}_K$: Kth vibrational wavenumber |
| Θ | | | $\Theta_{r_1 x} = hc\widetilde{B}_{0,x}/k_B$ | $\theta_{\upsilon,K} = hc\tilde{\upsilon}_K/k_B$ |
| q | $q_t = \left(\frac{2\pi m k_B T}{h^2}\right)^{3/2} V$ | $q_e = \omega_0$ degeneracy of the electronic energy level | $q_r = \frac{1}{\sigma_r}\left(\frac{T}{\Theta_r}\right)$ $q_r = \frac{\pi^{1/2}}{\sigma_r}\left(\frac{T^{3/2}}{\sqrt{\Theta_{r_1 x}\Theta_{r_1 y}\Theta_{r_1 z}}}\right)$ | $q_{v,K} = \frac{e^{\Theta_{v,K}/2T}}{1 - e^{-\Theta_{v,K}/T}}$ |
| S | $S_t = R(\ln q_t + 1 + 3/2)$ | $S_t = R(\ln q_e + 0)$ | $S_t = R(\ln q_r + 1)$ | $S_v = R(\ln(q_v) + T\left(\frac{\partial lnq}{\partial T}\right))_V$ |
| $E_{corr}(T)$ | $E_t = \frac{3}{2}RT$ | 0 | $E_r$= RT | $E_V = R\sum_K \Theta_{v,K}\left(\frac{1}{2} + \frac{1}{e^{-\Theta_{v,K}/T} - 1}\right)$ |
| $C_v$ | $C_t = \frac{3}{2}R$ | 0 | $C_r = R$ | $C_V = R\sum_K e^{\Theta_{v,K/T}}\left(\frac{\Theta_{v,k}/T}{e^{-\Theta_{v,K}/T} - 1}\right)^2$ |

*Thermodynamics of the molecule*

The total electronic energy ($E_{tot}$) of the molecular system under study relative to separate nuclei and electrons, after various corrections are applied. The zero-point energy (ZPE) is calculated using only the non-imaginary frequencies, results from the vibrational motion of molecular systems and is calculated for a harmonic oscillator model as a sum of contributions from all i vibrational modes of the system. The zero-point corrected total energy ($E_0$) is the sum of the $E_{tot}$ and ZPVE. Thermal corrected energy E°(T) included the total electronic energy and electric energy. This is the total electronic energy plus $H_{corr}$ with the unscaled zero-point energy removed. The standard Gibbs free energy (G°) is calculated form the sum of $G_{corr}$ and total electronic energy.

**Table 4**: Nomenclature and derivation of the most important thermochemical properties from corrections.

| | |
|---|---|
| $E_0 \equiv Etot+ZPVE$ | Zero-point corrected total energy |
| $E°(T) \equiv E_{tot}+E_{corr}(T)$ | Thermal-corrected energy |
| $H°(T)=E°(T)+RT=E_{tot}+H_{corr}(T)$ | Standard enthalpy (pV=nRT!) |
| $G°(T,p) \equiv H°(T)-TS°(T,p)=E_{tot}+G_{corr}(T,p)$ | Standard Gibbs free energy |
| $H_{corr}(T) = E_{corr}(T)+RT$ | Corrected Enthalpy |
| $G_{corr} = E_{corr}(T)+RT-TS°(T,p)$ | Corrected Gibbs free energy |

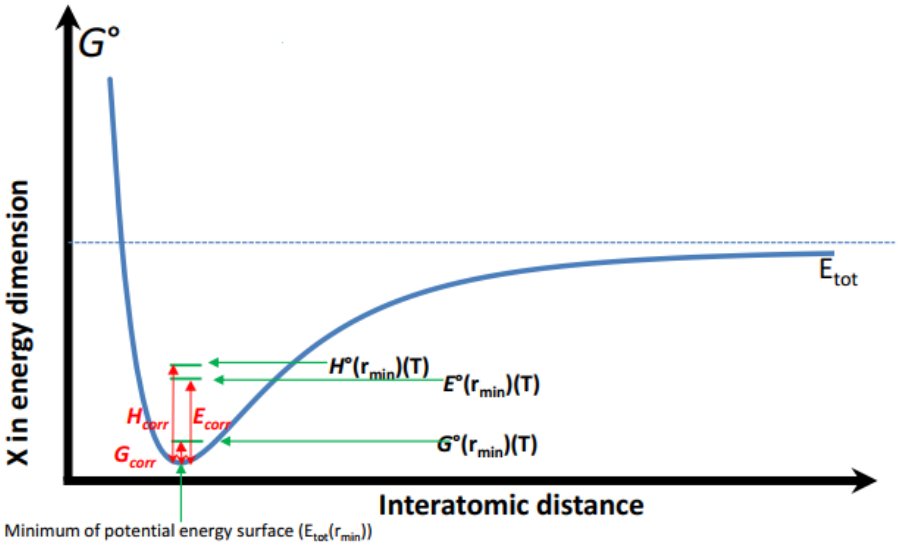


**Figure 11**: Schematic plot of the potential energy surface as a function of distance. Thermal corrections are also indicated.

## 2.5 Macroscopic properties

The macroscopic characteristics describes those features which is enough to be visible in the ordinary sense (such as temperature, pressure, entropy, free energy, heat capacity, chemical potential, viscosity, spectra, reaction rates, etc.). From the view of chemical reaction mechanism the determination of standard enthalpy of formation ($\Delta_f H°$), standard reaction enthalpy ($\Delta_r H°$), heat capacity $C_v(p,T)$, entropy $S(T,p)$ is essential.

### *2.5.1 Standard reaction enthalpy*

The standard reaction enthalpy of a chemical reaction is represented as $\Delta_r H°$ and refers to the enthalpy change associated with one mole of a specified reactant when all reactants and products are in their standard state[99]. It is the amount of heat absorbed (endothermic) or evolved (exothermic) in the transformation of the reactants into the products.

One way to calculate enthalpy of reaction is to calculate standard enthalpies of formation for the species involved and take the appropriate sums.

The standard reaction enthalpies ($\Delta_{r,298.15K} H°$) are calculated by subtracting the sum of the reactant from the sum of the products according to the stoichiometry of the reaction. In computational chemistry it is more practical to use the calculated enthalpies (here the reference state is the non-interacting nuclei and electrons) which is unpractical in experimental points of view but simple for ab initio.

The calculation is demonstrated using MDA as an example.

$$CH_2O + 2C_6H_5NH_2 = MDA + H_2O$$

$$\Delta_{r,298.15K} H° = (\Delta_{f,298.15K} H°(MDA) + \Delta_{f,298.15K} H°(H_2O)) - (\Delta_{f,298.15K} H°(CH_2O) + 2\Delta_{f,298.15K} H°(C_6H_5NH_2))$$

In the case of G3MP2B3 the $\Delta_{r,298.15K} H°$ is the following:

$$\Delta_{r,298.15K} H° = [(-612.302313 \text{ Hartree} + (-76.341863 \text{ Hartree}) - (2 \cdot (-287.120066 \text{ Hartree})$$

$$-114.354203 \text{ Hartree})] \cdot 2625.5 \text{ kJ/(mol Hartree)} = \mathbf{-130.9 \text{ kJ/mol}}$$

### 2.5.2 Standard Enthalpy of Formation

Standard enthalpy of formation ($\Delta_{f,298.15K}H°$) of a compound is the standard reaction enthalpy for the formation of one mole of molecule from its constituent elements with all substances in their standard states (at 1 bar and at temperature of interest)[99]. The formation energies of the elements are 0 kJ/mol, while the accurate experimental formation energies of atoms in gas phase and molecules can be found in databases. The determination of $\Delta_{f,298.15K}H°$ can be accomplished via atomization scheme (AS) and considering as isodesmic reaction (IR).

*Determination of $\Delta_{f,298.15K}H°$ on atomization level (AS)*

The calculation steps of the atomization scheme are the followings using the result of MDA formation at G3MP2B3 as an example:

1. Firstly, the relative standard enthalpy values of the atoms are calculated at G3MP2B3, which are added together according to the appropriate stoichiometry. The multiplicity of the atoms is different which also needs to be set up before we calculate it.

$$H_{calc}°(^3C(g)) = -37.788425 \text{ Hartree}$$

$$H_{calc}°(^2H(g)) = -0.499780 \text{ Hartree}$$

$$H_{calc}°(^4N(g)) = -54.524582 \text{ Hartree}$$

$$\Delta_{f,298.15K}H_{atoms}°(C_{13}H_{14}N_2(g)) = 13H_{calc}°(^3C(g)) + 14H_{calc}°(^2H(g)) + 2H_{calc}°(^4N(g)) = -607.295609 \text{ Hartree}$$

2. In the next step the enthalpy value of the molecule (e.g. MDA) is calculated in gas phase which is $H_{calc}°(MDA(g)) = -612.302313$ Hartree. The calculated atomic standard enthalpy value - *calculated in the previous step* - is then subtracted from this result.

$$H_{calc}°(MDA(g)) - \Delta H_{atoms}°(C_{13}H_{14}N_2(g)) = -5.006704 \text{ Hartree}$$

3. Afterwards, the accurate standard enthalpies of formation at 298.15K for the atoms are collected from Rusicic's[100] which are the following in our case:

$$\Delta_{f,\,298.15\,K}H_{exp}°(^3C(g)) = 716.88 \pm 0.055 \text{ kJ/mol}$$

$$\Delta_{f,298.15K}H_{exp}°(^2H(g)) = 217.998 \pm 0.000 \text{ kJ/mol}$$

$$\Delta_{f,298.16K}H_{exp}°(^4N(g)) = 472.43 \pm 0.024 \text{ kJ/mol}$$

4. The experimental atomization enthalpy can be calculated by sum of the enthalpies of the atoms according to their stoichiometries in MDA:

$$13\ C(graphite) + 7\ H_2(g) + N_2(g) = 13 \cdot {}^3C\ (g) + 7 \cdot {}^2H\ (g) + {}^4N\ (g)$$

$$\Delta_{atom.}H_{exp}^\circ = 13H_{exp}^\circ({}^3C(g)) + 14H_{exp}^\circ({}^2H(g)) + 2H_{exp}^\circ({}^4N(g)) =$$

$$= 13 \cdot 716.88 + 14 \cdot 217.998 + 2 \cdot 472.43 =$$

$$13316.3\ kJ/mol$$

5. Finally, the $\Delta_{f,298.15K}H^\circ$ of the molecule - in this case, the MDA - is calculated as adding the ($\Delta H_{calc}^\circ$(MDA(g)) and sum of standard atomization enthalpy values of the atoms:

$$\Delta_{f,298.15K}H^\circ(g) = \Delta_{f,298.15K}H^\circ(MDA)(g) + \Delta_{atomization}H_{exp}^\circ(g)$$

$$\Delta_{f,298.15K}H^\circ(MDA(g)) = -13145.10135\ kJ/mol + 13316.282\ kJ/mol =$$

$$= 171.2\ kJ/mol$$

*Determination of $\Delta_{f,298.15K}H^\circ$ considering an isodesmic reaction*

Isodesmic reactions are usually defined as transformations in which the number of electron pairs of the reactants and products are the same. These reactions can also be hypothetical. In this section the $\Delta_{f,298.15K}H^\circ$ of MDA on G3MP2B is represented as an example.

1. In the first step, the relative standard enthalpy values of the molecules are calculated. The reactants are added together and are substratcted from the sum of the products according to the sociometry of the reaction.

$$CH_2O(g) + 2C_6H_5NH_2(g) = MDA(g) + H_2O(g)$$

$$H_{calc}^\circ(CH_2O(g)) = -114.354203\ Hartree$$

$$H_{calc}^\circ(C_6H_5NH_2(g)) = -287.120061\ Hartree$$

$$H_{calc}^\circ(H_2O(g)) = -76.341863\ Hartree$$

$$H_{calc}(MDA(g) = -612.302313\ Hartree$$

$$\Delta_r H^\circ = \mathbf{-130.9\ kJ/mol}$$

The calculated relative standard enthalpy of formation in the first step of the isodesmic calculation way is the same as that the value achieved in the case of 2.5.1. section.

2. In the next step the accurate literature values[101] for the standard enthalpy of formation is needed in this case:

$$\Delta_{f,298.15K}H°_{exp}(CH_2O(g)) = -109.2\pm0.11 \text{ kJ/mol}$$

$$\Delta_{f,298.15K}H°_{exp}(C_6H_5NH_2(g)) = 87.04\pm0.88 \text{ kJ/mol}$$

$$\Delta_{f,298.15K}H°_{exp}(H_2O(g)) = -241.83\pm0.03 \text{ kJ/mol}$$

Then the $\Delta_{f,298.15K}H°$ of MDA is calculated by subtracted the sum of the experimental formation of the reactants according to the sociometry (step 2) from the calculated $\Delta_{r,298.15K}H°$ (kJ/mol) (step 1):

$$\Delta_{f,298.15K}H°(MDA)(g) = (\Delta_{r,298.15K}H°(MDA) - \Delta_{f,298.15K}H_{exp}°(H_2O)) + (\Delta_{f,298.15K}H_{exp}°(CH_2O) + 2\Delta_{f,298.15K}H_{exp}°(C_6H_5NH_2)$$

$$\Delta_{f,298.15K}H°(MDA)(g) = \textit{-130.9 kJ/mol-( -241.83kJ/mol) + (-2·87.04kJ/mol) + -109.2kJ/mol)} = \mathbf{175.9\ kJ/mol}$$

The calculated standard enthalpy of formation values, determinate by atomization ($\Delta_{f,298.15K}H°$=-130.9 kJ/mol) and by isodesmic reaction ($\Delta_{f,298.15K}H°$=175.9 kJ/mol) will be compared with the literature data (Section 2.7).

## 2.6 Applied Computational Methods

During my PhD research the main reaction mechanisms occurring in the industrial MDI production were studied using computational chemistry tools. To explore the important reaction mechanisms, structure of the reactants, transition states (TS), complexes, intermediates (IM) and products were necessary to be characterized accurately. Normal mode analysis was carried out on optimized structure both in vacuum and in solvent. To proof the corresponding structures connected with each other, intrinsic reaction coordinate (IRC) calculations of the minimal energy pathways (MEP) were also carried out. Furthermore, for these optimized structures, thermodynamic properties (zero-point corrected relative energy ($\Delta E_0$), relative enthalpy ($\Delta H°$), heat of formation [($\Delta_{f,298.15K}H°$(g), relative Gibbs free energy ($\Delta G°$), and entropy (S°)] were computed using methods described above.

All our systems were explored using this functional in combination with the 6-31G(d)[102] basis set and B3LYP functional. As a refinement of B3LYP/6-31G(d) level of theory, more

robust and accurate **G3MP2B3**[86] composite method was also selected from the Gaussian thermochemistry family whenever it was feasible. Due to its computationally demanding QCISD(T)/6-31G(d) calculation the use of G3MP2B3 is limited to the thermodynamic properties of larger systems were computed using another popular, new-generation functional, that is Truhlar's **M06-2X**[75] functional with the 6-31G(d,p) basis set. For verification purposes, the newest member of Gaussian thermochemistry family **G4**[88], **G4MP2**[103], and Peterson's **CBS-QB3**[104] composite methods were applied to estimate the accuracy of the used computational method.

All the geometry optimizations and frequency calculations were carried out using Gaussian09[105] program package.

The applied levels of theory in this thesis are summarized in *Table 5.*

**Table 5**: Applied theoretical methods studying the reaction steps of MDI synthesis and side reaction.

| Level of theory | Theoretical reaction mechanism of | | Thermodynamic properties of |
|---|---|---|---|
| | MDA synthesis | MDI synthesis | MDI dimers |
| B3LYP/6-31G(d) | ✓ | ✓ | ✓ |
| G3MP2B3 | ✓ | ✓ | - |
| M06-2X/6-31G(d,p) | ✓ | - | ✓ |
| G4 | ✓ | ✓ | - |
| G4MP2 | - | ✓ | - |
| CBS-QB3 | ✓ | - | - |

## 2.7 Benchmark of computational methods

In order to estimate the accuracy of the applied computational methods, the standard reaction enthalpy of MDA formation ($\Delta_{r,298.15K}H°$) and standard heat of formation ($\Delta_{f,298.15K}H°$) were calculated (*Table 6)* in gas phase using G3MP2B3 (B3LYP/6-31G*(d)), CBS-QB3 (6-311G (2d.d,p)) and M062X(6-31G(d,p)) levels of theory. Only two different $\Delta_{r,298.15K}H°$ values, -134.96[40] and -221.752 kJ/mol[106] in *Table 6*, were reported in the literature estimated by group additivity method suggested by Benson and Joback[107],

respectively. The standard reaction enthalpies obtained from CBS-QB3 and G3MP2B3 computations are excellent agreement with each other, since the difference is just 0.5 kJ/mol and these values are also close to the -134.94 kJ/mol obtained by Joback/Benson method. The M06-2X/6-31G(d,p) result is lower than the CBS-QB3 and G3MP2B3.Therefore, only the calculations obtained by composite methods are discussed later.

**Table 6**. Standard reaction enthalpies of MDA formation and heat of formation values for MDA.

| Level of theory | 2AN+FA=MDA+WAT | Atomization scheme (AS) | Isodesmic reaction (IR) |
|---|---|---|---|
| | $\Delta_{r,298.15K}H°$(kJ/mol) | $\Delta_{f,298.15K}H°$(MDA) (kJ/mol) | |
| G3MP2B3 | -130.9 | 171.2 | 175.9 |
| M06-2X/6-31G(d,p) | -155.8 | 139.5 | 151.4 |
| CBS-QB3 | -130.4 | 191.8 | 176.8 |
| literature data *(group additivity)* | -221.7[106] | 206.1[108] | |
| | -134.9[40] | 165.6[40] | |

The literature $\Delta_{f,298.15K}H°$ values are quite different (see the values of 206.05 and 165.6[108] kJ/mol in *Table 6)* which may be due to the different phases (e.g liquid/solid) but unfortunately that information was not reported in the original paper. In the case of G3MP2B3, $\Delta_{f,298.15K}H°$ values derived from AS and IR are consistent with each other and the $\Delta_{f,298.15K}H°$ result obtained from the IR by CBS-QB3 is also very close to the G3MP2B3 values, the largest deviation is just 0.5 kJ/mol. Based on these calculations, we recommend their average value as our best estimation of the $\Delta_{f,298.15K}H°$(MDA), that is 171.2 kJ/mol, with the uncertainty of 5 kJ/mol. Actually, one of the literatures $\Delta_{f,298.15K}H°$(MDA) value (165.6 kJ/mol) has relatively small deviation (5.6 kJ/mol) from our recommendation. The $\Delta_{f,298.15K}H°$(MDA) obtained from AS using CBS-QB3 results is higher than the recommended value due to the fact that CBS-QB3 is less robust than G3MP2B3 in such calculations. It is also worthy to mention that the CBS-QB3 was more computationally intensive than G3MP2B3 either, therefore only the G3MP2B3 results will be presented in the further discussion.

# 3 RESULTS AND DISCUSSION

## 3.1 Reaction mechanism of MDA synthesis

The purpose of this chapter is to explore and characterize thermodynamically the detailed reaction mechanism of the current industrial MDA production using quantum chemical calculations including the effect of the surrounding media. Furthermore, the protonation states of the intermediates are also determined as well as few important competing reaction channels are also included to provide theoretically established evidence for by-products.

### *3.1.1 Main reaction mechanism in gas phase*

Although, the MDA synthesis is carried in liquid phase, firstly the gas phase mechanism is examined as a reference. The solvent effect as the presence of solvent can make a significant difference on the reaction energy profile. According to the X-ray scattering experiment of aniline[109] closest intermolecular distance between nitrogen atoms in a pair of aniline (A) molecules is 3.31 Å, which is close to the distance (3.159 Å) found in the V-shape non-covalent bonded aniline dimer ($A_2$) computed at G3MP2B3 in gas phase. This short distance and orientational preference are due to the strong hydrogen bond between two amine groups explaining the large viscosity of liquid aniline[110]. Therefore, in our calculations, $A_2$ structure had been selected as initial structure (see right side of *Figure 13*). The energy reference used in *Figure 12* (also given in *Table 7*) corresponds to the sum of non-covalent $A_2$ dimer, formaldehyde (F) and protonated aniline ($AH^+$). The latter species supposes to mimic the acidic environment used by chemical industry.

In our reaction mechanism we assume that the protonated aniline dimer ($A_2$) approaches the formaldehyde (F) to form the pre-reactive complex (IM0, see *Figure 13*), in which formaldehyde is strongly hydrogen bonded to one of the anilines ($r_{O\text{-}H}$ = 2.108 Å) and its carbon atom approaches the nitrogen atom of the other amine ($r_{C\text{-}N}$ = 2.671 Å). This structure is 29.2 kJ/mol lower in energy compared to the separated formaldehyde, protonated aniline and aniline dimer (reference state). As seen in *Figure 14* , the transition state for formaldehyde addition to the aniline (TS1) is a six-membered ring structure, where the carbon of F got closer to the nitrogen of the amine by roughly 1 Å ($r_{C\text{-}N}$ = 1.644 Å) compared to the IM0. Simultaneously, attacked nitrogen releases a hydrogen

which is transferred to the oxygen of formaldehyde through the other aniline amine group.

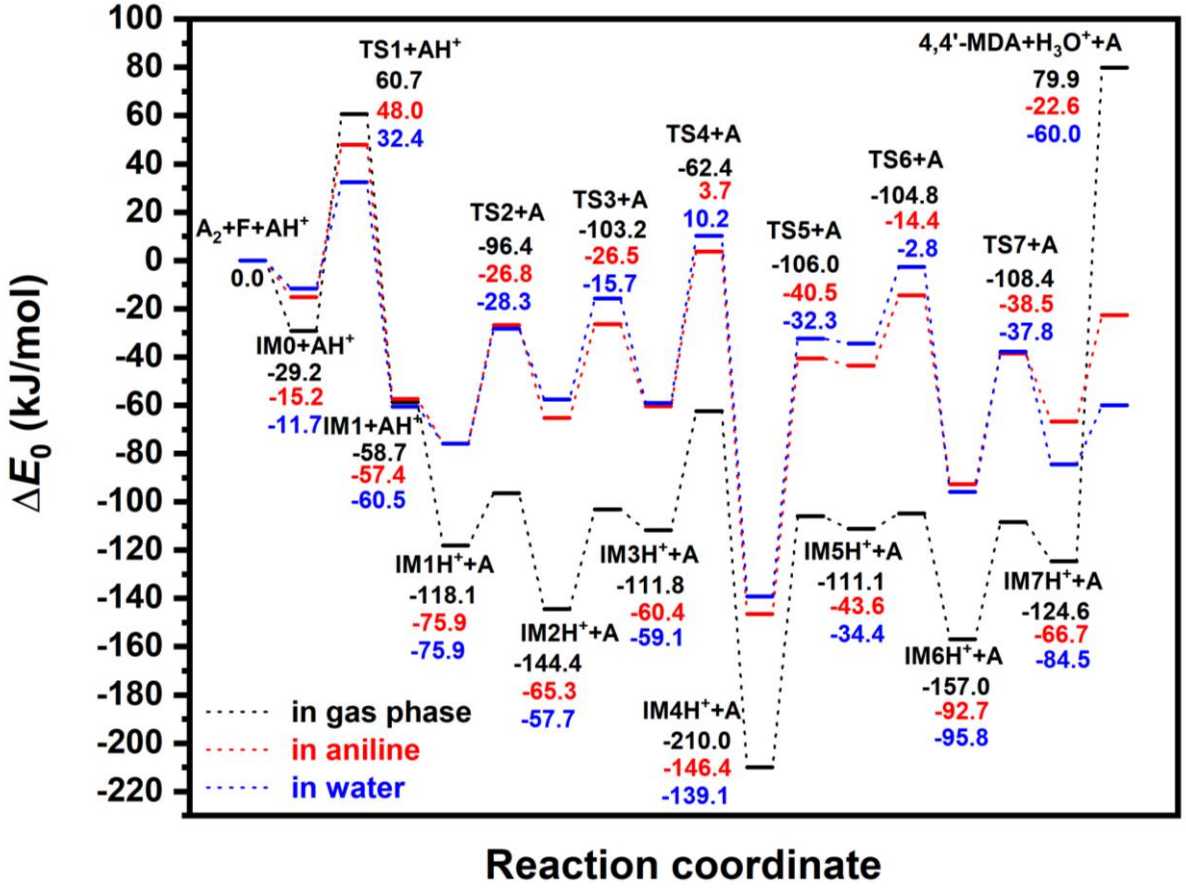


**Figure 12**: G3MPB3 energy profile (zero-point corrected) for MDA synthesis in gas phase (black), in aniline (red) and in water (blue).

The corresponding energy is 60.7 kJ/mol higher than that of the reactants making this structure as the highest energy TS along the entire reaction mechanism studied here (*Figure 12*). As next step, the resulted N-hydroxymethylaniline (IM1) forms molecular complex with protonated aniline ($AH^+$), noted as $IM1H^+$, in which the protonated amine group is in vicinity of the OH group of N-hydroxymethylaniline ($r_{O\text{-}H}$ = 1.599 Å). This protonated complex has significantly lower in energy (-118.1 kJ/mol) compared to the previous neutral complex (-58.7 kJ/mol).

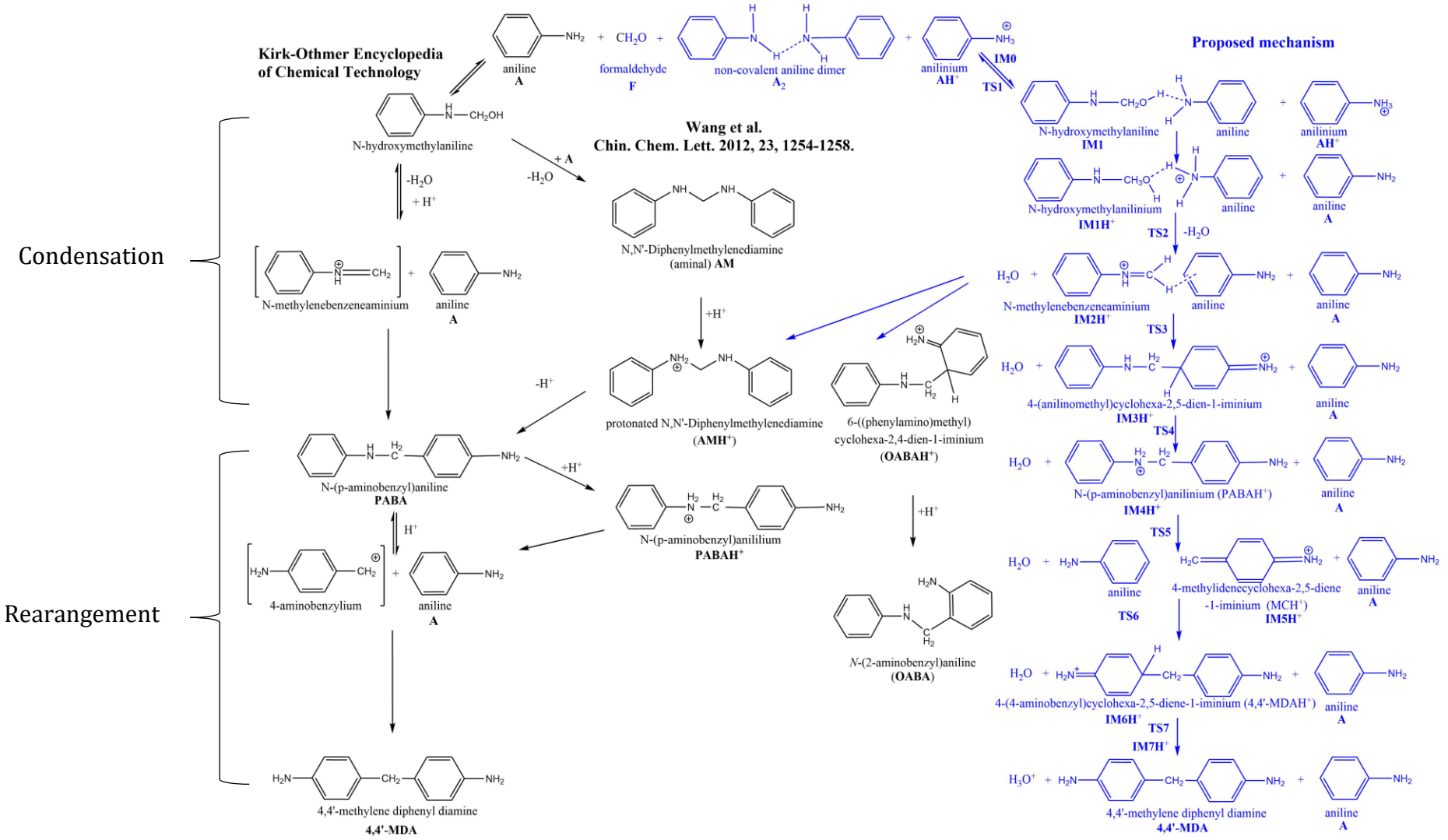


**Figure 13**: Overall reaction mechanism for methylene diphenyl diamine (methylenedianiline, MDA) synthesis according Kirk–Othmer Encyclopedia of Chemical Technology[17] as well as Wang[30] compared with our proposed mechanism based on G3MP2B3 computation.

**Table 7**: G3MP2B3 thermochemical properties calculated in gas phase, in aniline and in water including zero-point corrected relative energies ($\Delta E_0$,G3MP2B3), relative enthalpies (ΔHG3MP2B3(T)) and relative Gibbs free energies (ΔGG3MP2B3(T,P)) at T=273.15 K, and p=1 atm.

| Species | $\Delta E_{0,G3MP2B3}$ | | | $\Delta H_{G3MP2B3}(T)$ | | | $\Delta G_{G3MP2B3}(T,P)$ | | |
|---|---|---|---|---|---|---|---|---|---|
| | gas | aniline | water | gas | aniline | water | gas | aniline | water |
| **$A_2$ + F + $AH^+$** | 0.0 | 0.0 | 0.0 | 0.0 | 0.0 | 0.0 | 0.0 | 0.0 | 0.0 |
| **IM0 + $AH^+$** | -29.2 | -15.2 | -11.7 | -30.0 | -15.2 | -11.7 | 17.2 | 26.3 | 31.3 |
| **TS1 + $AH^+$** | 60.7 | 48.0 | 32.4 | 52.4 | 40.2 | 24.6 | 121.7 | 106.3 | 92.5 |
| **IM1 + $AH^+$** | -58.7 | -57.4 | -60.5 | -64.0 | -61.9 | -65.6 | -6.2 | -10.1 | -8.3 |
| **IM1$H^+$ + A** | -118.1 | -75.9 | -75.9 | -123.3 | -80.3 | -81.0 | -68.6 | -26.4 | -23.8 |
| **TS2 + A** | -96.4 | -26.8 | -28.3 | -121.6 | -53.0 | -53.8 | 38.2 | 106.2 | 102.3 |
| **IM2$H^+$ + A** | -144.4 | -65.3 | -57.7 | -162.4 | -83.2 | -75.2 | -18.5 | 58.0 | 64.0 |
| **TS3 + A** | -103.2 | -26.4 | -15.7 | -124.4 | -46.3 | -35.1 | 30.9 | 104.1 | 114.2 |
| **IM3$H^+$ + A** | -111.8 | -60.4 | -59.1 | -132.9 | -80.5 | -79.6 | 23.8 | 70.0 | 72.7 |
| **TS4 + A** | -62.4 | 3.7 | 10.2 | -88.3 | -20.5 | -13.6 | 81.1 | 141.0 | 148.1 |
| **IM4$H^+$ + A** | -210.0 | -146.4 | -139.1 | -231.8 | -167.5 | -160.5 | -72.9 | -14.6 | -6.9 |
| **TS5 + A** | -106.0 | -40.5 | -32.3 | -125.0 | -57.7 | -49.9 | 21.0 | 79.9 | 87.8 |
| **IM5$H^+$ + A** | -111.1 | -43.6 | -34.4 | -127.3 | -58.9 | -49.3 | 15.1 | 72.3 | 83.0 |
| **TS6 + A** | -104.8 | -14.4 | -2.8 | -123.0 | -29.9 | -20.7 | 28.0 | 108.8 | 128.2 |
| **IM6$H^+$ + A** | -157.0 | -92.7 | -95.8 | -177.3 | -110.7 | -114.3 | -20.0 | 34.5 | 33.4 |
| **TS7 + A** | -108.4 | -38.5 | -37.8 | -132.3 | -60.5 | -60.1 | 35.7 | 98.4 | 101.2 |
| **IM7$H^+$ + A** | -124.6 | -66.7 | -84.5 | -147.3 | -88.1 | -106.3 | 17.0 | 69.0 | 53.1 |
| **4,4'-MDA + $H_3O^+$ + A** | 79.9 | -22.6 | -60.0 | 60.0 | -41.5 | -79.3 | 176.7 | 67.6 | 32.8 |

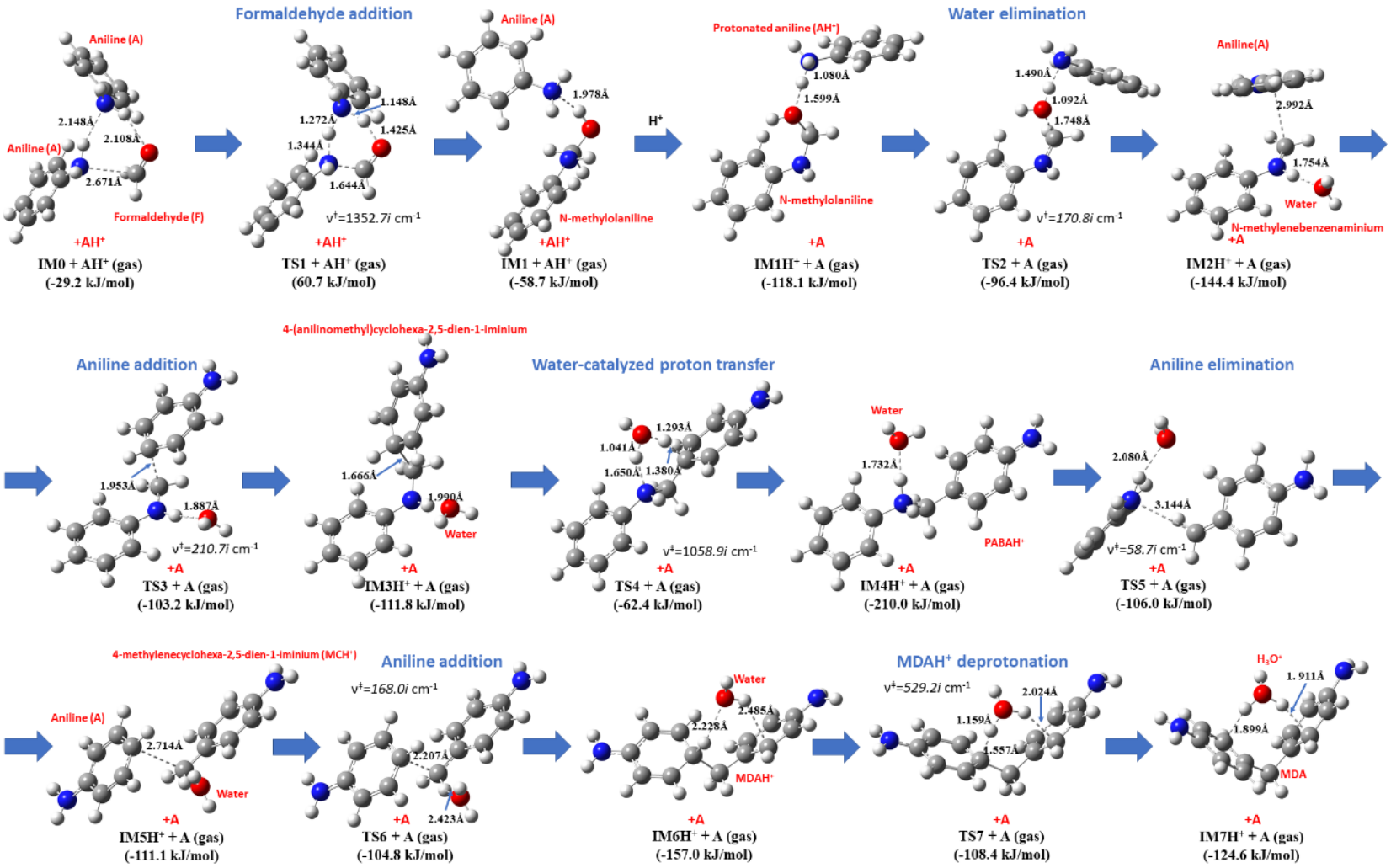


**Figure 14:** Transition state structures (obtained at B3LYP/6-31G(d) level of theory) for MDA synthesis in gas phase. The G3MP2B3 relative energies are also given.

Transition state of the water elimination (TS2) is structurally similar to the previous $IM1H^+$, although the O-H being formed become significantly shorter (rO-H = 1.092 Å), while the C-O bond expanded to 1.748 Å. TS2 is 21.7 kJ/mol higher than $IM1H^+$. The product of this exothermic reaction ($IM2H^+$) is a trimolecular complex (aniline-water and N-methylenebenzeneaminium) having -144.4 kJ/mol of relative energy) *(Table 7*). In this structure, the carbon of the aniline at para position is just 2.992 Å far from the methylene group of N-methylenebenzenaminium and the water oxygen is hydrogen bonded to the hydrogen atom of the secondary amine group. The critical C-C distance is 1.953 Å in the transition state structure of the aniline addition (TS3) and water is only slightly rotated around the elongated hydrogen bond (1.887 Å) (*Figure 14).* The activation energy of TS3 is 41.2 kJ/mol, while its relative energy become -103.2 kJ/mol. By linking these two aromatic ring structures, water complex of 4-(anilinomethyl)cyclohexa-2,5-dien-1-iminium is formed ($IM3H^+$) in a slightly endothermic reaction ($\Delta_r H°$ = 29.5 kJ/mol obtained from data in *Table 7*). Despite of the loss of aromatic nature of the aniline, the $IM3H^+$ structure is -111.8 kJ/mol lower than the reference energy. In the next step of the proposed mechanism, the water reoriented to initiate the transfer of the positive charge to the amine nitrogen in such a way that the second aromatic ring can also be formed (TS4). This six-centered transition state with the activation energy of 49.4 kJ/mol resulted in the product (noted as $IM4H^+$) with the lowest relative energy ($\Delta E_0(IM4H^+)$ = -210.0 kJ/mol) structures in the entire mechanism, the hydrogen bonded complex of the N-(p-aminobenzyl)anilinium ($PABAH^+$) and water. Due to the proton of the amine, $PABAH^+$ is activated to dissociate to aniline (A) and 4-methylidenecyclohexa-2,5-diene-1-iminium ($MCH^+$) noted as $IM5H^+$ via C-C bond scission (TS5). The activation energy of this reaction step is 104.0 kJ/mol. To make rearrangement of the released aniline happen, the formed $PABAH^+$ should be chemically activated and stabilization of $PABAH^+$ should be avoided (e.g. through deprotonation of $PABAH^+$). Firstly, we considered the aniline addition occurs at para position to the $MCH^+$ to form protonated 4,4'-methylenedianiline (4,4'-$MDAH^+$) noted as $IM6H^+$. After the formation of the loosely bounded complex of $MCH^+$ and aniline ($IM5H^+$), these two species can form TS6 structure in which C-C bonds being formed is 2.207 Å. Only small rotational motion of the water molecule contributes to the reaction coordinate ($\nu‡ = 168.0i\ cm^{-1}$) in this case. The energy level of TS6 is -104.8 kJ/mol compared to the entrance level.

In $IM6H^+$, water binds to the $MDAH^+$ by hydrogen bond and interaction occurs of its other hydrogen and the aromatic ring. This structure shows similarity for the deprotonation transition state, that is TS7, in which the distance of C-H being broken is significantly elongated (1.557 Å) and the critical distance of H-O bond is short (1.159 Å). Moving along the reaction coordinate the water molecule reoriented again and its one of the alone pairs is now pointed toward the extra proton of $IM6H^+$ making the post-reaction complex, $IM7H^+$ after a slight reorientation of the $H_3O^+$ cation. This structural change resulted in an energy decrease by 16.2 kJ/mol ($\Delta E_0(IM7H^+)$ = -124.6 kJ/mol). The relative energy of last three transition states is also energetically close to each other ($\Delta E_0$(TS5) = -106.0 kJ/mol, $\Delta E_0$(TS6) = -104.8 kJ/mol and $\Delta E_0$(TS7) = -108.4 kJ/mol). Finally, the post-reaction complex converted into the final product that is the 4,4'-MDA ($\Delta E_0$(4,4'-MDA) = 79.9 kJ/mol) which has the highest relative energy considering the whole reaction coordinate in gas phase. This mechanism shows high similarity to the mechanism found in Kirk-Othmer Encyclopedia of Chemical Technology[17], but three new intermediate elementary steps have also been identified (formation of $IM3H^+$, $IM4H^+$ and $IM6H^+$). Amongst these new species, $IM4H^+$ differs only in the protonation state from the suggested PABA intermediate in Ref.[17]. On the other hand, the one step formation of aminal (AM) suggested by Wang[30] is unlikely, since the corresponding hypothetical transition state would be crowdy around the methylene carbon, therefore reaction of N-methylenebenzeneaminium and aniline is considered as a formation of protonated aminal ($AMH^+$) instead (for its detailed discussion see Important side reactions section). Before the solvent effect is discussed the gas phase thermochemistry of the species playing role is evaluated.

#### *3.1.1.1* Gas phase thermodynamic properties of reactants, intermediates and products

As shown in *Table 8*, the calculated standard enthalpies of formation for aniline, 4,4' MDA and all intermediates are endothermic, while the formation of formaldehyde (-111.5 kJ/mol) and N-hydroxymethylaniline (-71.8 kJ/mol) are exothermic. Highly accurate standard enthalpy of formation ($\Delta_{f,298.15K}H_0$) value is only reported for aniline and formaldehyde in the literature[100,101]. The largest error for their G3MP2B3 computation is 2.3 kJ/mol, which is significantly smaller than those for CBS-QB3, therefore only the G3MP2B3 results are discussed latter. While the G3MP2B3 value for 4,4'-MDA (171.2 kJ/mol) is also consistent with the estimated values based on group

additivity rules by Benson[30] and Benson and Stein[111,107] and (165.6 kJ/mol and 172.0 kJ/mol, respectively), only CBS-QB3 estimates more endothermic enthalpy of formation for 4,4'-MDA. Interestingly, ortho and meta isomers of MDA (2,4-MDA, 2',4-MDA and 3,4-MDA) have less endothermic formation than 4,4'-MDA, while among their protonated forms 2,4-MDA and 4,4'-MDA found to be less endothermic. For these species, only modest difference in molar entropy had been found.

**Table 8**: Gas phase thermochemical properties for reactants, products and all the intermediates MDA synthesis as well as MDA and $MDAH^+$ isomers. Standard enthalpy of formation ($\Delta_{f,298.15K}H°(g)$) is calculated from G3MP2B3 and CBS-QB3 enthalpies by means of atomization scheme (AS) at 1 atm pressure at 298.15 K. Absolute deviation is given in parenthesis.

| Species | $\Delta_{f,298.15K}H°$ (g) | Method | Ref. | $S_0$(g) | $C_v$(g) | Ref. |
|---|---|---|---|---|---|---|
| | kJ/mol | | | J/molK | J/molK | |
| **aniline (A)** | 86.5 (0.5) | AS(G3MP2B3) | 112 | 319.0 | 96.6 | 112 |
| | 96.0 (9.0) | AS(CBS-QB3) | 1 | 317.3 | 97.4 | |
| | 87.0±0.88 | Burcat | 101 | 311.6 | 104.5 | 101 |
| **non-covalent aniline dimer ($A_2$)** | 156.2 | AS(G3MP2B3) | 311.7 | 529.6 | 214.3 | 112 |
| **formaldehyde (F)** | -111.5 (2.3) | AS(G3MP2B3) | 112 | 224.4 | 26.8 | 112 |
| | -113.3 (4.1) | AS(CBS-QB3) | 112 | 224.3 | 26.8 | |
| | -109.2±0.11 | Ruscic ATcT | 100 | 218.8 | 35.4 | 113 |
| **4,4'-MDA** | 171.2 | AS(G3MP2B3) | 33 | 500.1 | 221.4 | 112 |
| | 191.5 | AS(CBS-QB3) | | 503.6 | 223.3 | |
| | 165.6 | additivity rule | 40 | 522.7 | n.d. | 40 |
| | 172 | additivity rule[114, 113] | NIST 113,115 | 511.6 | 234.7 | 115 |
| **2,4-MDA** | 159.4 | AS(G3MP2B3) | 112 | 490.4 | 220.6 | 112 |
| **2',4-MDA** | 168 | AS(G3MP2B3) | 112 | 484.0 | 219.8 | 112 |
| **3,4-MDA** | 168.3 | AS(G3MP2B3) | 112 | 499.4 | 221.3 | 112 |
| **PABA** | 202.4 | AS(G3MP2B3) | 112 | 496.3 | 216.5 | 112 |
| | 201.3 | additivity rule | | 514.4 | n.d. | |
| **N-hydroxymethylaniline** | -71.8 | AS(G3MP2B3) | 112 | 379.3 | 129.3 | 112 |
| **$AH^+$** | 739.4 | AS(G3MP2B3) | 112 | 339.9 | 97.2 | 112 |
| **N-methylenebenzeneaminium** | 828.6 | AS(G3MP2B3) | 112 | 346.2 | 107.9 | 112 |
| **4-(anilinomethyl)cyclo-hexa-2,5-dien-1-iminium** | 858.5 | AS(G3MP2B3) | 112 | 491.2 | 220.0 | 112 |
| **$PABAH^+$** | 785.1 | AS(G3MP2B3) | 112 | 501.2 | 219.4 | 112 |
| **$MCH^+$** | 802.8 | AS(G3MP2B3) | 112 | 340.9 | 113.7 | 112 |
| **4,4'-$MDAH^+$** | 814.3 | AS(G3MP2B3) | 112 | 494.8 | 225.1 | 112 |
| **2,4-$MDAH^+$** | 812.2 | AS(G3MP2B3) | 112 | 494.7 | 226.4 | 112 |
| **2',4-$MDAH^+$** | 830.9 | AS(G3MP2B3) | 112 | 487.1 | 224.4 | 112 |
| **3,4-$MDAH^+$** | 858.6 | AS(G3MP2B3) | 112 | 534.2 | 236.5 | 112 |

Furthermore, G3MP2B3 and the group additivity values are also consistent with each other in the case of PABA. To the best of our knowledge, no literature $\Delta_{f,298.15K}H_0$ was found for other intermediates presented here *(Table 8).* The computed standard molar entropy (S°(g)) and molar heat capacity (CV(g)) values are also tabulated in *Table 8*, and their deviation from accurate literature values[101,116] less than 8.6 J/molK, while larger deviation is observed from the results obtained form group additivity (22.6 J/molK for 4,4'-MDA) which is probably due to missing correction terms in the group additivity.

### *3.1.2 Solvent effect*

Based on the industrial synthesis of MDA - via the reaction of formalin, aniline using HCl solution as catalyst - two possible solvent effect is considerable: aniline and water. It is unclear in which phase the reaction occurs. The presence of solvents (aniline and water) changes significantly energy profile of the reaction as shown in *Figure 12*, the solvent effect is very similar regardless which solvent is considered. The most dramatic change is the stabilization of the final product (see 4,4'-MDA+$H_3O^+$+A in *Table 7*) by 102.5 kJ/mol for aniline solution and by 139.9 kJ/mol for aqueous solution which is mainly due to the solvation energy difference between protonated aniline ($AH^+$) and oxonium cation ($H_3O^+$). The highest lying barrier in gas phase, that is TS1, is also decreased due to solvation by 12.7 kJ/mol (in aniline) and 28.3 kJ/mol (in water). While its pre-reaction (IM0+$AH^+$) and post-reaction (IM1+$AH^+$) complexes are destabilized slightly (14.0 kJ/mol and 1.3 kJ/mol in aniline, respectively), large destabilization effect can be observed for the intermediates and transition states after the protonation of IM1 intermediates (IMx and TSx, where 2≤x), its magnitude is in the range of 42.2-90.5 kJ/mol for the aniline solution, while it is 40.1-102.1 kJ/mol for the aqueous solution (about 60 kJ/mol in average). The largest increase in relative energy belongs to the transition state of the second aniline addition (TS6) for both solutions, this energy shift was 90.5 kJ/mol and 102.1 kJ/mol for aniline and for aqueous solution, respectively. Similarly, the transition state for first aniline addition (TS3) and its pre-complex (IM2$H^+$) are also significantly destabilized by solvation compared to the other TSs and intermediates (in the range of 76.8-87.5 kJ/mol).

As *Table 6* shows, relative enthalpies ($\Delta H°$) present same trend as $\Delta E_0$, $\Delta H°$ values tend to be larger, but not more than 26.6 kJ/mol. Most of the cases, difference in relative enthalpies ($\Delta\Delta H°_{an\rightarrow aq}$) by comparing aniline to aqueous phase is less than 9.2 kJ/mol.

Larger difference in $\Delta H°$ values found in those cases, where large solvation effect for $\Delta E_0$ had already been observed, such as TS1, TS3, TS6, $IM7H^+$ and 4,4'-MDA.

The calculated $\Delta H°$ results are:

- $\Delta\Delta H°_{an\rightarrow aq}$(TS1) = -15.6 kJ/mol, $\Delta\Delta H°_{an\rightarrow aq}$(TS3) = 10.7 kJ/mol,
- $\Delta\Delta H°_{an\rightarrow aq}$(TS6) = 11.6 kJ/mol, $\Delta\Delta H°_{an\rightarrow aq}(IM7H^+)$ = -17.8 kJ/mol
- $\Delta\Delta H°_{an\rightarrow aq}$(4,4'-MDA) = -37.3 kJ/mol).

Analysis of the relative Gibbs free energies (ΔG°) in *Table 7* shows also that solvation Gibbs free energies ($\Delta G_{solv}°$) and $\Delta E_{0,solv}$ are in linear relationship for both surrounding media.

### *3.1.2.1 Proton dissociation constants ($pK_a$) of intermediates*

The species in proposed mechanism are proton activated, their possible deprotonation can lead to side reactions and appearance of deactivated intermediates in the industrial process. Therefore, the affinity of these compounds for deprotonation is important and it can be described by site-specific acid dissociation constant (p*K*a)[117,118]. Ghalami-Choobar[119] et al. performed calculation for aqueous $pK_b$ values of aniline and its substituted derivatives with good accuracy. Behjatmanesh-Ardakani[120] and Lu[121] also reported calculated $pK_a$ for some aniline derivatives.

The acid dissociation constant ($pK_{a,aq}$) in aqueous solution of the intermediates were also derived from G3MP2B3 calculations. The $pK_{a,aq}$ values can be calculated using Gibbs free energy of the gas phase species in neutral and cationic form (noted as $G(A_g)$ and $G(AH^+_g)$, respectively) which corrected by the solvation Gibbs free energies ($\Delta G_{solv}$) of the species involved[122]:

$$pK_{a,aq}=[G(A_g)-G(AH^+_g)+\Delta G_{solv}(A)-\Delta G_{solv}(AH^+)+G_{gas}(H^+)+G_{solv}(H^+)+RT\ln(V_m)]/RT\ln 10$$

where gas phase Gibbs free energy for proton $G_{gas}(H^+)$ comes from Sackur-Tetrode equation (26.3 kJ/mol[122]) and solvation Gibbs free energy for proton, $\Delta G_{solv}(H^+)$, is -1107.1 kJ/mol[123] Molar volume ($V_m$) at reference state is 24.46 $dm^3$. Although, such direct $pK_a$ calculation *via* thermodynamics cycle usually suffers from larger error, therefore proton exchange scheme was applied to improve the accuracy of a $pK_a$ calculation ($pK_a$ of anilinium, $AH^+$, used as reference).

Although, direct $pK_a$ calculation via thermodynamics cycle usually suffers from larger error than the relative method. In this study, the G3MP2B3-SMD based absolute $pK_a$ value of anilinium ($AH^+$) was found to be 2.86 in aqueous phase using the direct $pK_a$ estimation

which is smaller by 1.74 p$K_a$ units than the reference value (p$K_{a,aq}$=4.60 in Ref.[120], so we have used the anilinium half-reaction as reference for the relative p$K_a$ calculation shown in *Table 9.* N-methylenebenzeneanilium, N-(p-aminobenzyl)anilinium and PABAH$^+$ have similar p$K_a$ values which corresponds to weak acid and they can lose their potential to turn into MDA by deprotonation, while acid strength of MCH$^+$ is far less therefore it likes to be protonated.

**Table 9**: Protonation dissociation constants (p$K_{a,aq}$) for the protonated intermediates in aqueous solution. The dissociative proton presented in red.

| **Species** | | **p$K_{a,aq}$** | **p$K_{a,aq}$** |
|---|---|---|---|
| **AH$^+$** | | 4.6[1] | 4.60 [120] |
| **N-methylenebenzeneanilium** | 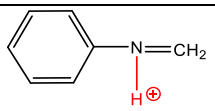 N-methylenebenzeneaminium | 4.2 | |
| **PABAH$^+$** | 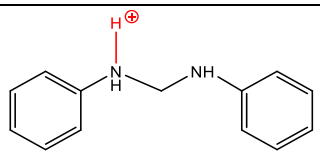 protonated N,N'-diphenylmethylenediamine | 6.7 | |
| **MCH$^+$** | 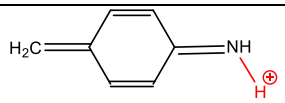 4-methylidenecyclohexa-2,5-diene-1-iminium | 11.4 | |
| **AMH$^+$** | 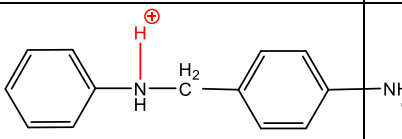 N-(p-aminobenzyl)anilinium | 5.1 | |

[1] used as reference

### *3.1.3 Important side reactions*

Alternative aniline addition reactions can also be proposed. One of these side reactions can be the protonated aminal formation (see AMH$^+$ in *Figure 13*), which is essentially an alternative to the formation of IM3H$^+$ from aniline to the N-methylenebenzeneaminium ('the first' aniline addition). However, the aniline addition occurs through the amine group instead of the aromatic carbon at para position. Interestingly, loose transition state had been found for this reaction in both condensed media, which was also proven by scan of the potential energy surface via the C-N bond stretching of the protonated aminal at B3LYP/6-31G(d) level of theory. The B3LYP curve was also reproduced by BHandHLYP and MP2 methods. In contrast, the formation of ortho adduct (o-aminobenzylaniline,

OABAH$^+$) undergoes tight submerged transition state ($\Delta^{\ddagger}E_0$ = -9.4 kJ/mol in aniline phase, $\Delta^{\ddagger}E_0$ = -5.0 kJ/mol in aqueous phase).

**Table 10**: Thermochemical properties for some side reactions of the formation of 4,4'-MDAH$^+$.

| **Reaction** | **Aminal formation** | | | **IM3H$^+$ formation** | | |
|---|---|---|---|---|---|---|
| | **gas** | **aniline** | **water** | **gas** | **aniline** | **water** |
| **$\Delta_r E_0$(kJ/mol)** | -90.7 | -75.2 | -77.2 | 32.7 | 4.9 | -1.4 |
| **$\Delta_r H°$(kJ/mol)** | -92.2 | -76.6 | -78.8 | 29.6 | 2.7 | -4.4 |
| **$\Delta_r G°$(kJ/mol)** | -41.1 | -26.5 | -28.6 | 42.2 | 12.0 | 8.7 |

As seen from *Table 10,* aminal (AMH$^+$) formation reaction is exothermic, but it has only moderate exergonicity in each media studied in contrast to the competitive reaction step, IM3H$^+$ formation. However, the thermochemical and kinetic favor of formation of AMH$^+$ over IM3H$^+$ is obvious, AMH$^+$ is without relevant new exit channel. Similarly, formation of OABAH$^+$ is more exothermic than that of IM3H$^+$, although it is more endergonic by 32.0 kJ/mol than in the case of IM3H$^+$.

Beside the formation of 4,4'-MDAH$^+$, the aniline addition to MCH$^+$ can also result in the formation of ortho and meta MDAH$^+$ isomers (2,4-MDAH$^+$, 2',4-MDAH$^+$ and 3,4-MDAH$^+$). The thermodynamic properties of these competitive reactions are collected in *Table 11*.

**Table 11**: Energetic description for aniline addition to 4-methylidene-cyclohexa-2,5-diene-1-iminium (MCH$^+$) reactions.

| **Reaction** | **$\Delta_r E_0$(kJ/mol)** | | **$\Delta^{\ddagger}E_0$(kJ/mol)** | |
|---|---|---|---|---|
| | **water** | **aniline** | **water** | **aniline** |
| **IM5H$^+$ + A → TS6 → IM6H$^+$ + A[1]** | -49.2 | -61.4 | 29.2 | 31.6 |
| **A+MCH$^+$ → TS6 → 4,4'-MDAH$^+$** | -62.2 | -64.4 | 17.8 | 22.5 |
| **A+MCH$^+$ → TS6* → 2,4 MDAH$^+$** | -45.1 | -49.0 | 15.5 | 18.9 |
| **A+MCH$^+$ → TS6* → 2',4-MDAH$^+$** | -52.7 | -53.6 | -1.9 | 2.3 |
| **A+MCH$^+$ → TS6* → 3,4-MDAH$^+$** | 48.4 | 45.2 | 54.8 | 57.4 |

[1] IM5H$^+$ represents complex of MCH$^+$, A and water while IM6H$^+$ stands for water complex of 4,4'-MDAH$^+$ (see *Figure 13*).

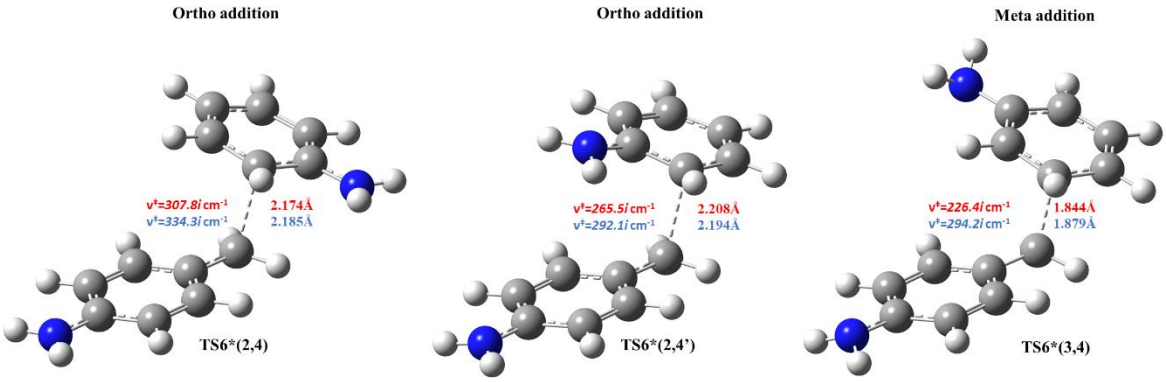


**Figure 15**: Transition state structures (obtained at B3LYP/6-31G(d) level of theory) for 4,4'-MDA isomer formation (critical distance are also given for both condensed phases).

Based on these results, significant amount of 2,4-MDA should be formed as a product of the title reaction which is in clear contradiction with laboratorial observations (more than 92 m/m% of the product is 4,4'-MDA while 7 m/m% is 2',4-MDA. This discrepany might be caused by incomplete quantum chemical description of the solvent effect and/or neglecting the role of the counter ion in the mechanism. On the other hand, 33.5 m/m% of the product is oligomeric and polymeric MDA[124]. Another hypothesis might be that the 2',4-MDA is more reactive towards aniline addition making oligomeric structures (e.g. 3-ring) overrepresented in these forms. To bear in mind that the above mentioned experiments are on the several minutes time scale, that makes reactive interferences between the intermediates and products possible (the w% of 4,4'-MDA became saturated at 20% after ca. 40 min in Knjasev experiment at T = 70°C, where the initial molar ratio of the mixture was A:F:HCl:$H_2O$=4:2:1:13[124]). An example for such interference is the highly preferred addition of the N-methylenebenzeneaminium (the '3-ring' structure) in the para position which is also supported by the $^{2}H$- and $^{13}C$-NMR-based observation by Knjasev[124]. This step can be followed by proton transfer which might make the dissociation of the adduct favorable to $MCH^{+}$ and PABA as it shown in *Figure 16*.

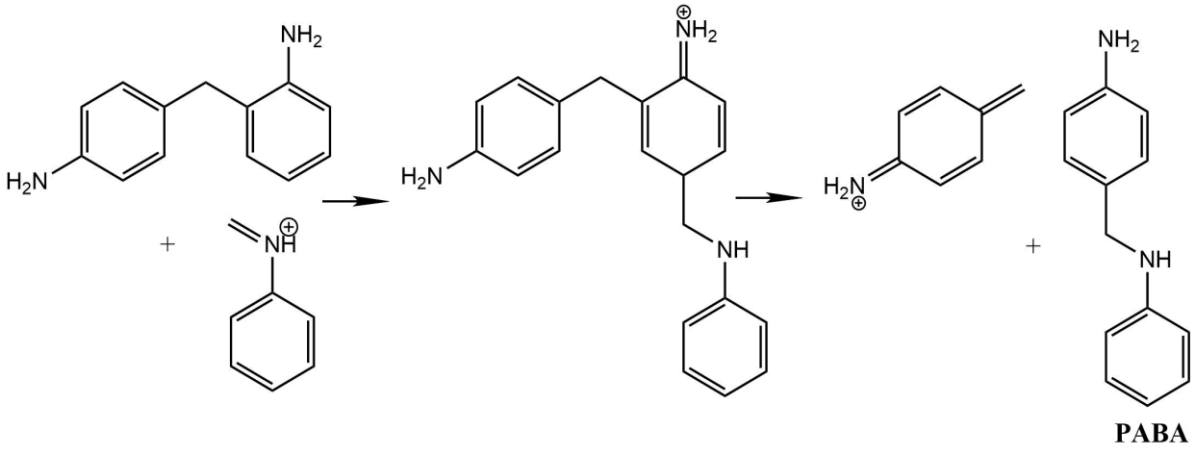


**Figure 16:** Schematic reaction mechanism of the formation of the 3-ring adduct and its dissociation to N-methylenebenzeneaminium and PABA.

### *3.1.4 Conclusions*

The detailed reaction mechanism of the current industrial MDA production was explored and characterized thermodynamically using G3MP2B3 quantum chemical calculations including solvent effect. Most important findings for this reaction mechanism are:

- Mechanism of MDA synthesis consists of eight elementary reaction steps including condensation and rearrangement steps. In the initial reaction step, a non-covalent aniline dimer is reacted with formaldehyde. This hypothetical aniline dimer is based on experimental observation (e.g. high viscosity of aniline, scattering experiments).
- The highest lying transition state (60.7 kJ/mol) corresponds to formaldehyde addition to aniline (TS1) leading to N-hydroxymethylaniline formation. After exothermic water elimination, aniline addition to N-methylenebenzenaminium took place through either tight transition state (resulted in 4-methylidenecyclohexa-2,5-diene-1-iminium, $MCH^+$).
- Afterwards, proton shift can undergo in 4-methylidenecyclohexa-2,5-diene-1-iminium to produce N-(p-aminobenzyl)anilinium (protonated PABA, $PABAH^+$), being the global minimum at this reactive potential energy surface, which can be also along with the line with experimental observation of PABA during MDA production. Two steps rearrangement of aniline resulted the protonated MDA isomers ($MDAH^+$).

- Gas phase thermodynamic properties for the reactants, products and intermediates were determined, accurate standard enthalpy of formation is recommended for the intermediates.
- The significant solvent effect (water and aniline) on the energetics of MDA mechanism was found. It lowers the highest lying transition state which belongs to formaldehyde addition by 12.7 kJ/mol.
- One of the important side reactions, that is the aminal formation ($AMH^+$), is both thermodynamically and kinetically preferable than the formation of $PABAH^+$, but $AMH^+$ is a kinetic dead-end in the same time.
- The species in proposed mechanism are proton activated and the acid strength ($pK_a$) of four important weak acid intermediates such as N-methylenebenzeneanilium (4.2), $PABAH^+$ (6.7), $MCH^+$ (11.4) and $AMH^+$ (5.1) had been calculated. They got more acidic in aniline (basic) environment which can then deactivate the intermediates.
- Aniline addition in ortho position (formation of 2,4'-MDA) is competitive with that of in the para position (formation of 4,4'-MDA) from both kinetic and thermodynamic points of view. The preference of the formation of 4,4'-MDA can be hypothesized over MDA oligomer formation as intermediate.

### *3.1.5 Experimental studies*

The computational results demonstrated the complexity of the whole MDA synthesis including eight reaction steps. The possible side reactions and by-products were explored. Above the calculations, MDA synthesis was carried out in the laboratory. The target was to identify the MDA composition during the synthesis and in the final product. The purpose of the laboratory experiments was to get more information about the MDA synthesis. The experiences are summarized in this chapter.

*MDA synthesis in the laboratory*

Based on the required molar ratio of hydrochloric-acid/aniline (HCl/A=0.33) the appropriate amount of aniline (99.9 g) of room temperature was measured into a glass reactor (*Figure 17*). The nitrogen stream was opened until the end of the synthesis. Afterwards, the hydrochloric-acid solution (32.1 m/m%, 40.30 g) was added continuously to the aniline and the temperature was set up to 60°C. The mixture was light brown color (*Figure 18*, *step (a)).* Then the formalin (aniline/formalin=2.3, 37 m/m%, 35.2 ml) was

introduced continuously to the system within about 60 min by an automatic feeder with 0.587 ml/min flow rate. The reaction mixture became lighter and turbid (*Figure 18, step (b)*). After the formalin fed the temperature was adjusted to 93°C. The reaction mixture was stirred for 90 min. Subsequently, the NaOH solution (49 m/m%, 37.61 g) was added to the reaction mixture within 10 minutes. The solution was stirred for 15 minutes and then the compound was left for 3 minutes. The organic and aqueous phases were separated *(Figure 18, step (c)*). The product MDA is in the organic phase. During the MDA synthesis samples were taken after the condensation step and in the rearrangement step. The composition of the examined samples is summarized *Table 12*.

The qualitative analysis of the samples including the isomer distribution were carried out by gas chromatography (column: Zebron 5HT 30m/250μm/0.1μm, maximum temperature: 415°C, FID detector) while the ring distribution was performed by gel permeation chromatography (PLgel, pore size: 100 Å, particle size: 3.0 μm, refractive index detector, 40°C).

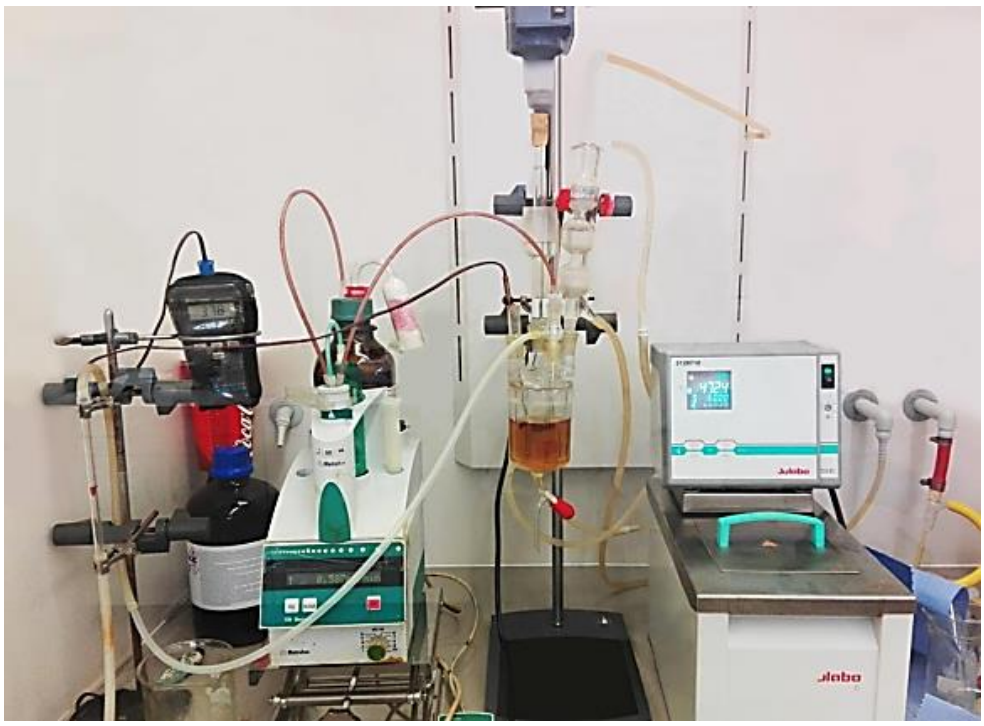

**Figure 17**: Laboratory equipment used for MDA synthesis.

*Step (a) - condensation* *Step (b) - rearangement* *Step (c) - neutralization*

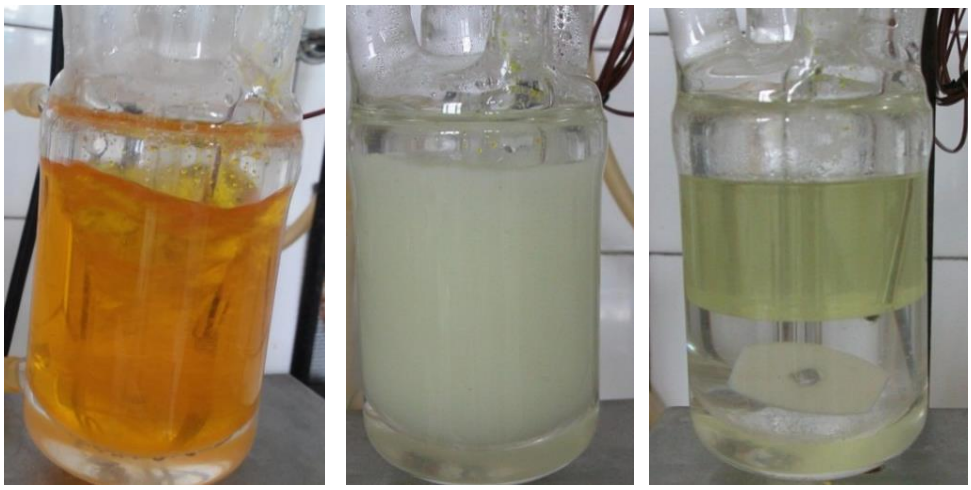

**Figure 18**: Different steps of MDA synthesis.

**Table 12**: Change of ring distribution during the MDA synthesis.

| HCl/aniline: 0.33<br>Aniline/formalin: 2.30 | After the condensation step | During the rearrangement step | | | | | Product |
|---|---|---|---|---|---|---|---|
| Temperature | 60°C | 90°C | | | | | |
| Composition | [m/m%] | [%] | [%] | [%] | [%] | [%] | [%] |
| Time (min) | **0** | **15** | **30** | **45** | **60** | **90** | **120** |
| **2-rings** | 39.6 | 62.2 | 65.2 | 65.7 | 66.8 | 67.2 | 67.4 |
| **3-rings** | 26.4 | 20.1 | 19.9 | 20.5 | 21.3 | 20.6 | 21.1 |
| **4-rings** | 15.5 | 10.2 | 9.1 | 8.6 | 7.7 | 7.8 | 7.5 |
| **5-rings** | 8.8 | 4.3 | 3.6 | 3.3 | 2.8 | 2.9 | 2.7 |
| **>5-rings** | 9.6 | 3.1 | 2.1 | 1.9 | 1.4 | 1.4 | 1.2 |

Considering the ring distribution, it was found that 39.6 m/m% of the 2-ring content was produced after the condensation step and nearly all of them (62.3 m/m%) was developed after 15 minutes. Almost 33 m/m% of the product MDA is oligomeric MDA containing three or more rings conforming the literature data[124]. Based on the results the formation of the 2-ring content is increasing while the number of the >2-ring content is decreasing during the reaction time. It can be assumed that the more membered-ring compounds are

decomposed into molecules of 2-ring. The ring distribution of the MDA product can be modified by changing the molar ratio of the reagents *as shown in Figure 19*. The number of the 2-membered ring MDA is increasing by adding more aniline to the formaldehyde. As lower the amount of the aniline is the less 2-membered ring can be formed. For the MDA formation at least 2:1 aniline formaldehyde molar ratio is necessary for the reaction. If the aniline content is higher it is supposed that the number of the non-covalent aniline-dimer molecules is also higher. The possibility of the interactions between aniline molecules and the intermediate N-methylenebenzeneanilium forming more 2-membered ring MDA is higher.

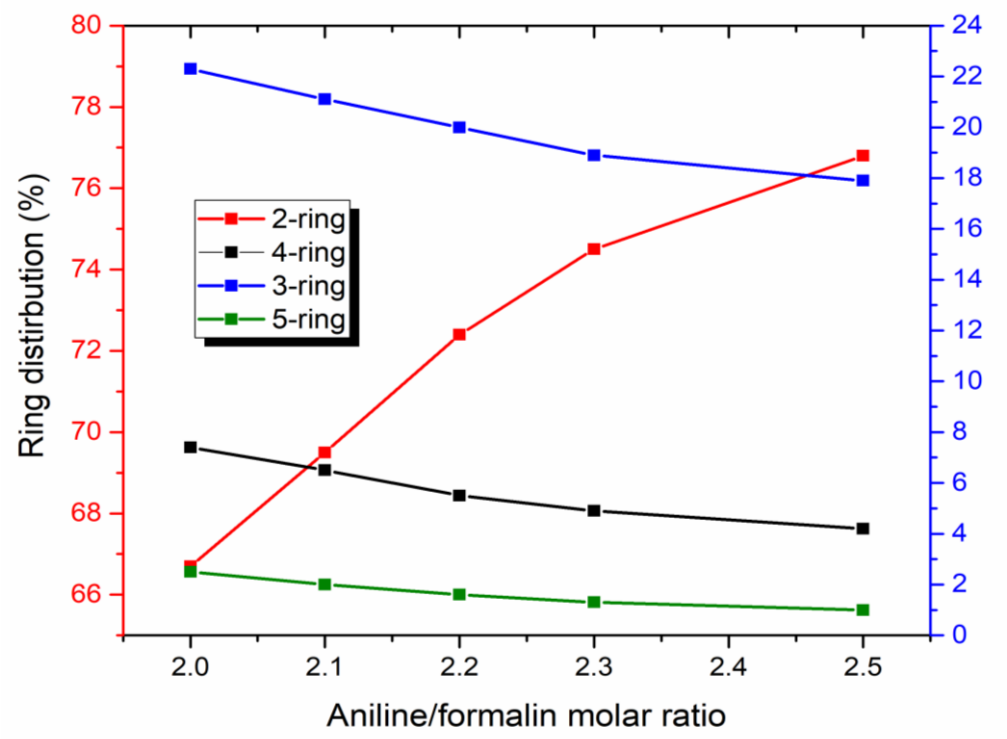


**Figure 19**: Ring distribution in the function of aniline/formalin molar ratio.

The isomer distribution of the 2-membered ring MDA is summarized in *Table 13*. The highest amount of MDA isomer was observed to be the 4,4'-MDA (67.4%) while the least was formed from the 2,2'-MDA.

**Table 13**: Isomer distribution of 2-membered ring MDA and the amount of PABA, oABA intermediates

| HCl/aniline: 0.33; Aniline/formalin: 2.30 | After the condensation step | During the rearrangement step | | | | | Product |
|---|---|---|---|---|---|---|---|
| Temperature | 60°C | 90°C | | | | | |
| Composition | [m/m%] | [%] | [%] | [%] | [%] | [%] | [%] |
| Time (min) | 0 | 15 | 30 | 45 | 60 | 90 | 120 |
| **4,4'- MDA** | **39.6** | **62.2** | **65.2** | **65.7** | **66.8** | **67.2** | **67.4** |
| **2,4- MDA** | **26.4** | **20.1** | **19.9** | **20.5** | **21.3** | **20.6** | **21.1** |
| **2,2'-MDA** | **15.5** | **10.2** | **9.1** | **8.6** | **7.7** | **7.8** | **7.5** |
| PABA | 40.4 | 1.1 | 0.2 | 0.1 | 0.1 | 0.0 | 0.0 |
| o-ABA | 8.8 | 4.3 | 3.6 | 3.3 | 2.8 | 2.9 | 2.7 |

Comparing the charge distribution between the monomer aniline and non-covalent aniline dimer (*Figure 20)* it was found that they slightly differ. The charge of carbon atoms in the para and ortho positions became more negative in the case of the non-covalent aniline dimer compared with the aniline monomer facilitating the electrophile addition of the $MCH^+$ cation into the para and ortho position producing 4,4'-MDA and 2,4-MDA. The formation of the MDA isomers with the assist of aniline dimer is more favourable increasing the possibility of our assumed reaction mechanism.

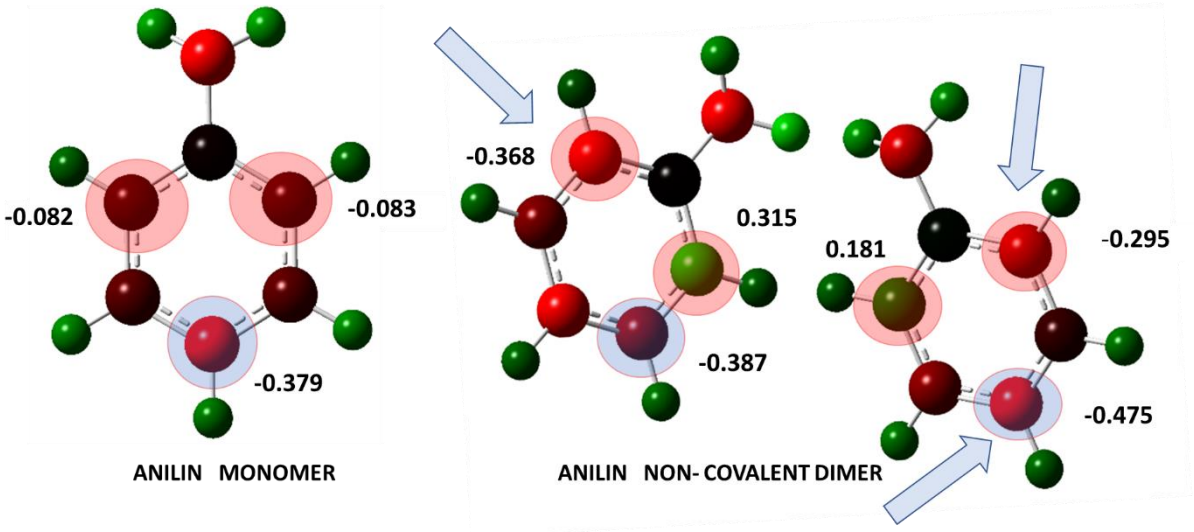


**Figure 20**: Charge distribution of monomer aniline and non-covalent aniline dimer.

Evaluating the experimental results, it can be seen that after the formalin had been added to the aniline within the first 15 minutes (at the end of the condensation and in the beginning of the rearrangement) an equilibrium state exists. The composition of the MDA became almost stable. Particularly, more than half of the 4,4'-MDA (51.3 m/m%) has been formed even after the condensation step (0 min), while the other significant compound was found to be the PABA intermediate (40.4 m/m%). The amount of the oABA was relatively small (<10m/m%). Within 15 minutes the intermediate PABA was almost totally converted into the product MDA (91.5m/m%) after a dissociation and recombination process.

*Experiences and main consequences*

Regarding the whole reaction pathway, it was found that the composition of the final product is highly determined in the first 15 minutes. The quality of the MDA can be mostly influenced after the condensation step in the first part of the rearrangement process. The main intermediates were found to be the amino-benzyl-aniline compounds (o-ABA, PABA). The isomer- and ring distribution was only slightly changed from the first 15 minutes.

The assumed reaction mechanism of the MDA synthesis is in correlation with the experimental results. The most probably supposed intermediate, the PABA (and oABA), were identified. According to the analytical data it was confirmed that the reaction run is divided into two main steps: condensation and rearrangement step as assumed in our mechanism. In the whole reaction mechanism of MDA synthesis, the 2-ring MDA components are dominant. The focus of our assumed reaction mechanism is also the 2-ring MDA formation.

## 3.2 Reaction mechanism of MDA phosgenation

The aim of this section is to study the reaction mechanism of the phosgenation of MDA, the second step of MDI production, using accurate quantum chemical calculations. The gas phase thermodynamic profiles of the possible main reaction pathways leading to the formation of the MDI are compared to those obtained in ODCB. The temperature and pressure effects on the thermodynamic profiles are also discussed together with the interference of the products formed in the case of the incorporation of phosgene into MDA. Additionally, the calculated thermodynamic properties of the important species

along the reaction coordinates are compared to the established literature values. The achieved results are introduced below.

### *3.2.1 Reaction mechanisms in gas phase*

Two reaction mechanism of MDA phosgenation were investigated. As it was mentioned in the introduction (*1.3 Section*) the basic differences between the mechanisms are the followings: 'Phosgenations first': both amino groups transformed to carbamoyl chloride groups giving [methylenebis(4,1-phenylene)]dicarbamic chloride and then two endothermic HCl-elimination steps occurs. 'Stepwise phosgenations': One of the amino groups of MDA turns into isocyanate by phosgene and then the other amine does. For easier overview *Figure 4* is shown in this chapter again representing the phosgenation mechanisms.

G3MP2B3 calculations were used to investigate the mechanism of the phosgenation reactions of 4,4'-MDA resulted in the formation of MDI, such as in the case of the MDA formation. The reactions were firstly examined in gas phase. The mechanisms of the 'phosgenation first' and 'stepwise phosgenations' are energetically compared. The results of the calculations are represented in *Figure 22*. The first gas phase elementary step of MDA phosgenation is the reactive complex formation (RC1) in which phosgene molecule approached the amine group of MDA. The zero-point corrected relative energy ($\Delta E_0$) of this species is -20.7 kJ/mol. The consecutive reaction step occurs via four-centered transition state (TS1 in Figure *23*) with high relative energy ($\Delta E_0$ (TS1) = 44.9 kJ/mol shown in *Figure 22*) resulted in formation of 4-[(4-aminobenzyl) phenyl] carbamate-chloride (IM1) and release of HCl ($\Delta E_0$ = -84.4 kJ/mol). TS1 structure manifested in the synchronous formation of the C-N and H-Cl bonds (with the critical distances of rC-N=1.522 Å and rH-Cl=2.042 Å), while one of the C-Cl bonds extremely elongated (rC-Cl=2.624 Å). Incorporation of the first phosgene molecule into MDA is highly exothermic ($\Delta H_0$ = -81.2 kJ/mol tabulated in *Table 14*).

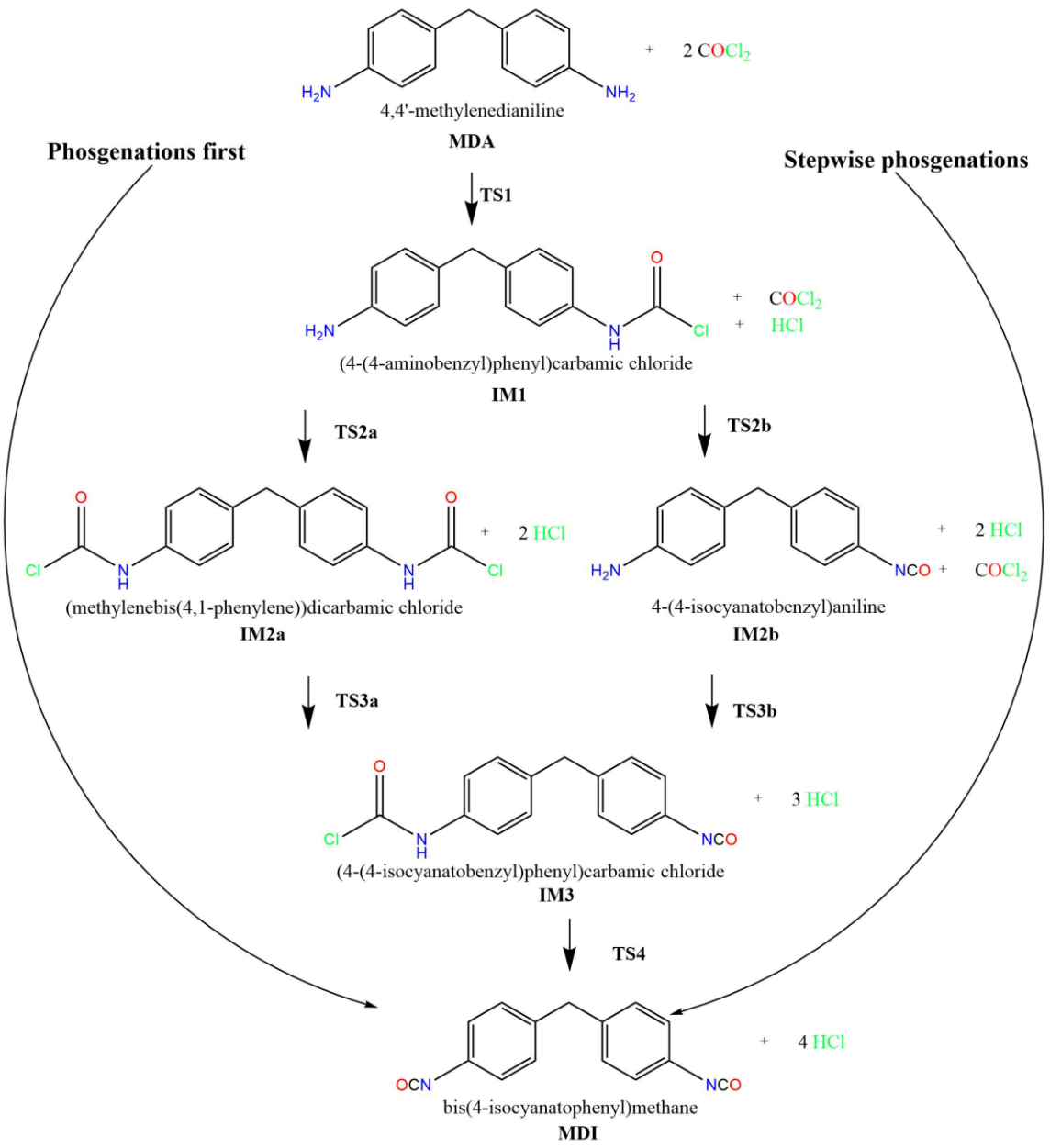


**Figure 21:** Possible reaction mechanism of MDA phosgenation.

When the 'phosgenations first' mechanism occurs the IM1 intermediate is converted into [methylenebis(4,1-phenylene)] dicarbamate)-chloride (IM2a), an energetically very low-lying structure ($\Delta E_0$ = -166.9 kJ/mol, see *Figure 22*) via a four-centered transition state (TS2a in *Figure 23*). The corresponding transition state, that is TS2a, is analogous to TS1 (compare rC-N, rH-Cl, rC-Cl for TS1 and TS2a in *Figure 23*). However, this reaction step has high reaction barrier (49.4 kJ/mol) the TS2a is still above the energy level of the MDA + 2$COCl_2$ by -35.0 kJ/mol as shown in *Figure 22* due to the exothermicity of the first phosgenation step. The subsequent elementary step, that is the HCl-elimination, was

proceeded through TS3a with the energy of -33.7 kJ/mol relative to the reactants (*Figure 22*).

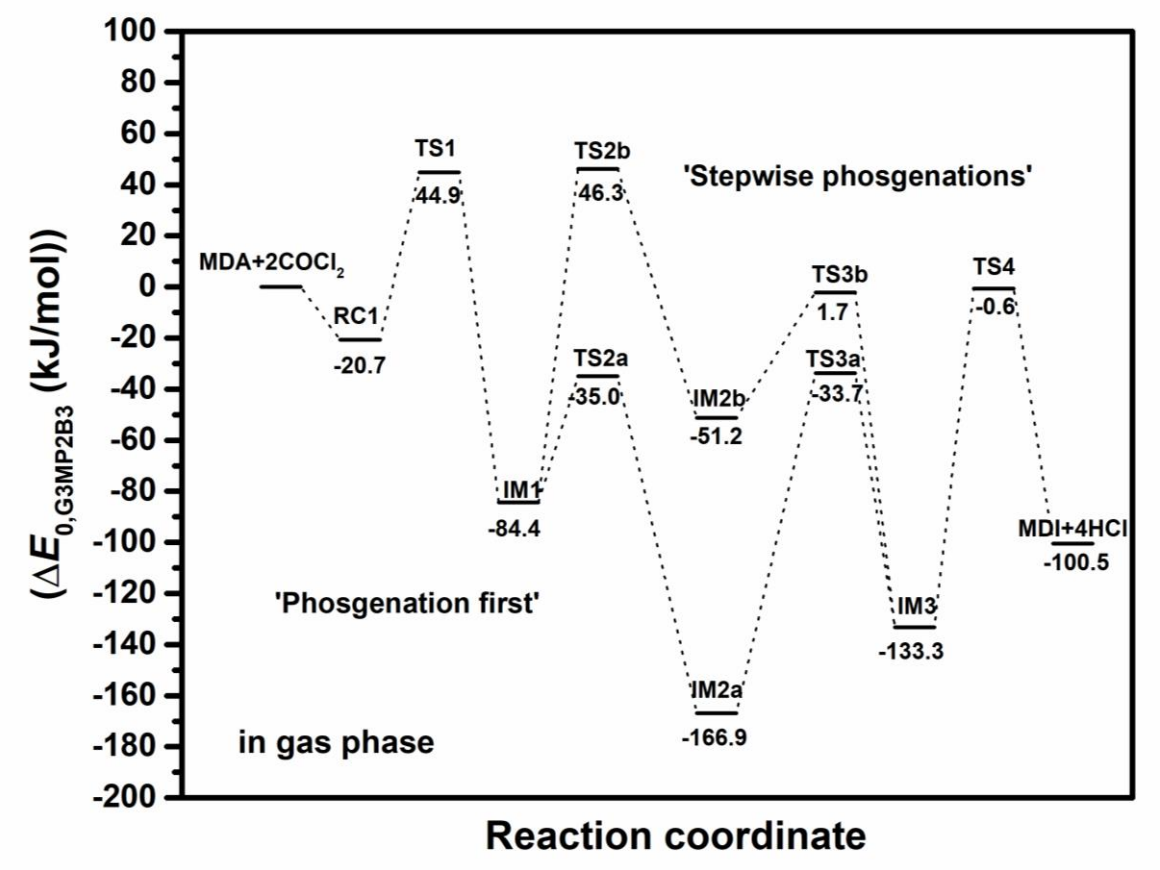


**Figure 22**: G3MPB3 energy profile (zero-point corrected) for the phosgenation of 4,4′-methylenedianiline (MDA) in gas phase.

As *Figure 23* shows, in four-centered transition state of TS3a, the critical bond distances are the followings: rC-N=1.271 Å and rH-Cl=1.761 Å rC-Cl=2.735 Å, making the transition state structure similar to the product, which is [4-(4-isocyanatobenzyl) phenyl]-carbamate-chloride (IM3). It is also important to mention that the relative energy of the product (IM3 + 3HCl, $\Delta E_0$ = -133.3 kJ/mol) is higher than that of IM2 + 2HCl ($\Delta E_0$ = -166.9 kJ/mol), therefore this reaction step is endothermic ($\Delta_r H°$=38.3 kJ/mol). In the 'stepwise phosgenations' mechanism, intermediate IM1 undergoes an endothermic HCl-elimination resulted in 4-(4-isocyanatobenzyl-aniline) noted as IM2b *(Figure 22*). Besides the endothermic nature of this HCl-elimination, the energy level of IM2b and HCl is lower than that of the reactant by 51.2 kJ/mol. The corresponding four-centered transition state (TS2b) with 46.3 kJ/mol zero-point corrected relative energy shows structural similarity to TS3a.

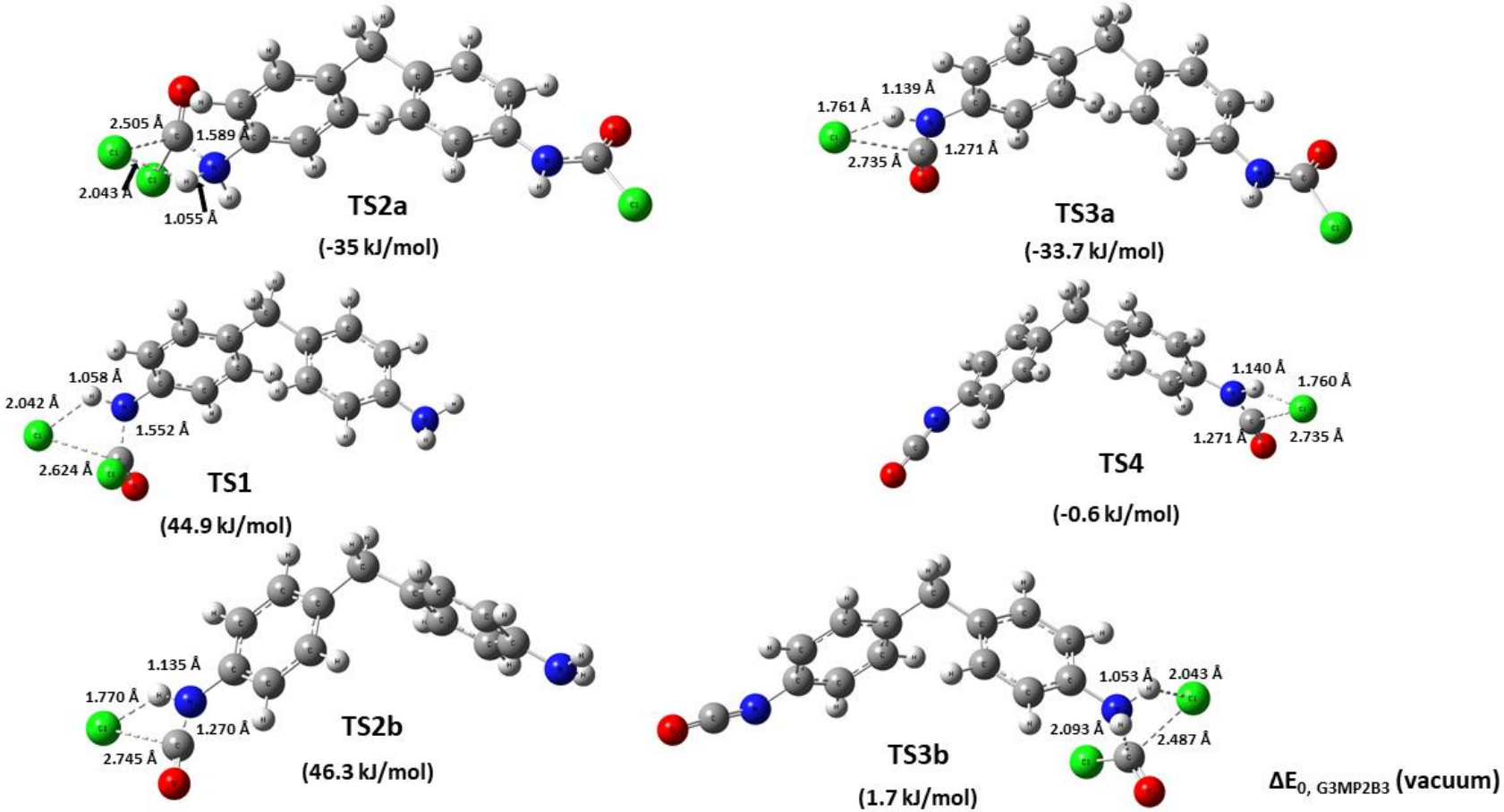


**Figure 23:** Transition state structures (obtained at B3LYP/6-31G(d) level of theory) for the phosgenation of 4,4′-methylenedianiline (MDA) in gas phase.

In the next phosgenation step, the previously mentioned IM3 is produced via transition state TS3b of 1.7 kJ/mol zero-point corrected energy (*Figure 22*). TS3b structure evolved in the simultaneous formation of H-Cl and C-N bonds with the distances of rH-Cl=2.043 Å and rC-N=2.093 Å (*Figure 23*). The structure of TS3b is similar to TS1 and TS2a. Incorporation of phosgene molecule into the IM2b is also exothermic. Comparing these mechanisms, the activation energy of the bimolecular transition state TS2a ($\Delta^{\ddagger}E_0$=49.4 kJ/mol) is lower by 81.3 kJ/mol than that of the unimolecular TS2b ($\Delta^{\ddagger}E_0$=130.7 kJ/mol) as seen in *Figure 22*. In the present of excess of $COCl_2$, this energy difference may allow us to speculate without the complex kinetic modelling of the procedure that the 'phosgenation first' mechanism dominates the gas phase reaction of MDA with phosgene, the relevant condition for the chemical industry. In the last elementary process, the HCl and MDI ($\Delta E_0$ = -100.5 kJ/mol) are formed from IM3 through HCl-elimination transition state (TS4) with a barrier height of 133.9 kJ/mol via endothermic elementary step (data provided in *Table 15*). The relative energy of TS4 is -0.6 kJ/mol. This transition state structure resembles TS2b and TS3a geometries. Comparing the two type of reaction mechanisms from the view of enthalpy change it could be concluded that the 'phosgenation first' mechanism has two exothermic processes at the beginning of the reaction (lead to the formation of IM1 and IM2a) and two endothermic at the end (result in the formation of IM3 and MDI) (*Table 15*). In the case of the 'stepwise phosgenations' consists of alternating exothermic and endothermic steps. Knowing the enthalpy profile of a reaction provides useful information for predicting the heat requirement of the system.

#### *3.2.1.1 Characterization of the molecular properties for relevant reaction intermediates*

Taking the advantages of the accurate calculation of the intermediates (reported average absolute deviation for G3MP2B3 is 5.2 kJ/mol), the thermodynamic properties can be computed for reactants and products and all the intermediates in the gas phase at standard condition. According to *Table 14*, the calculated standard enthalpies of formation for MDI, MDA and IM2b are endothermic, while the formation of IM1, IM2a and IM3 are exothermic. Besides the highly accurate literature $\Delta_{f,298.15K}H°$ values for $COCl_2$ and HCl, to the best of our knowledge, standard enthalpies of formation are reported in the literature only for MDA and MDI. As can be seen from *Table 14*, the G3MP2B3 heats of formation for $COCl_2$ and HCl are close to the highly accurate literature value available in the ATcT database[100], which can support the reliability of our G3MP2B3 results. It is

worthy to note that G3MP2B3 performs even better than G4MP2 for these species. The largest error in the computed G3MP2B3 $\Delta_{f,298.15K}H°$ values are found in the case of $COCl_2$, where the deviation is 6.7 kJ/mol. While the G3MP2B3 value for MDA (171.0 kJ/mol) is also consistent with the estimated values based on group additivity rules by Benson[114] and Benson and Stein[113] and (165.6[40] and 172.0 kJ/mol, respectively), the NIST recommended value of 189 ± 21 kJ/mol for $\Delta_{f,298.15K}H°$ (MDI) is significantly larger compared to our G3MP2B3 result (14.8 kJ/mol). The NIST recommendation is based on the work by Zhuravlev et al.[41] As can be seen in *Table 14* significantly lower $\Delta_{f,298.15K}H°$ (MDI) values can be derived from heat of combustion results obtained from bomb calorimetric measurement ($\Delta_cH°$(MDI)=7.28 MJ/mol) and Handrick estimation ($\Delta_cH°$ (MDI) =7.27 MJ/mol) by Selivanov et al.[125] Using the first reported heat of combustion for MDI (6.91 MJ/mol)[126], even exothermic $\Delta_{f,298.15K}H°$(MDI) can be obtained with large uncertainty (-200.6 ± 52.3 kJ/mol). Our G3MP2B3 results (14.8 kJ/mol) is in between the reported extreme $\Delta_{f,298.15K}H°$(MDI) values. However, none of the above-mentioned publications provide information about the experimental condition, all seems to underestimate our measured $\Delta_cH°$(MDI) value (7.346 ± 0.005 MJ/mol).

No literature $\Delta_{f,298.15K}H°$ found for any intermediates presented here, group based estimation of standard enthalpy of formation is also not possible since no group increments ($\Delta_{f,i}H°$) available for the isocyanate (-NCO) and carbamoyl chloride (-NHCOCl) linked to aromatic ring. However, calculated G3MP2B3 enthalpies of formation allow us to derive the corresponding Benson and Stein's group increment value ($\Delta_{f,i}H°$) for these group: $\Delta_{f,i}H°$(-NCO) = -61.2 kJ/mol and $\Delta_{f,i}H°$(-NHCOCl) = -195.0 kJ/mol with the uncertainty of G3MP2B3 (± 5.2 kJ/mol). These values can later be used for chemical process simulations.

The computed standard molar entropy (S°(g)) and molar heat capacity (CV(g)) values are also tabulated in *Table 14* and their deviation from the established literature values is less than 8.7 J/molK

**Table 14**: Gas phase thermochemical properties for reactants, products and all the intermediates of the phosgenation of the MDA. The standard enthalpy of formation is calculated from G3MP2B3and G4MP2 enthalpies by means of atomization scheme (AS). Standard molar enthalpy of formation ($\Delta_{f,298.15K}H°$(g)), standard molar entropy ($S°$(g)) and molar heat capacity ($CV$(g)) were obtained at 1 atm pressure at 298.15 K. Entropy and heat capacity values are obtained from scaled B3LYP/6-31G(d) frequencies. Enthalpy of combustion ($\Delta_c H°$) was estimated as HHV (higher heating value) from molar enthalpy of formation obtained by G3MP2B3.

| **Species** | **$\Delta_{f,298.15K}H°$(g)(kJ/mol)** | | | **$\Delta_c H°$** | | | **$S°$ (g)** | **$C_v$(g)** | |
|---|---|---|---|---|---|---|---|---|---|
| | **Value** | **Method** | **Ref.** | **MJ/mol** | **MJ/kg** | **Ref.** | **J/molK** | **J/molK** | **Ref.** |
| **$COCl_2$** | -225.8/-227.3 | AS using G3MP2B3/G4MP2 | [33] | | | | 290.3 | 50.4 | [33] |
| | -219.13 ± 0.27 | Ruscic ATcT | Ref.[100] | | | | 283.8 | 57.69 | CCCBDB[111] |
| **HCl** | -95.0/-95.1 | AS using G3MP2B3 / G4MP2 | [33] | | | | 186.7 | 20.8 | [33] |
| | -92.173 ± 0.0062 | Ruscic ATcT | Ref.[100] | | | | 186.9 | 29.14 | CCCBDB[111] |
| **MDA** | 171.1/171.9 | AS using G3MP2B3 / G4MP2 | [33] | | | | 500.0 | 230.6 | this work |
| | 165.6 | Benson's additivity rule | Ref.[40] | | | | 522.70 | | Ref[40] |
| | 172.0 | Additivity rule by Benson and Stein[114,113] | NIST[116] | | | | 511.66 | 234.7[a] | NIST[116] |
| **MDI** | 14.8/24.5 | AS using G3MP2B3 / G4MP2 | [33] | 7.346 ± 0.005 | 29.35 ± 0.02[b] | this work | 580.4 | 259.0 | [33] |
| | | | | 7.363 ± 0.03 | 29.421 ± 0.128[c] | this work | | | |
| | 189 ± 21 | NIST recommendation | Ref.[41] | | | Ref.[41] | | | |
| | 164.7 ± 12.6 | Static bomb calorimetry | Ref.[125] | 7.28 ± 12.6 | | Ref.[125] | | | |
| | 159.3 | Handrick's group additivity[127] | Ref.[125] | 7.27 | | Ref.[125] | | | |
| | -200.6 ± 52.3 | from heat of combustion value | Ref.[126] | 6.91 ± 52.3 | | Ref.[126] | | | |
| **IM1** | -41.0/-38.6 | AS using G3MP2B3 / G4MP2 | [33] | | | | 573.2 | 267.8 | [33] |
| **IM2a** | -251.0/-247.1 | AS using G3MP2B3 / G4MP2 | [33] | | | | 653.8 | 304.8 | [33] |
| **IM2b** | 92.0/97.3 | AS using G3MP2B3 / G4MP2 | [33] | | | | 542.0 | 245.0 | [33] |
| **IM3** | -117.8/-111.0 | AS using G3MP2B3 / G4MP2 | [33] | | | | 616.9 | 281.9 | [33] |

[a] at 300 K

[b] gas phase

[c] solid phase

### *3.2.2 Solvent effect*

In chemical industry, phosgenation of the MDA is carried out mainly in a suitable inert solvent such as ODCB. The effect of the surrounding ODCB media on the energy profile of the reaction is shown in *Figure 24* and relative energies are tabulated in *Table 15* . The zero-point corrected relative energies ($\Delta E_0$) of the transition states are dramatically decreased (by roughly 50 kJ/mol), while the $\Delta E_0$ of the intermediates lowered only by 10 kJ/mol. The only exception is the energy difference between the reactive complex RC1 and the reactants ($\Delta E_0$ (RC1) = -7.4 kJ/mol), which increased by 13.3 kJ/mol (see in *Figure 24)*

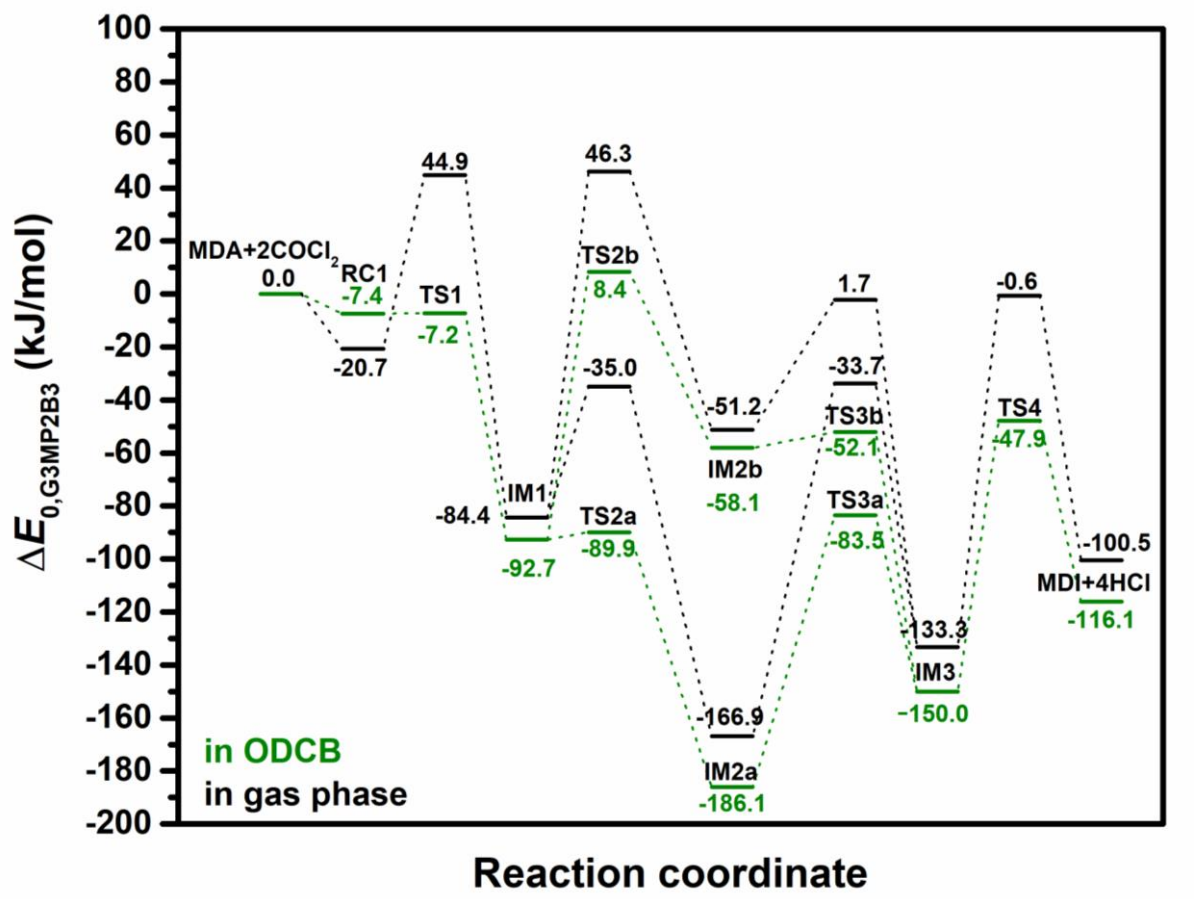


**Figure 24**: G3MPB3 energy profile (zero-point corrected) for the phosgenation of 4,4′-methylenedianiline (MDA) in ortho-dichlorobenzene (ODCB) media (in green) and in gas phase (in black).

The consequence of the fall of $\Delta E_0$ for transition states, the incorporation of the first phosgene molecule occurs via submerged transition state and therefore we suspect that reaction rate mainly determined by the diffusion rate of the molecules. Besides the dramatic change in the relative energy of TS1, the structure of TS1 shows structural similarity to its four-membered gas phase counterparts. However, the C-Cl and Cl-H bond

distances were increased, while the H-N and C-N were decreased (rC-H=2.457 Å; rC-Cl=2.715 Å; rH-N=1.032 Å; rN-C=1.522 Å) as shown in *Figure 25*. Due to simultaneous phosgene addition and HCl-elimination via TS1, solvated IM1 is formed *Figure 24.*

Similar to the incorporation of the first phosgene, the simultaneous addition of the second phosgene and HCl-elimination *(Figure 24*) goes through a low-lying transition state TS2a ($\Delta E_0$(TS2a) = -89.9 kJ/mol) starting from ODCB solvated IM1 + $COCl_2$, resulted in the formation of IM2a and HCl. As seen from the structure of TS2a in *Figure 25*, the Cl-H bond distance was increased, while the others were decreased such as rCl-H=2.400 Å; rC-Cl=2.433 Å; rH-N=1.031 Å; rN-C=1.567 Å compared to its gas phase counterpart. In this exothermic reaction step, the products found to have the lowest zero-point corrected energy along the reaction coordinate toward the formation of MDI ($\Delta E_0$ = -186.1 kJ/mol) shown in *Figure 23.*

In the next step of the 'phosgenation first' mechanism, endothermic HCl-elimination occurred through a transition state (TS3a) step giving solvated IM3 intermediate ($\Delta E_0$ (IM3) = -150.0 kJ/mol). In this ODCB phase transition state structure (noted as TS3a in *Figure 25*), critical distances are slightly different compared to its gas phase analogue: the rCl-H and rC-Cl were elongated, while the rH-N and rN-C were shortened (rCl-H=2.00 Å; rC-Cl=2.866 Å; rH-N=1.069 Å; rN-C=1.268 Å). It is important to mention that starting from IM2a + HCl, the energy barrier of the forward unimolecular HCl-elimination via TS3b and the bimolecular reverse reaction though TS2a are energetically close to each other. In the case of the 'stepwise phosgenations', conversion of IM1 into IM2b (IM2b, $\Delta E_0$ = -58.1 kJ/mol) (*Figure 24)* became energetically easily accessible due to the low-lying solvated TS2b transition state ($\Delta E_0$ = 8.4 kJ/mol).

Additionally, IM3 ($\Delta E_0$ (IM3) = -150.0 kJ/mol) can be formed by overcoming small energy barrier of 6 kJ/mol via TS3b ($\Delta E_0$ (TS3b) = -52.1 kJ/mol) *Figure 24*. This transition state lies with 53.8 kJ/mol lower in zero-point corrected energy in ODCB than in gas phase. Only significant structural change between TS structures optimized in the gas phase and the ODCB is the Cl-H bond, which was elongated in ODCB compared with the gas phase rCl-H=2.431 Å; rC-Cl=2.427 Å; rH-N=1.031 Å; rN-C=1.584 Å (TS3b in *Figure 25*). The subsequent elementary step was proceeded via TS4 (TS4, $\Delta E_0$ = -47.9 kJ/mol) with threshold energy of 102.1 kJ/mol (seen in *Figure 24)* resulted in MDI formation by releasing HCl ($\Delta E_0$ = -116.1 kJ/mol). The zero-point corrected relative energy of TS4 is also lower than in gas phase by 47.3 kJ/mol. Describing the structure of TS4 in ODCB the

bond distances slightly differ from the gas phase as follows; the Cl-H and C-Cl bonds are elongated; the others are shortened (phase rCl-H=1.999 Å; rC-Cl=2.888 Å; rH-N=1.069 Å; rN-C=1.268 Å (TS4 in *Figure 25*). In general, the ODCB solvation changes the energy profile dramatically making energetically more accessible both 'phosgenations first' and 'consecutive phosgenations' mechanism. The activation barriers for both phosgenation mechanisms were found to be high in the gas phase, while all the zero-point corrected relative energies ($\Delta E_0$) of the transition states dramatically reduced by roughly 50 kJ/mol, while the $\Delta E_0$ of the intermediates lowered only by 10 kJ/mol. However, complex kinetic evaluation of different reaction conditions is out of our scope, one may speculate that the molar ratio of phosgene and MDA can make a switch between the two reaction mechanisms. Stability of the product complexes (as we see later in the case of the charge separated complex of $IM1H^+$ and $Cl^-$) can also change this kinetic picture.

### *3.2.3 Thermochemistry of the studied reactions at different condition*

In the industrial phosgenation of MDA the two main parameters are the pressure and temperature. The efficiency of the phosgenation, the possibility of the side reactions highly depends on the adjustment of these conditions. To get more information about the phosgenation of MDA in ODCB we examined the influence of different temperature and pressure values to explore the temperature and pressure dependence of the thermodynamics of the reaction system. Relative enthalpies and Gibbs free energies obtained at 25°C, 90°C and 150°C under 1, 6 and 11 bar are summarized in *Table 15*. Concluded the results it can be said that the computed relative enthalpies of the species (ΔHG3MP2B3(T)) were not significantly changed (varied between -1.0 and 0.1 kJ/mol) by increasing the temperature from 90°C and 150°C.

This effect is enhanced in the case of the relative Gibbs free energies ($\Delta G_0$), although this increase is moderate (-14.0 - 11.9 kJ/mol), but still larger than the changes according to the increase of 6 bar to 11 bar (-2.1 - 4.3 kJ/mol).

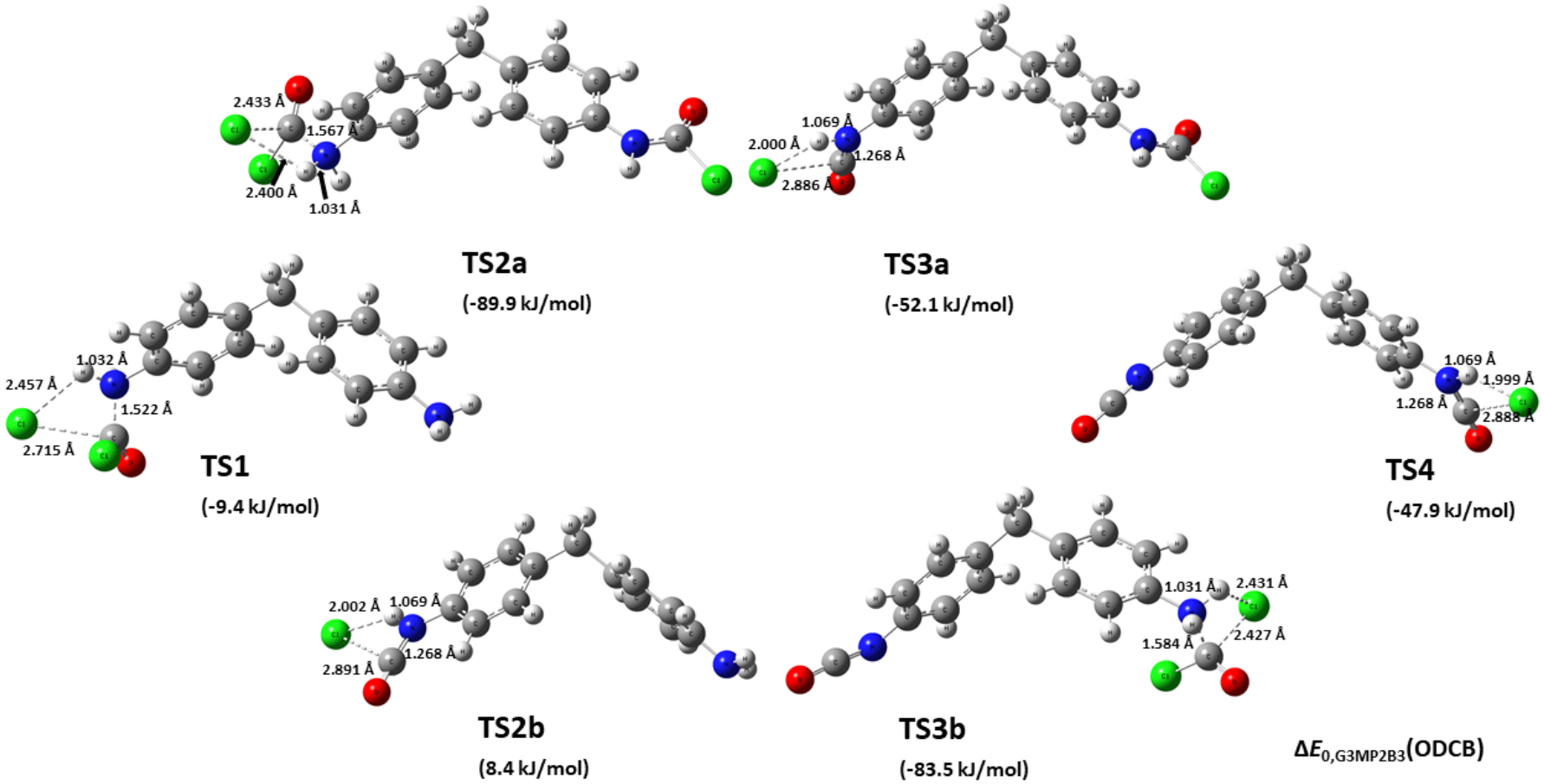


**Figure 25:** Transition state structures (obtained at B3LYP/6-31G(d) level of theory) for the phosgenation of 4,4′-methylenedianiline (MDA) in ortho-dichlorobenzene (ODCB) media.

**Table 15:** G3MP2B3 thermochemical properties calculated in gas phase and in ortho-dichlorobenzene (ODCB) including zero-point corrected relative energies ($\Delta E_0$, G3MP2B3), relative enthalpies (ΔHG3MP2B3(T)) and relative Gibbs free energies ($\Delta G$G3MP2B3(T,P)).

| | $\Delta E_{0,G3MP2B3}$ | | $\Delta H_{G3MP2B3}(T)$ | | | | $\Delta G_{G3MP2B3}(T,P)$ | | | | | |
|---|---|---|---|---|---|---|---|---|---|---|---|---|
| **Solvent** | **-** | **ODCB** | **-** | **ODCB** | **ODCB** | **ODCB** | **-** | **ODCB** | **ODCB** | **ODCB** | **ODCB** | **ODCB** |
| **T/°C** | 25 | 25 | 25 | 25 | 90 | 150 | 25 | 25 | 90 | 90 | 150 | 150 |
| **P/bar** | 1.0 | 1.0 | 1.0 | 1.0 | 6.0 | 6.0 | 1.0 | 1.0 | 6.0 | 11.0 | 6.0 | 11.0 |
| **MDA + 2 $COCl_2$** | 0.0 | 0.0 | 0.0 | 0.0 | 0.0 | 0.0 | 0.0 | 0.0 | 0.0 | 0.0 | 0.0 | 0.0 |
| **RC1** | -20.7 | -7.4 | -17.5 | -7.6 | -7.1 | -6.7 | 16.5 | 44.8 | 50.8 | 49.0 | 60.3 | 58.2 |
| **TS1a + $COCl_2$** | 44.9 | -7.2 | 43.5 | -8.6 | -8.7 | -8.8 | 96.9 | 44.8 | 51.0 | 49.2 | 60.9 | 58.8 |
| **IM1 + $COCl_2$ + HCl** | -84.4 | -92.7 | -81.2 | -89.6 | -89.2 | -88.9 | -72.1 | -80.3 | -78.3 | -78.3 | -76.5 | -76.5 |
| **TS2a + HCl** | -35.0 | -89.9 | -33.1 | -88.2 | -87.8 | -87.5 | 28.2 | -24.5 | -16.0 | -17.8 | -4.1 | -6.3 |
| **IM2a + 2 HCl** | -166.9 | -186.1 | -160.5 | -179.7 | -178.8 | -178.0 | -144.5 | -163.3 | -159.9 | -159.9 | -156.8 | -156.8 |
| **TS3a + 2 HCl** | -33.7 | -83.5 | -26.3 | -76.4 | -75.6 | -75.1 | -13.6 | -62.1 | -59.0 | -59.0 | -56.3 | -56.3 |
| **TS2b + $COCl_2$ + HCl** | 46.3 | 8.4 | 50.5 | 12.5 | 12.9 | 13.1 | 54.3 | 13.6 | 13.8 | 13.8 | 13.9 | 13.9 |
| **IM2b + $COCl_2$ + 2HCl** | -51.2 | -58.1 | -43.3 | -50.0 | -49.2 | -48.7 | -80.5 | -87.8 | -90.8 | -89.0 | -97.7 | -95.6 |
| **TS3b + 2HCl** | 1.7 | -52.1 | 8.3 | -45.4 | -44.7 | -44.3 | 24.6 | -29.8 | -26.4 | -26.4 | -23.4 | -23.4 |
| **IM3 + 3HCl** | -133.3 | -150.0 | -122.2 | -139.0 | -137.8 | -137.0 | -150.9 | -166.2 | -166.8 | -165.0 | -171.7 | -169.6 |
| **TS4 + 3HCl** | -0.6 | -47.9 | 11.6 | -36.3 | -35.7 | -35.0 | -22.8 | -66.2 | -68.5 | -66.6 | -73.9 | -71.8 |
| **MDI + 4HCl** | -100.5 | -116.1 | -84.6 | -99.8 | -98.3 | -97.3 | -158.0 | -176.2 | -182.3 | -178.6 | -196.3 | -192.0 |

#### *3.2.3.1 Thermochemical properties of the product complex of the incorporation of the first phosgene into MDA*

In the previous sections, we neglected all the interference of the products formed. However, the HCl molecules is hardly solvated in ODCB and HCl may stay in strong interaction with IM1 to form dimer giving the following possibilities:

(1) Molecular complex of IM1 and HCl in which the HCl oriented parallel to the C=O bond of the carbamoyl chloride (IM1 × HCl)

(2) Protonated IM1 separated from solvated chloride ion (IM1H++ $Cl^-$)

(3) Charge separated complex of protonated IM1 and chloride ion (IM1H+ × Cl-)

We use them as a proxy to measure the stability of the amine hydrochloride salts in ODCB. The calculated thermodynamics properties are shown in *Table 16.* The formation of the molecular complex (IM1 + HCl → IM1 × HCl) is slightly exothermic, but the Gibbs free energy of its formation from separated ODCB solvated IM1 and HCl is positive due to the entropy effect. Obviously, the charge separation cannot be an option either due to its high Gibbs free energy at any condition studied. However, the ionic complex (see IM1H+ × Cl- in *Table 16*) has relatively high stability at these conditions which might inhibit the second phosgene to incorporate both sterically and energetically. One can also speculate that the freshly introduced MDA can also form such charge separated complex with HCl (when there is a large excess HCl in the reactor) due to such thermodynamically preference. This may decrease the reactivity of MDA towards phosgene. The ionic complex (complex of hydrochloric acid and 4-(4-aminobenzyl)phenyl)carbamic chloride, IM1H+ × Cl-) has relatively high stability ($\Delta E_0$ = -52.0 kJ/mol) at industrial conditions which might inhibit the second phosgene to incorporate both sterically and energetically. MDA can also form such charge separated complex with HCl (when there is a large excess HCl in the reactor) due to such thermodynamically preference. This may decrease the reactivity of MDA towards phosgene.

**Table 16:** Thermochemical properties for IM1 intermediates of the phosgenation of the MDA obtained from G3MP2B3 calculations. The reference state is the infinitely separated IM1 and HCl in ODCB.

| | $\Delta E_{0,G3MP2B3}$ | $\Delta H°_{G3MP2B3}(T)$ | | | $\Delta G°_{G3MP2B3}(T,P)$ | | | | |
|---|---|---|---|---|---|---|---|---|---|
| **Solvent** | **ODCB** | **ODCB** | **ODCB** | **ODCB** | **ODCB** | **ODCB** | **ODCB** | **ODCB** | **ODCB** |
| **T/°C=** | 25 | 25 | 90 | 150 | 25 | 90 | 90 | 150 | 150 |
| **P/atm=** | 1.0 | 1.0 | 6.0 | 6.0 | 1.0 | 6.0 | 11.0 | 6.0 | 11.0 |
| **IM1 + HCl** | 0.0 | 0.0 | 0.0 | 0.0 | 0.0 | 0.0 | 0.0 | 0.0 | 0.0 |
| **IM1 × HCl** | -5.4 | -3.3 | -2.5 | -1.7 | 18.6 | 17.9 | 16.0 | 21.2 | 19.1 |
| **$IM1H^+ + Cl^-$** | 24.4 | 22.5 | 22.0 | 21.5 | 30.7 | 32.5 | 32.5 | 34.3 | 34.3 |
| **$IM1H^+ \times Cl^-$** | -52.0 | -55.3 | -55.7 | -56.0 | -17.0 | -14.0 | -15.8 | -7.1 | -9.2 |

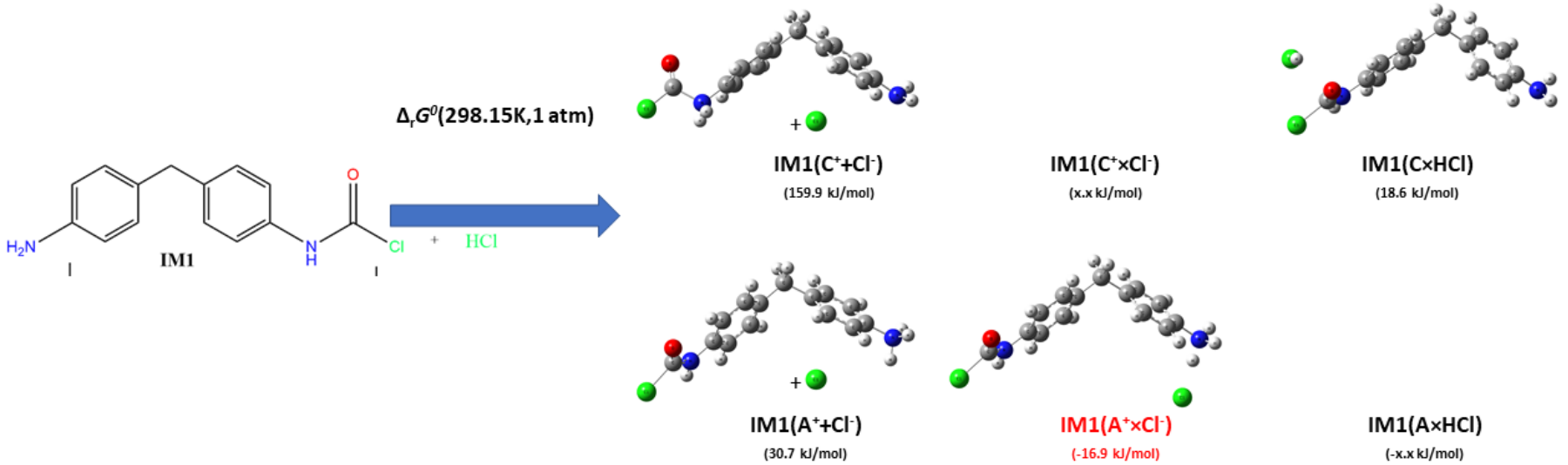


**Figure 26**: Stability of HCl complexes (IM1) in ODCB.

### *3.2.4 Conclusions*

The possible main reaction pathways of MDA phosgenation were computed in gas-phase and in ortho-dichlorobenzene (ODCB). It was found that:

- The formation of MDI can be possible via two different mechanisms: 'Phosgenations first': both amino groups transformed to carbamoyl chloride groups giving [methylenebis(4,1-phenylene)]dicarbamic chloride and then two endothermic HCl-elimination steps occurs. Stepwise phosgenations': One of the amino groups of MDA turns into isocyanate by phosgene and then the other amine does.
- Accurate standard enthalpy of formation was determined for MDI (14.8 kJ/mol) with the uncertainty of 5.2 kJ/mol. This value was compared with the uncertain literature standard enthalpies of formation for MDI.
- The activation barriers for both phosgenation mechanisms were found to be high in the gas phase, while all the reaction barriers are dramatically reduced making the incorporation of the first phosgene occurred in ODCB via submerge transition state. The reaction with the second phosgene has also low-lying transition state in this case.
- Only moderate effect on the relative enthalpies and Gibbs free energies found by changing in the temperature and pressure range of the industrial operation
- ($90°C < T < 160°C$ and $6 \text{ bar} < P < 11 \text{ bar}$).
- The ionic complex ($IM1H^+ \times Cl^-$) has relatively high stability at industrial conditions which might inhibit the second phosgene to incorporate both sterically and energetically. MDA can also form such charge separated complex with HCl (when there is a large excess HCl in the reactor) due to such thermodynamically preference. This may decrease the reactivity of MDA towards phosgene.

### *3.2.5 Experimental studies*

The execution of MDA phosgenation in the laboratory is quite circumstantial therefore in the case the phosgenation step we focused on the examination of ([methylenebis(4,1-phenylene)]dicarbamic chloride intermediate found as the global minimum of the reaction coordinate. Firstly, our purpose was to examine the characteristic of this compound by synthetizing it. Afterwards, we planned to in situ generate this intermediate and examine its decomposition ability at different temperatures.

*Synthesis of [methylenebis(4,1-phenylene)]dicarbamic chloride*

According to our assumption, if we add HCl gas to the pure MDI (4,4'-MDI) [methylenebis(4,1-phenylene)]dicarbamic chloride will be formed. The conversion is a reversible process. The product [methylenebis(4,1-phenylene)]dicarbamic chloride can be decomposed at higher temperature releasing HCl gas as by-product *Scheme 2.*

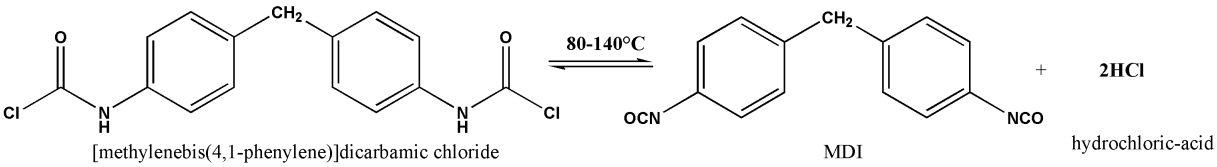


**Scheme 2:** Formation and decomposition of [methylenebis(4,1-phenylene)]dicarbamic chloride.

In the laboratory this intermediate was synthetized by adding pure HCl (10g) gas to 4,4'-MDI (100 g). The synthesis was carried out in a three-neck round-bottomed flask reactor. A condenser was fitted to the top of the flask with the output connected to the tap. In one of the necks HCl gas was flowed into the reactor passing through a flow meter within 15 minutes. In third neck a thermometer was put. During the HCl gas feed the color of the MDI was continuously changed *Figure 27*. As a result, a high viscosity material was formed, which was difficult to handle.

**Figure 27**: Change of the 4,4'-MDI after the HCl gas was added to the pure 4,4'-MDI.

At the end of the synthesis the product became solid (*Figure 28*). The synthetized compound was analyzed by infrared spectroscopy. The IR spectrum is introduced in *Figure 29.*

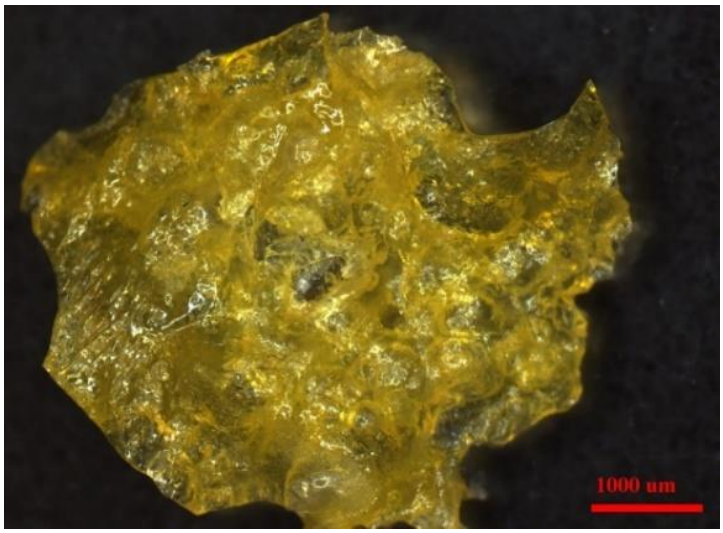


**Figure 28**: The synthetized [methylenebis(4,1-phenylene)]dicarbamic chloride product.

According to the IR results the [methylenebis(4,1-phenylene)]dicarbamic chloride was successfully synthetized. The characteristic CO bond appeared at 1740 $cm^{-1}$ (connected to the Cl atom) and at 3300 $cm^{-1}$ (connected to the -NH group) *(Figure 29*), however the characteristic NCO peak (2270 $cm^{-1}$) can also be found referring to the presence of unreacted MDI.

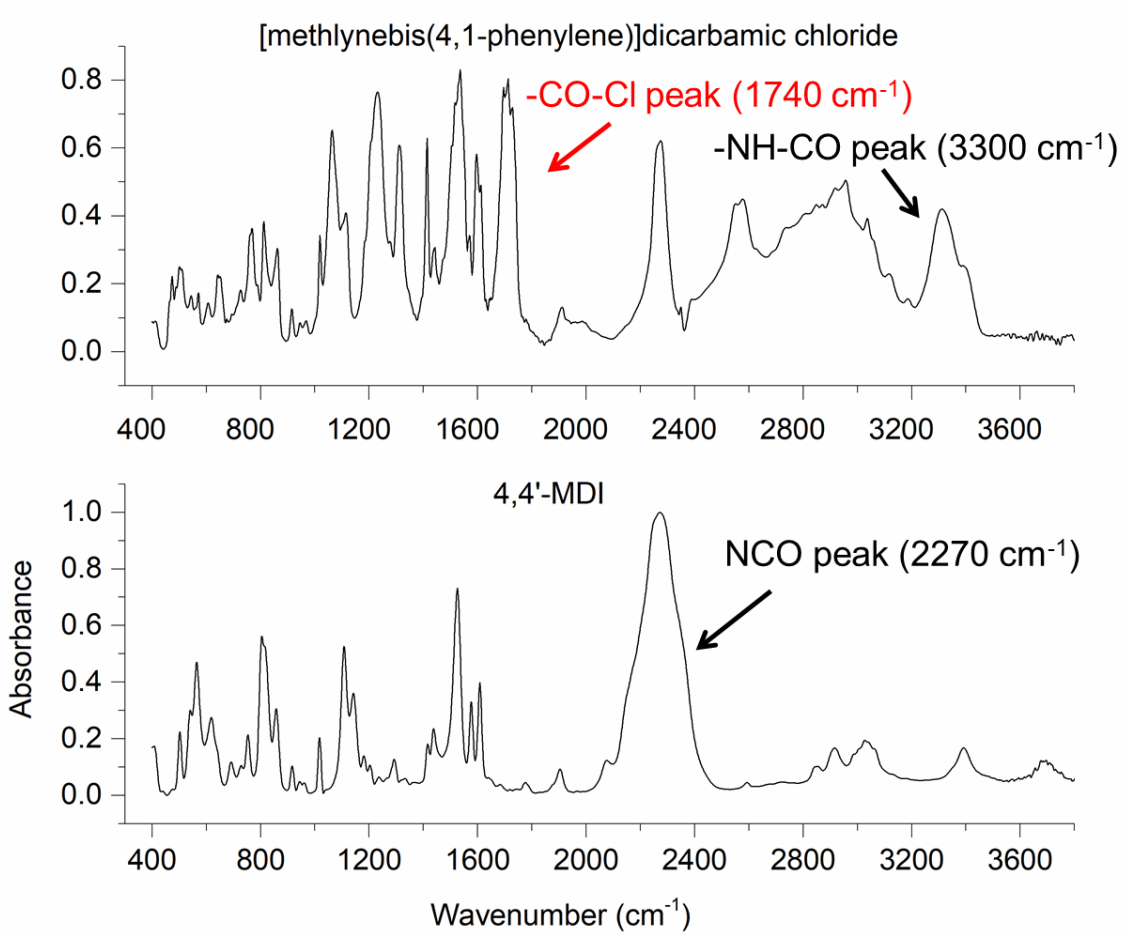


**Figure 29**: IR spectrum of the synthetized [methylenebis(4,1-phenylene)]dicarbamic chloride.

*Study the decomposition of the methylenebis(4,1-phenylene)]dicarbamic chloride at different temperatures*

The target was to measure the decomposition of the in situ generated [methylenebis(4,1-phenylene)]dicarbamic chloride (IM2a) by monitoring the HCl elimination from the system.

The stability examination of the [methylenebis(4,1-phenylene)]dicarbamic chloride was accomplished using an own-developed laboratory equipment *(Figure 30*). The 4,4'-MDI was fed into a three-necked double walled glass reactor connected with a laboratory cooler. The reactor was heated using oil-bath thermostat. In one of the necks nitrogen gas was flowed into the reactor passing through a gas inlet. The out-blown HCl gas was introduced into a four-necked round-bottomed flask reactor filled with distilled water. The pH value of the water was measured continuously by a pH meter. In the case of acidic medium (by the incame HCl gas) sodium-hydroxide (10 m/m%) was added to the water

by an automatic feeder to neutralize the solution. The amount of the NaOH was measured continuously. From the added NaOH quantity the released HCl was calculated and represented in the function of time. We wanted to compare the effect of temperature on this conversion. In the technology usually high temperature (140-160°C) is used to decompose [methylenebis(4,1-phenylene)]dicarbamic chloride.


**Figure 30**: Laboratory apparatus used for the stability examination of [methylenebis(4,1-phenylene)]dicarbamic chloride.

Experiments were carried out at different temperatures. The conversions of HCl amount are shown in the function of time *Figure 31*. Temperature has a significant effect on the decomposition of the [methylenebis(4,1-phenylene)]dicarbamic chloride. Increasing the temperature, the decomposition reaction of the examined intermediate is faster. According to these results it could be stated that even 80°C-90°C might be enough for the decomposition of [methylenebis(4,1-phenylene)]dicarbamic chloride. The highest decomposition efficiency can achieved at 130°C. The decomposition ability of the studied in situ generated intermediate refers to the fact that adding extra heat to the system promote the reaction run towards the MDI synthesis. The low lying exothermic IM2 intermediate can be shifted out from the lowest minimum of the reaction coordinate by this way.

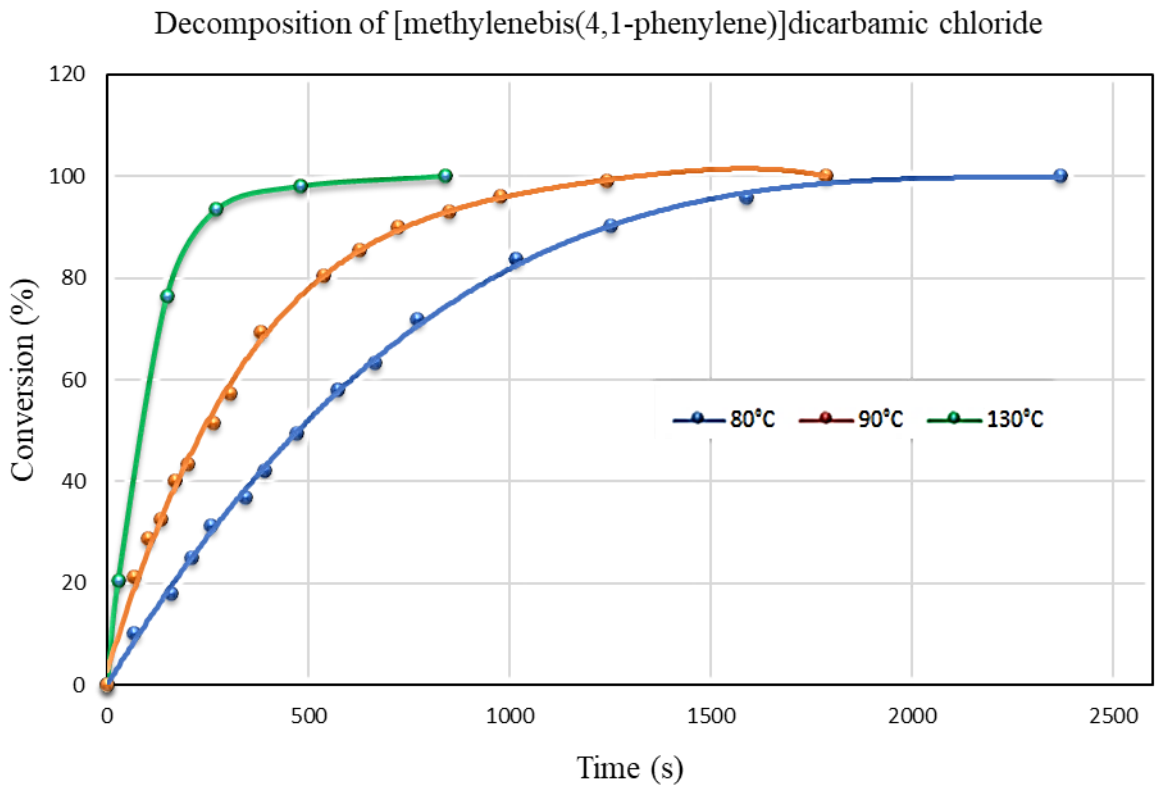


**Figure 31:** Decomposition of [methylenebis(4,1-phenylene)]dicarbamic chloride at different temperatures by measuring the released HCl.

*Industrial application of computational results*

As it was mentioned previously in 3.2.4 section, from the industrial point of view the most important characteristic of a system is the enthalpy profile of it. Knowing the exothermic and endothermic point of a reaction pathway might help to calculate the heat-balance of the examined technology. The industrial experiences are in correlation with the calculated results according which by changing temperature and pressure range (90°C < T <160°C and 6 bar < P < 11 bar) the relative enthalpies and Gibbs free energies are not altering significantly. The recommended standard enthalpy of formation for MDI (14.8 kJ/mol) was similar with those date predicted only by experiences so far. The calculated group additivity increments for NCO and NHOCl groups linked to phenyl ring ($\Delta_{f,i}H°$(-NCO)=-61.2 kJ/mol and ($\Delta_{f,i}H°$(-NHCOCl)=-195.0 kJ/mol) is going to be used in the currently applied simulation software assisting more precious calculations.

*Experiences and main consequences*

Based on the calculations the 'phosgenation first' type of mechanism is the preferable one with the most stable intermediate, methylenebis(4,1-phenylene)]dicarbamic chloride (IM2a). The stability of this intermediate was confirmed

by its successful synthesis. It was formed easily by adding HCl gas to the 4,4'-MDI. The in situ generated IM2a intermediate was decomposed at higher temperature (>80°C) by releasing HCl. The conversion of low-lying IM2a intermediate to the product MDI can be facilitated by heating of the system.

## 3.3 MDI dimers

Industrially, 4,4'-MDI is maintained in the molten state to facilitate pumping and minimize dimer formation. By examining the thermodynamic properties of the possible MDI dimers at the molecular level could give a possibility to minimize the dimerization of MDI in another way also. The geometry optimizations and frequency calculations were carried out using the M06-2X[75] functional as implemental in the Gaussian 09 program package, in combination with the 6-31 G (d,p)[91] basis set. The results of the calculations are introduced in this section. The structures of the MDI dimers are examined.

### *3.3.1 MDI monomers*

The stability and the reactivity of the dimers are influenced by the structure of their monomeric components. The MDI monomer has three main possible isomers according to the position of the isocyanate groups located on the aromatic ring, namely 2,2'-MDI, 2,4-MDI and 4,4'-MDI. The formation of the meta isomers is infinitesimal[128] therefore it is out of the interest of this research. The optimized structures of the main isomers can be seen in *Figure 32.*

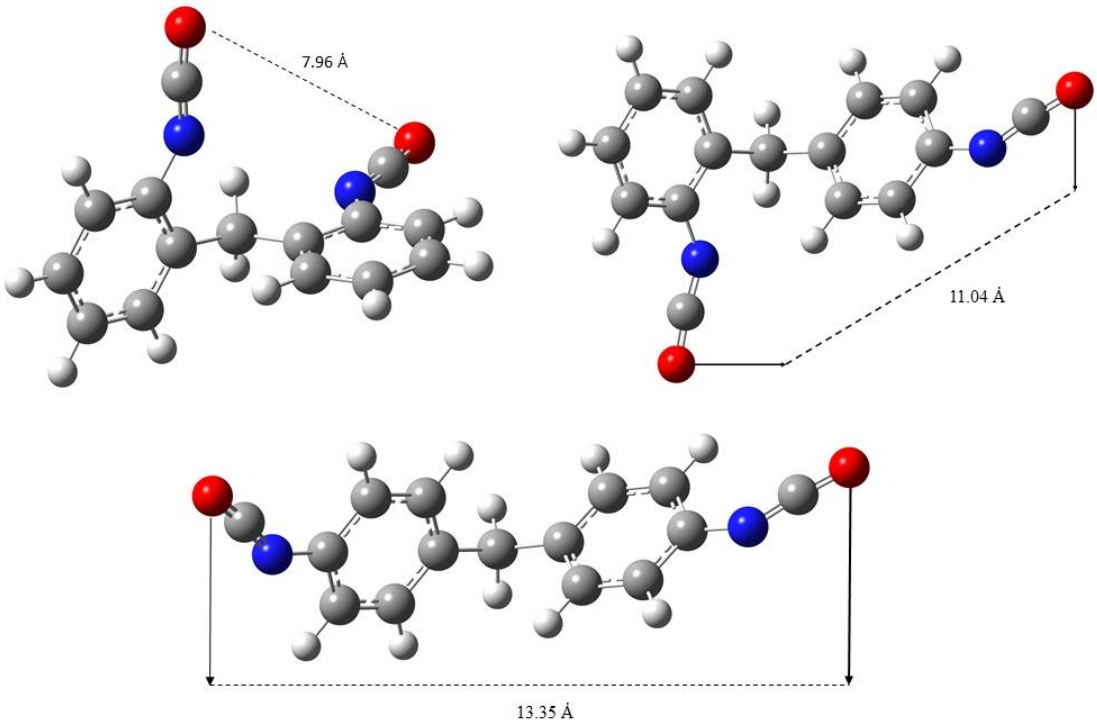


**Figure 32**: Optimized structures of the MDI isomers.

The relative positions of the isocyanate groups are influenced by the related positions of the aromatic rings. The delocalization of the two aromatic rings are hindered by the methylene group located between them. The isocyanate groups are in one plane with the adjacent aromatic ring, facilitating the delocalization between the electrons of the π orbitals of the benzene rings and isocyanate groups. The distance between the nitrogen atoms of the isocyanate groups were measured, and in the case of the 2,2'-MDI the isocyanate groups are nearest to each other (7.96 Å), the 2,4-MDI's functional groups are located further (11.04 Å) from each other, and the isocyanate groups of the 4,4'-MDI are the furthest (13.35 Å). However, the structure of the 2,2'-MDI had seemed to be the most unstable one because the adjacent isocyanate groups occupy a certain amount of molecular field, producing steric hindrance, but the possibility of weaker interactions is higher as well.

Sterically, the 2,4-MDI seems to be more stable than the 2,2'-MDI at constant pressure and temperature ($\Delta G°$) and even at that condition where stability is independent from these conditions ($\Delta E°$) (Section 2.4.2, *Table 2*). Although structurally the 4,4'-MDI appears to be the most stable one, the computed results are in contrast with this assumption. The structure of the 2,2'-isomer might adopt a conformation where rotation through the methylene group allows the two isocyanate groups to be in the nearest

position to each other. This could permit for an interaction to take place between the carbon atom of one isocyanate group and the oxygen atom of the other isocyanate group. The carbon atom has a partial positive charge which can interact with the negative charge of the oxygen atom of the other isocyanate. Another interference could be a so-called π-stacking between the two aromatic rings due to the π bonds. The rings can have a T-shaped or parallel-displaced conformation, which is essentially isoenergetic and represents an energy minimum. The third possible interaction could be the hydrogen bonds between the nitrogen atom of one isocyanate group and the hydrogen atom of the methylene group, which could make this structure more stable than the others. Rodziewicz et al[129] confirmed the presence of weak C–H···π hydrogen bonds by molecules analysis and found to be responsible for the low energy barriers. Comparing the main isomers, the 4,4'-isomer is the most reactive, because the group at the para-position is approximately four times more reactive than the group at the ortho position[1].

**Table 17**: Thermodynamic properties of MDI isomers calculated at M06-2X/6-31G(d,p) level of theory including relative electric energy (Δ*E*°), relative enthalpies (Δ*H*°), relative Gibbs free energies (Δ*G*°) and entropies (S°).

| MDI isomers | Δ*E*° (kJ/mol) | Δ*H*° (kJ/mol) | Δ*G*° (kJ/mol) | *S*° (J/molK) |
|---|---|---|---|---|
| **2,2** | 0.0 | 0.0 | 0.0 | 570.4 |
| **2,4** | 5.7 | 5.5 | 8.9 | 558.9 |
| **4,4'** | 6.8 | 6.9 | 7.2 | 569.2 |

The 2,2'-MDI has the lowest relative total energy, Gibbs free energy and enthalpy. The 2,2' isomer is the most stable one because of its intramolecular interactions. In the case of the complete dimers, these interactions play a significant role. The relative energy, enthalpy, and Gibbs free energy of the 2,4-MDI differs infinitesimally (2-5 kJ/mol) from that of the 4,4'-MDI. The entropy values vary depending on the different conformers. The 2,2'-MDI has the highest entropy.

### *3.3.2 Dimerization via different membered rings*

Different sized rings can be formed in the self-reactions of monomers. The two isocyanate groups can create four-, five- or six membered rings. The three different membered rings can stabilize the dimers (*Figure 33*). As it was previously mentioned

(*Section 1.5*) the possibility of the four membered ring (uretidinone ring) is the highest feasible[2].

The relative stability of the four-, five-, and six-membered rings are listed in *Table 18* and the structures of the different sized rings can be seen in *Figure 34.* From the calculated thermodynamic data computed using M06-2X/6-31G(d,p), it could be concluded that the four-membered ring is the most stable ring, while the six-membered ring is the least stable. The difference between the four- and five-membered rings is about 260 kJ/mol, and the relative energies, enthalpies, and Gibbs free energies of the six-membered ring are within about 400 kJ/mol less stable than the five-membered one.

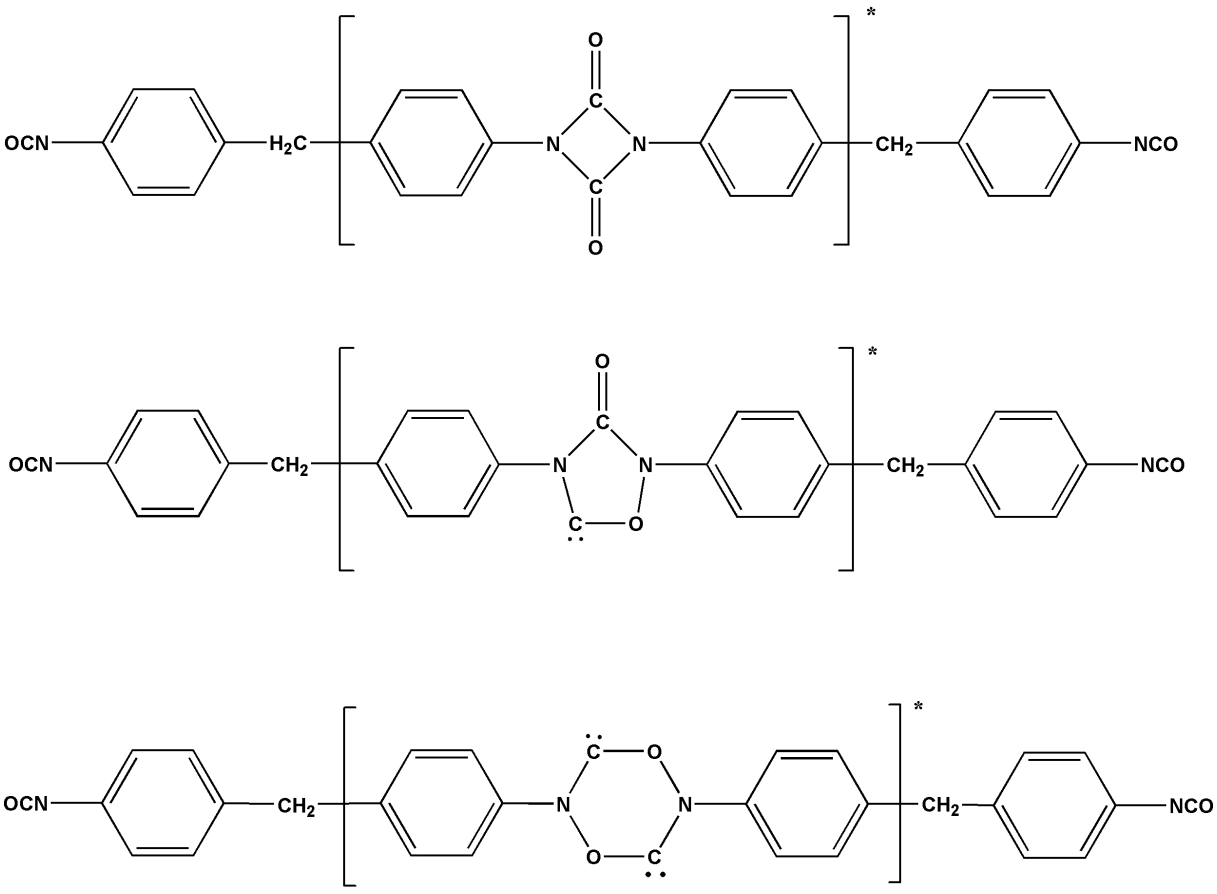


*Only this part of the molecule was calculated

**Figure 33**: MDI dimers with different suzed-rings.

**Table 18**: Relative stability and entropy of the different sized rings formed in the dimerization reaction of the two monomers. thermodynamic properties calculated at M06-2X/6-31G(d,p) level of theory.

| | **$\Delta E°$** | **$\Delta H°$** | **$\Delta G°$** | **$S°$** |
|---|---|---|---|---|
| Type of the ring | *(kJ/mol)* | | | *(J/mol K)* |
| **4-membered ring** | 0.0 | 0.0 | 0.0 | 519.7 |
| **5-membered ring** | 262.5 | 260.6 | 266.6 | 499.7 |
| **6-membered ring** | 660.9 | 659.8 | 664.9 | 502.6 |

Potentially, the -membered ring is the most stable one due to a conjugation inside the ring, which does not occur in the case of the two other rings. It has aromatic properties with 6π electrons *(Figure 34*).

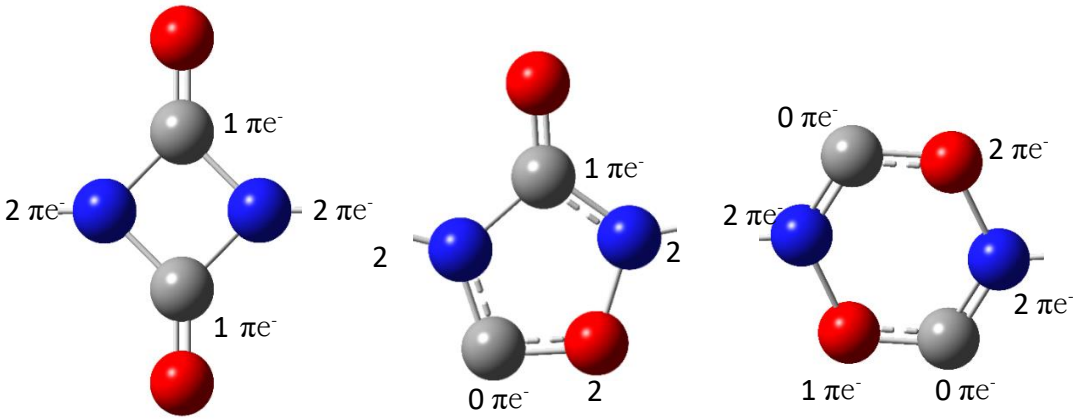


**6 πe⁻** **7 πe⁻** **8 πe⁻**

**Figure 34**: Electron distribution of the 4, 5 and 6 membered rings in the middle of the dimer models of MDI.

This aromatic stabilization overrides the ring strain. The five-membered ring has a divalent carbene-like carbon (it has a σ lone pair and an empty π orbital) which destabilizes this structure. The six-membered ring has 2 carbene-like carbons, which make the structure about twice as destabilized as the four-membered ring. It is anti-aromatic with 8 electrons in π orbitals.

The six-membered ring is twice as unstable as the five-membered ring and the four-membered ring dimers are the most stable ones, thus only those dimers are examined. The entropy values differ only slightly from each other. It is very interesting that the relative total energy, enthalpy, and Gibbs free energy values are very similar within one type of ring.

### *3.3.3 MDI dimers*

Based on the results shown in the previous section the MDI dimers are formed via the reaction of the isocyanate groups, establishing a four-membered (uretidione) ring. With the combination of the three different types of isomers altogether ten dimers can construct. The relative stability and the entropies of the dimers are summarized in *Table 19*. The characterization of the dimers is mostly carried out without considering the thermodynamic conditions (pressure, temperature) (*Table 2).*

Three different clusters are characterized by their relative energies: A, B and C. According to the relative total energy, enthalpy, and Gibbs free energy, there are no significant differences between the dimers in cluster A. These dimers have numerous intrinsic interactions due to the 2,2'-isomers. Cluster B contains another three similar dimers. The differences between the relative energies of these MDI dimers are infinitesimal and the number of secondary bonds is lower. Cluster C includes four dimers which have higher relative energies and enthalpies than the rest. Also, the amount of intrinsic interactions is the lowest. There is a linear correlation between the isomers' interactions and their dimers'. Concerning all of the dimers it could be observed that those having 2,2' or 2,4 isomers are more stable under the examined condition where the effect of the pressure and temperature is neglected. The possibility of H-bond formation within these dimers is even higher. If the methylene group is in the ortho-position in reference to the four-membered ring, the formation of weaker interactions is favorable. In contrast, dimers which have 4,4'- or 4,2 isomers are less stable comparing the relative energies. In these cases, there are fewer possibilities for weak interactions. When the methylene group of the monomer is in the para-position, and the four-membered ring and the benzene ring are in one plane, the probability of the intrinsic interactions occurring is very small. In addition, dimers with 2,4- or 4,4'-isomers are unstable, as the free isocyanate group in the para-position destabilizes the structure. All of the dimers are compared to the most stable dimer, the 4,2-2,4-MDI dimer. The least stable dimer, on the other hand, is the 4,4'-2,4-MDI dimer considering the relative energies. However, in the case of that condition when the pressure and temperature is constant, the most thermodynamically stable dimer is the 4,4'4,4'-MDI dimer.

**Table 19**: Gas phase thermodynamic properties of MDI dimers including relative total electric energy (ΔE°), relative enthalpies (ΔH°), relative Gibbs free energies (ΔG°) and entropies (S°) under standard condition calculated using M06-2X/6-31G(d,p) level of theory.

| Cluster | MDI isomer | **Δ*E*°** | **Δ*H*°** | **Δ*G*°** | **S°** |
|---|---|---|---|---|---|
| | | *kJ/mol* | | | *J /mol K* |
| A | **4,2-2,4** | **0.0** | **0.0** | **5.9** | **860.7** |
| | **2,2-2,4** | 5.2 | 5.4 | 7.2 | 874.3 |
| | **2,2'-2,2'** | 5.7 | 6.1 | 7.7 | 874.8 |
| B | **4,4'-4,2** | 14.1 | 16.6 | 1.3 | 931.8 |
| | **2,4-4,2** | 14.4 | 16.5 | 4.8 | 919.8 |
| | **4,4'-4,4'** | 16.1 | 19.0 | 0.0 | 944.1 |
| C | **2,2'-4,4'** | 18.8 | 20.8 | 7.6 | 924.7 |
| | **2,2'-4,2** | 19.5 | 21.4 | 6.1 | 931.6 |
| | **4,2-4,2** | 22.2 | 23.8 | 14.8 | 910.6 |
| | **4,4-2,4** | 22.3 | 24.4 | 12.5 | 920.2 |

The entropy clustering informs us of the differences of the internal interactions. Two main entropy cluster can be distinguished. In cluster A more, secondary interactions can be formed (lower entropy values) while in cluster B and C only negligible secondary interactions (highest entropy values) occur. The well-ordered dimers (cluster A) have stronger interactions between their isocyanate groups which results in an additional ring formation.

Those dimers which have their methylene groups in the ortho position to the four-membered ring display entropies from 860.7 to 874.8 J/mol K, but dimers which have these groups in the para-position or even in the para- and ortho-positions have entropies in the range of 910.6-944.1 J/mol K. These results are in good correlation with the fact that in the case of the first cluster the central four-membered ring and the adjacent two benzene rings are in one plane, generating higher entropy due to the aromatic property of the four-membered ring and the delocalized 18 electrons. However, when one or two benzene rings are moved from the plane, the entropy was lowered.

The possible dimerization reactions of the monomers, which form differently structured dimers, were also studied. The dimerization reactions were found to be mostly exothermic. From the dimerization reaction, Gibbs free energies and equilibrium constants were calculated at 25°C, 43°C (storage temperature) and 180°C (decomposition

temperature) (*Table 20*). If our system were to contain different monomers, 4,4'-monomer would form the most common dimer. The results are consistent with the experiences. At room temperature the dimer formation is favorable, while at 43-45°C (storage temperature) the dimer formation deceases. At high temperature (for example at 180°C) the dimers are decomposed.

**Table 20**: Reaction Gibbs free energies ($\Delta_r G°$) and equilibrium constants (K) of the dimerization processes calculated on M06-2X level of theory using 6-31G(d,p) basis set.

| MDI dimers | $\Delta_r G°$ (kJ/mol) | K | | |
|---|---|---|---|---|
| | | T=25°C | T=43°C | T=180°C |
| 4,2-2,4 | -9.7 | 50.1 | 40.1 | 33.2 |
| 2,2-2,4 | 0.5 | 0.8 | 0.8 | 0.8 |
| 2,2'-2,2' | 10.0 | 0.0 | 0.0 | 0.0 |
| 4,4'-4,2 | -12.6 | 161.2 | 120.7 | 94.5 |
| 2,4-4,2 | -10.8 | 78.0 | 60.8 | 49.4 |
| 4,4'-4,4' | -12.2 | 137.2 | 103.7 | 81.8 |
| 2,2'-4,4' | 2.6 | 0.3 | 0.4 | 0.4 |
| 2,2'-4,2 | -0.5 | 1.2 | 1.24 | 1.2 |
| 4,2-4,2 | -0.8 | 1.4 | 1.4 | 1.3 |
| 4,4-2,4 | -1.4 | 1.8 | 1.7 | 1.6 |

These computed results prove the assumption that the most reactive isomer is the 4,4'-monomer. The systems containing monomers and dimers are not initially in equilibrium but tend to achieve this state over time. This intermediate status is examined via the dimerization process. The optimized structures of the most likely formed (4,4'-4,2-MDI dimers) and least likely formed product (2,2'-2,2'-MDI dimer) of the dimerization process can be seen in *Figure 35*. In the structures of the most and least likely formed dimers, the positions of the isocyanate groups are different. In the case of the 4,4'-4,2-MDI dimers, these groups are far from each other, thus they have no possibility for intrinsic interactions. The structure of the dimer is in correlation with the monomer structure. In the case of the 4,4-MDI the isocyanate groups are also far from each other, having no steric hindrance and allowing for the monomers to be more reactive. The dimers are formed from the more reactive components. The isocyanate groups are close to each other in the 2,2'–2,2'-MDI dimer. Therefore, the possibility of the intrinsic interactions is higher, but

the reactivity of the 2,2'-monomer components are lower which results in fewer dimers being formed. The results of *Table 20* confirmed the importance of the temperature on the dimerization process.

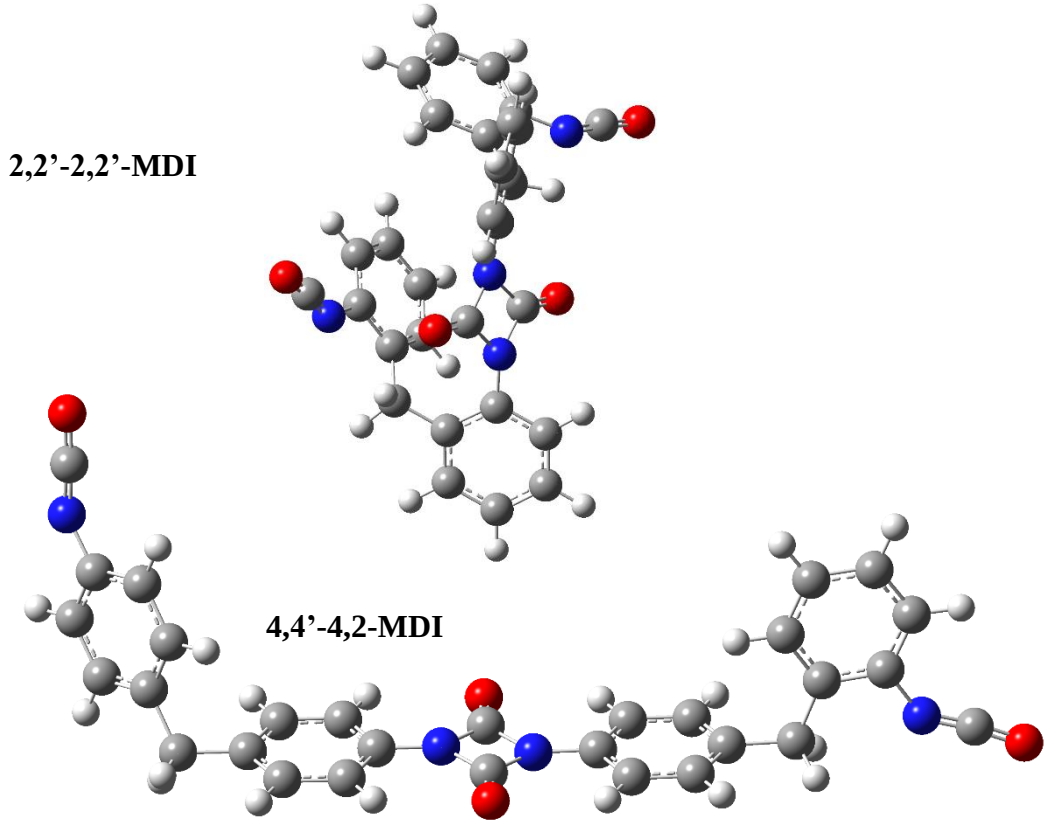


**Figure 35**: Optimized structure of the most preferable MDI dimer (4,4'-4,2) and least preferable MDI dimer (2,2'-2,2').

### *3.3.4 Conclusion*

MDI covalent dimers causes several quality issues during the usage of MDI (e.g. '4-ring structures'), therefore their thermodynamic and structural properties need a better understanding in order to minimize their effect. The following points were explored in our study:

- Among the MDI monomers, the 2,2'-MDI was found to be the most thermodynamically stable, while the industrially preferred isomer, that is 4,4'-MDI isomer, is 7.2 kJ/mol higher in Gibbs free energy according to our results at M06-2X/6-31G(d,p) level of theory.
- Dimers with four-membered ring are the most stable due to the aromatic electronic structure of the uretidione ring. The relative stability of the dimers is therefore influenced by the steric effects and the relative positions of isocyanate groups.

- While MDI dimer with the lowest energy is the 4,2-2,4-MDI dimer, the most thermodynamically stable is turned out to be the 4,4'-4,4'-MDI dimer, however the 4,4'-4,2 dimer has only 1.3 kJ/mol higher standard Gibbs free energy.
- From the thermodynamic point of view, it seems that all the MDI isomers can form dimer with high stability. The reaction Gibbs free energy is the lowest for the 4,4'-4,2-MDI ($\Delta_r G°$=-12.6 kJ/mol),

### *3.3.5 Experimental studies*

As the importance of the MDI dimerization is significant the examination of this side reaction was started from experimental point of view also. To provide exact solution for minimizing the dimerization firstly it might be useful to get more information about the MDI dimer as a pure material. For this purpose, one target of the experimental research was to synthetize pure MDI dimer which can be also used as a standard for analytical measurements.

*Synthesis of MDI dimer*

Based on the literature MDI dimers can be usually synthetized by adding a catalyst to the pure 4,4'-MDI in inert solvent. MDI dimerization can be catalyzed applying catalysts such as trialkyl-phosphines, pyridines, 1,2-dimethyl imidazole, dimethyl-amino pyridine[130]. For stopping the dimerization reaction chloroacetic acid, trichloroacetic acid, methanesulphonic acid, phosphoric acid, chloroformic acid, benzoyl chloride, dimethyl carbamide acid, acetic acid anhydride, succinic acid anhydride, toluene sulphonic acid methyl ester or mixtures thereof can be used as deactivators. As solvents those are generally used which are inert to NCO groups (benzene, toluene, xylene, chlorobenzene, nitrobenzene, acetone, methylethylketone, acetic ester, dioxane, tetrahydrofuran, aliphatic hydrocarbons, ethyl-acetate).

In our research work attempts were made to synthetize 4,4'-MDI dimer according to Kaplan et al[131]. For the synthesis the following chemicals were used: pure 4,4'-MDI, ethylene-acetate, 4-N,N-dimethylamino-pyridine, benzoyl-chloride. The reaction apparatus consisted of a double-walled, cylindrical reaction vessel heated by water-thermostat. To one neck of the reactor a double-walled dropping funnel was connected while to the other neck a gas inlet and a KPG stirrer. The steps of the synthesis were the followings:

- In the reaction vessel temperature controlled to 35°C, 500 ml ethyl-acetate containing 1.0 g 4-N,N-dimethylamino-pyridine was introduced by means of a dropping funnel
- 130.0 g MDI melted at 50°C was added via a dropping funnel temperature controlled to 50°C within 45 min with stirring (the temperature in the reaction vessel remained 35 °C). The stirring took place for another 2 hours at 35 °C
- Thereafter, 1.27 g benzoyl-chloride dissolved in 5 ml ethyl-acetate was added via a dropping funnel within 10 minutes and stirred for another 15 minutes
- Subsequent the batch was cooled to 23°C, and the filtered product was washed twice with 100 ml ethyl-acetate. The inert condition was ensured by nitrogen stream.

The product was light yellow solid material *(Figure 36*).

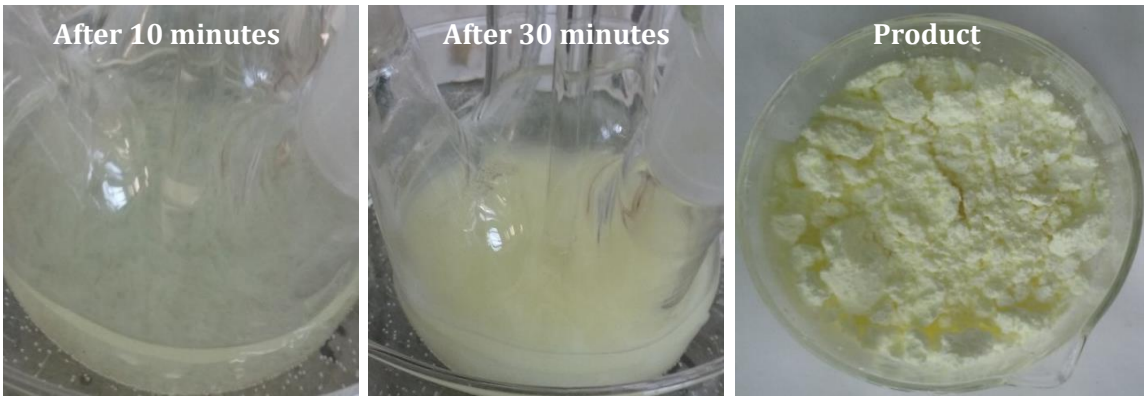


**Figure 36**: Reaction steps of MDI dimer synthesis.

The synthetized MDI dimer was insoluble in several solvents. The tested solvents were the followings: acetone, isopropanol, 1,4-dioxane, tetrahydrofuran toluene, dimethyl sulfoxide, dichloromethane. Samples were treated by ultrasonic process, but the solubility of the dimer remained poor. Boiling of the solvent-dimer mixture had no effect on the solubility. Because of the insolubility of the MDI dimer the accurate analysis of it was impossible. The only analytical techniques which was able to be applied was the infrared spectroscopy (IR, Section 3.2.4). This method is good for determining the dimer ratio or dimer percentage, taking the ratio of the phenyl ring and carbonyl ring. but inappropriate for qualitative analysis. Based on the bottle-neck of the sample preparation the precious analytical identification of the synthetized MDI dimer was not finished in the current research but is it the target of the subsequent study.

*Decomposition of MDI dimer*

Industrially it could be a serious problem if the product MDI has high dimer content. It is necessary to find out an efficient method to decrease the dimer content. Based on the calculations the structure of the dimer highly influences its stability. The formed uretidione ring makes the structure very stable which cause problems in the decomposition of the dimers. The most important parameter which influences the dimer formation is the temperature. Based on the industrial experiences[52,128] the MDI is stored at 40-45°C or in frozen state to avoid the dimer formation. For the decomposition of the dimers there is pure information in the literature. The target of our experiment was to find the appropriate temperature at which the dimer content can be reduced within a short time. Some MDI samples were stored under inappropriate condition for a longer time to generate dimer formation inside. After that the samples were heated up to 180 and 200°C. The results are illustrated in *Figure 37*. The dimer ratio was decreased from the initial 4.9/4.7 dimer ratio to <2 within 10 minutes and achieved 1 ratio after 30 minutes. The higher temperature (200°C) was more efficient but there was no big difference between the two tested temperature degrees. Evaluating the achieved results for the dimer decomposition it is suggested to heat up the sample to at least 180°C until at least 10 minutes. For higher efficiency 30 minutes residence time is recommended

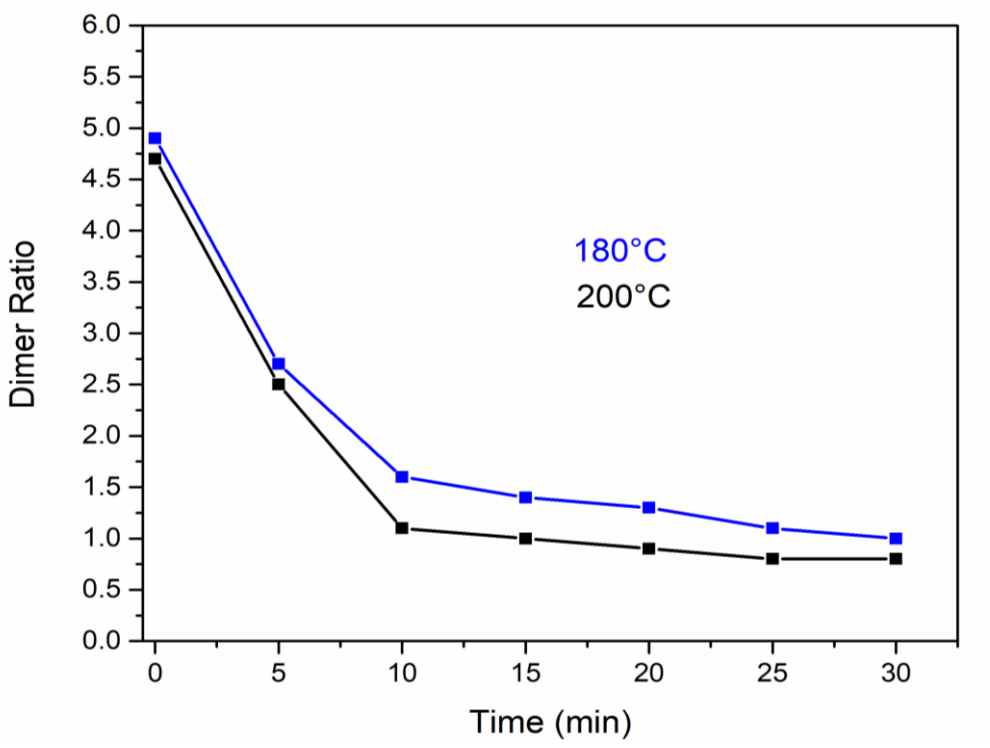


**Figure 37**: Dimer ratio as function of time.

*Experiences and main consequences*

Based on the calculations it was found that dimerization of MDI resulted in ten different type of MDI dimer structures. Most probably dimers via 4-membered ring containing 4,4'-isomers are formed. Due to the stable uretidione ring dimers should be stable materials. The synthesis of MDI dimers confirmed the stability of this material. The produced MDI dimer was solid, yellow, non-degradable, tangible, easy to handle material. The synthesis was simple, the product was precipitated easily. MDI dimer was insoluble in solvents which makes impossible to analyze it preciously by standard analytical methods such as HPLC. The decomposition of dimer content of the pure 4,4'-MDI was achieved only at very high temperature (min 180 °C). This experience also refers to the ascertainment that the MDI dimers are stable compounds. The formation of them highly depends on the temperature which plays a key parameter during the storage and transport of the MDI.

# 4 NEW SCIENTIFIC RESULTS – THESES

As a consequence of the results of MDI production study introduced in Section 3 the following main conclusions were decided as new scientific results:

*Reaction Mechanism of MDA synthesis*

**1st Thesis**

A new reaction mechanism of MDA synthesis has been explored on elementary level consisting of eight reaction steps including condensation and rearrangement steps. Novelty of this study is that in the initial reaction step a non-covalent aniline dimer is reacted with formaldehyde. This hypothetical aniline dimer is based on experimental observation (e.g. high viscosity of aniline, scattering experiments).

- The global minimum at this reactive potential energy surface was found to be the N-(p-aminobenzyl)anilinium (protonated PABA, $PABAH^+$), being along with the line with experimental observation of PABA during MDA production. Two steps rearrangement of aniline resulted the protonated MDA isomers ($MDAH^+$). The species in our proposed mechanism are proton activated. They got more acidic in aniline (basic) environment which can then deactivate the intermediates.

- The significant solvent effect (water and aniline) on the energetics of MDA mechanism was found. It lowers the highest lying transition (N-hydroxymethylaniline) state by 12.7 kJ/mol.

**2nd Thesis**

Among the main reaction mechanism uncertain side reactions were also examined by computation. Our results confirmed that the aminal formation ($AMH^+$), is both thermodynamically and kinetically preferable than the formation of $PABAH^+$ but it is a kinetic dead-end in the same time. The aniline addition in ortho position (formation of 2,4'-MDA) is competitive with that of in the para position (formation of 4,4'-MDA) from both kinetic and thermodynamic points of view. The preference of the formation of 4,4'-MDA can be hypothesized over MDA oligomer formation as intermediate.

*Reaction Mechanism of MDA phosgenation*

**3rd Thesis**

'Phosgenations first': both amino groups transformed to carbamoyl chloride groups giving [methylenebis(4,1-phenylene)]dicarbamic chloride and then two endothermic HCl-elimination steps occurs. 'Stepwise phosgenations': One of the amino groups of MDA turns into isocyanate by phosgene and then the other amine does. The 'Phosgenation first' mechanism is the energetically more favourable pathway.

**4th Thesis**

The activation barriers for both phosgenation mechanisms were found to be high in the gas phase, while all the reaction barriers are dramatically reduced in ODCB. making the incorporation of the first phosgene occurred in ODCB via submerge transition state. The reaction with the second phosgene has also low-lying transition state in this case.

- Accurate standard enthalpy of formation was determined for MDI (14.8 kJ/mol) with the uncertainty of 5.2 kJ/mol. This value was compared with the uncertain literature standard enthalpies of formation for MDI.
- The ionic complex ($IM1H^+ \times Cl^-$) has relatively high stability at industrial conditions which might inhibit the second phosgene to incorporate both sterically and energetically. MDA can also form such charge separated complex with HCl (when

there is a large excess HCl in the reactor) due to such thermodynamically preference. This may decrease the reactivity of MDA towards phosgene.

- Only moderate effect on the relative enthalpies and Gibbs free energies found by changing in the temperature and pressure range of the industrial operation (90°C < T < 160°C and 6 bar < p < 11 bar).

*MDI Dimer Structures*

**5thThesis**

The 4,4'-MDI dimer with four-membered ring is the most stable among the studied dimers due to its aromatic electronic structure of the uretidione ring.

- The relative stability of the dimers is influenced by the steric effects and the relative positions of isocyanate groups.
- Among the MDI monomers, the 2,2'-MDI was found to be the most thermodynamically stable, while the industrially preferred isomer, that is the 4,4'-MDI.

**6th Thesis**

While MDI dimer with the lowest energy is the 4,2-2,4-MDI dimer formed from a 4,2 and a 2,2'-MDI monomer, the most thermodynamically stable is turned out to be 4,4'-4,4'-MDI dimer.

- Considering equilibrium for the MDI dimerization, the reaction Gibbs free energy is the lowest for the 4,4'-4,2'-MDI ($\Delta_r G°$=-12.6 kJ/mol), but the formation of 4,4'-4,4'-MDI is just slightly more endergonic ($\Delta_r G°$=-12.2 kJ/mol).

# 5 SUMMARY

However, methylene diphenyl diisocyanate (MDI) is one of the most important raw material of polyurethane industry the reaction mechanism of its synthesis is poorly understood. The purpose of this research was to study the reactions of the industrial MDI production at molecular level. The MDI production consists of two main reaction processes: the appropriate amine formation, that is methylene diphenyl diamine (MDA) and phosgenation of the previously synthetized MDA. Amongst the large number of side reactions at different stage of the MDI synthesis, for instance, dimerization of the MDI is identified as serious issues in polyurethane production (e.g. plugging).

Reaction mechanism of the MDA formation from aniline and formaldehyde was explored using G3MP2B3 quantum chemical method in gas phase and in industrially relevant solvents (aniline and water). It was found that the non-covalent aniline dimer approaches formaldehyde to form the pre-reactive complex from which eight elementary reaction steps resulted in 4,4'-MDA as the final product including the formation of the protonated N-(p-aminobenzyl)anilin (PABA) intermediate. The formation of the neutral PABA was confirmed by gas chromatography. Theoretical mechanism including the condensation and rearrangement can also be supported by the experimental finding shown in this work. The hypothesis of the formation and disintegration of larger ring structures which needed for the explanation of the MDA isomer distribution is proven by the measured values. The isomer- and ring (defined as a number of phenyl group in the MDI monomer)-distribution in the MDI product is mainly established during the MDA formation. Results in gas phase were compared to mechanism in aqueous and aniline solutions where the highest lying transition state, which belongs to formaldehyde addition, was lowered by at 12.7 kJ/mol. The highest decrease in relative energy was observed in the case of the deprotonation of the $MDAH^+$.

The consecutive industrial process is the phosgenation of the produced MDA, which can be carried out in ODCB solvent under pressure (90-150°C and 6-11 bar pressure). The reaction mechanism of phosgenation was also accomplished using G3MP2B3 composite method such as in the case of MDA synthesis. The formation of MDI is possible via two different mechanisms: 'Phosgenations first' and 'Stepwise phosgenations'. The activation barriers for both phosgenation mechanisms are high in the gas phase, while all the reaction barriers are dramatically reduced in ODCB. The most stable intermediate (IM2A)

of the phosgenation is confirmed by IR spectroscopy. Promoting the decomposition of the *in situ* generated intermediate toward the product MDI formation the sample of intermediate was heated to 90-140$^0$C to overcome the high activation barrier (102.6 kJ/mol). In the theoretical investigation, we found that the thermodynamically stabile charge separated amine hydrochloride intermediate can mask the amine toward phosgene. Gas phase thermodynamic properties were also determined in the case of MDA and MDI synthesis. Accurate standard enthalpy of formation was recommended for the reactants, products and intermediates compared to the literature values.

Group additivity increments for NCO and NHCOCl groups linked to phenyl ring were proposed ($\Delta_{f,i}H°$(-NCO) = -61.2 kJ/mol and $\Delta_{f,i}H°$(-NHCOCl)=-195.0 kJ/mol). These data were provided for industrial application.

The last section of this study deals with one of the important side reaction of MDI synthesis, that is the dimerization of MDI isomers causing issues during storage or transport. Beside the thermodynamic description of the MDI isomers, the most plausible dimers were characterized structurally and thermodynamically. Altogether ten different dimers can be formed via a four-membered ring (uretidione) depending on the relative positions of isocyanate groups. The most thermodynamically stable dimer was found to be the 4,4'-4,4'-MDI dimer. The stability of the MDI dimers was proven experimentally by the fact that they were able to be decomposed only above 180°C.

# 6 ÖSSZEFOGLALÓ

A metilén difenil diizocianát (MDI) a poliuretángyártás egyik legfontosabb alapanyaga, előállításának reakciómechanizmusáról ennek ellenére nagyon keveset tudunk. Az alábbi tanulmány célja az volt, hogy az ipari előállítás folyamatait molekuláris szinten vizsgálja, ezáltal is közelebb kerülve a folyamatok megértéséhez. Az MDI előállítása két fő lépésből áll: a szükséges amin metilén difenil diamin (MDA) előállítása majd ezt követően annak foszgénezése. A fő reakciók mellett, azonban számolni kell mellékreakciók lejátszódásával is, amelyek közöl a dimerképződés az egyik legjelentősebb (pl. okozhat alkalmazástechnikai problémákat).

Vizsgálatainkat az első lépés - *MDA szintézis* - tanulmányozásával kezdtük. A termék izomer- és gyűrűeloszlását ennél a lépésnél határozzuk meg. Az MDI gyártásban kulcsfontosságú ez a folyamat, hiszen az itt képződött melléktermékek befolyásolni fogják a késztermék minőségét. Az MDA előállítása anilin és formaldehid reakciójával sósav katalizátor jelenlétében történik. A reakció mechanizmusát G3MP2B3 kvantumkémiai módszert alkalmazva, gázfázisban és ipari szempontból releváns oldószerekben (anilin és vízz) vizsgáltuk. Az irodalomban felvázolt reakciómechanizmust módosítottuk, figyelembe véve a legvalószínűbb mellékreakciókat, illetve a kulcsfontosságú köztitermékek savi erősségét. Feltételezzük, hogy a reakció első lépésében nem kovalens kötésű anilin dimer lép reakcióba a formaldehiddel pre-reaktív komplexet képezve, amelyet követően nyolc elemi lépésen keresztül történik meg a termék kialakulása protonált N-(p-aminobenzil)anilin (PABA) köztiterméken keresztül. A PABA képződését gázkromatográfiás vizsgálattal igazoltuk. A felvázolt reakciómechanizmusban taglalt kondenzációs és átrendeződéses lépések lefolyását kísérleti úton bizonyítottuk. Az MDA izomerek kialakulásához vezető többgyűrűs molekulák képződését, valamint szétesését a kísérleti eredmények alátámasztják. Az oldószerekben (víz és anilin) számolt eredményeket összevetettük a gázfázisú mechanizmussal, ahol azt tapasztaltuk, hogy a formaldehid addíciójához tartozó legmagasabb relatív energiájú átmeneti állapot 12.7 kJ/mol energiával csökkent. A legnagyobb relatív energia csökkenést az utolsó lépésnél tapasztaltuk, az $MDAH^+$ deprotonálódásánál.

Vizsgálatainkat az MDI gyártás következő lépésének, az MDA foszgénezés reakciómechanizmusának tanulmányozásával folytattuk, amelyet orto-diklórbenzol oldószerben, 90-150°C-on és 6-11 bar is végezhetnek. A foszgénezés mechanizmusát is G3MP2B3 kompozit módszerrel vizsgáltuk, az MDA mechanizmusához hasonlóan. Két

reakcióútvonal lehetséges a „foszgénezés először” illetve a „lépcsőzetes foszgénezés”. A „foszgénezés először” típusú mechanizmus energetikailag kedvezőbbnek bizonyult. Az aktiválási gátak mindkét reakció esetében gázfázisban jelentősen magasak, míg az összes reakciógát drasztikusan lecsökken már az első foszgén beépülésekor ODCB oldószerben un. negatív aktiválási energiájú átmeneti állapoton keresztül. A foszgénezés legstabilabb intermedierét (IM2A) infravörös spektroszkópiával (IR) bizonyítottuk. Az *in situ* előállított köztitermék bomlását termikusan (90-130°C) vizsgáltuk, ehhez a lépéshez tartozó a magas energiagátat (102.6 kJ/mol) sikerült áthidalni. Azt tapasztaltuk, hogy a termodinamikailag stabil töltésszeparált amin-hidroklorid köztitermék jelenléte gátolja a foszgén molekula reakcióját az aminnal. A gázfázisú számolások útján G3MP2B3 elméleti módszerrel meghatároztuk az egyes köztitermékek, reaktánsok és termékek standard képződési entalpiát, entrópiát és hőkapacitást atomizációs séma szerint. Javaslatot tettünk csoportadditív hozzájárulások kiszámolására a fenil gyűrűhöz kapcsolódó NCO és NHCOCl funkciós csoportok esetében ($\Delta_{f,i}H°$(-NCO)=-61.2 kJ/mol and $\Delta_{f,i}H°$(-NHCOCl)=-195.0 kJ/mol. Ezeket az adatokat javasoltuk ipari használatra, amelyeket alkalmazva a számolások pontosabbá váltak

Az alábbi tanulmány utolsó része az MDI szintézis egyik jelentős mellékreakcióval foglalkozik, az MDI dimerizálódásával, amely nem megfelelő tárolás és szállítás esetében jelentkezik. Az MDI izomerek termodinamikai tárgyalása mellett, a legjelentősebb dimer szerkezeteket határoztuk meg. Összesen tíz különböző típusú MDI dimer képződhet egy négytagú gyűrű (uretidion) kialakulásával. Szerkezetük kialakulására befolyással van az izocianát csoportok sztérikus hatása és relatív helyzete. A termodinamikailag legstabilisabnak a 4,4’-4,4’-MDI dimer mutatkozott. Az MDI dimerek stabilitását támasztja alá az a kísérleti tapasztalat, miszerint csak magas hőmérsékelten (180°C) bomlanak.

# 7 REFERENCES


(1) Randall, D.; Lee, S. *The Polyurethanes Book*; Huntsman International LLC Polyurethanes, 2002.

(2) Sonnenschein, M. F. *Polyurethanes: Science, Technology, Markets, and Trends*; John Wiley & Sons, Inc, 2014.

(3) Bayer, O. Das Di-Isocyanat-Polyadditionsverfahren (Polyurethane). *Angew. Chemie* **1947**, *59* (9), 257–272.

(4) Wurtz, A. Ueber Die Verbindungen Der Cyanursaure Und Cynaure Mit Aethyloxyd, Methyloxyd, Amyoxyd Und Dies Daraus Enstehenden Prosucte; Acetyl- Und Metacetylharnstoff, Methylamin, Aethylamin, Valeramin. *241* (1848), 326–342.

(5) Maisonneuve, L.; Lamarzelle, O.; Rix, E.; Grau, E.; Cramail, H. Isocyanate-Free Routes to Polyurethanes and Poly(Hydroxy Urethane)S. *Chem. Rev.* **2015**, *115* (22), 12407–12439.

(6) Delebecq, E.; Pascault, J.; Boutevin, B.; Ganachaud, F. On the Versatility of Urethane/Urea Bonds: Reversibility , Blocked. *Chem. Rev.* **2013**, *113*, 80–118.

(7) Kathalewar, M. S.; Joshi, P. B.; Sabnis, A. S.; Malshe, V. C. Non-Isocyanate Polyurethanes: From Chemistry to Applications. *RSC Adv.* **2013**, *3* (13), 4110–4129.

(8) Guan, J.; Song, Y.; Lin, Y.; Yin, X.; Zuo, M.; Zhao, Y.; Tao, X.; Zheng, Q. Progress in Study of Non-Isocyanate Polyurethane. *Ind. Eng. Chem. Res.* **2011**, *50* (11), 6517–6527.

(9) Pyo, S.-H.; Persson, P.; Mollaahmad, M. A.; Sörensen, K.; Lundmark, S.; Hatti-Kaul, R. Cyclic Carbonates as Monomers for Phosgene- and Isocyanate-Free Polyurethanes and Polyccarbonates. *Pure Appl. Chem* **2012**, *84* (3), 637–661.

(10) Blattmann, H.; Fleischer, M.; Bähr, M.; Mülhaupt, R. Isocyanate- and Phosgene-Free Routes to Polyfunctional Cyclic Carbonates and Green Polyurethanes by Fixation of Carbon Dioxide. *Macromol. Rapid Commun.* **2014**, *35* (14), 1238–1254.

(11) Szycher, M. *Szycher's Handbook of Polyurethanes*; 2010.

(12) Hofmann, A. W. Annalen Der Chemie Und Pharmacie. **1850**, *74* (2).

(13) Hentschel, W. Phosgenroute Ersterwähnung. *Chem. Ber* **1884**, *17*, 1284–1289.

(14) Allport, D. C.; Gilbert, D. S.; Outterside, S. M. *MDI and TDI: Safety, Health and the Environment: A Source Book and Practical Guide*; 2003.

(15) Wegener, G.; Brandt, M.; Duda, L.; Hofmann, J.; Klesczewski, B.; Koch, D.; Kumpf, R. J.; Orzesek, H.; Pirkl, H. G.; Six, C.; et al. Trends in Industrial Catalysis in the Polyurethane Industry. *Appl. Catal. A Gen.* **2001**, *221* (1–2), 303–335.

(16) Mordor Intelligence. *Global Methylene Diphenyl Di-Isocyanate (MDI) Market*; 2018.

(17) Moore, W. M. Amines, Aromatic, Methylenedianiline. In *Kirk-Othmer Encyclopedia of Chemical Technology*; Grayson, M., Ed.; John Wiley and Sons, 2007; pp 338–348.

(18) Metcalf, R. L. Insect Control. *Ullmann's Encycl. Ind. Chem.* **2000**, 264–322.

(19) Haynes, W. M. *CRC Handbook of Chemistry and Physics*, 91st ed.; CRC Press Inc., 2010.

(20) Ulrich, H. *Chemistry and Technology of Isocyanates*; J. Wiley & Sons: New York, 1996.

(21) Mustata, F. R.; Tudorachi, N.; Bicu, I. Epoxy Resins Cross-Linked with Bisphenol A/Methylenedianiline Novolac Resin Type: Curing and Thermal Behavior Study. *Ind. Eng. Chem. Res.* **2012**, *51* (25), 8415–8424.

(22) Perkins, G. T. Process for the Preparation of 4,4'-Methylenedianiline. U.S. Patent 3,367,969, 1968.

(23) Botella, P.; Corma, A.; Carr, R. H.; Mitchell, C. J. Towards an Industrial Synthesis of Diamino Diphenyl Methane (DADPM) Using Novel Delaminated Materials: A Breakthrough Step in the Production of Isocyanates for Polyurethanes. *Appl. Catal. A Gen.* **2011**, *398* (1–2), 143–149.

(24) de Angelis, A.; Ingallina, P.; Perego, C. Solid Acid Catalysts for Industrial Condensations of Ketones and Aldehydes with Aromatics. *Ind. Eng. Chem. Res.* **2004**, *43* (5), 1169–1178.

(25) Nafziger, I. J. L.; Jackson, L.; Rader, L. A.; Seward, I. J.; Jackson, L. Process for Preparing Polyamines with Ion Exchange Resin Catalysts. U.S. Patent 4,554,378, 1985.

(26) Corma, A.; Botella, P.; Mitchell, C. Replacing HCl by Solid Acids in Industrial Processes: Synthesis of Diamino Diphenyl Methane (DADPM) for Producing Polyurethanes. *Chem. Commun.* **2004**, *10* (17), 2008–2010.

(27) Salzinger, M.; Fichtl, M. B.; Lercher, J. A. On the Influence of Pore Geometry and Acidity on the Activity of Parent and Modified Zeolites in the Synthesis of Methylenedianiline. *Appl. Catal. A Gen.* **2011**, *393* (1–2), 189–194.

(28) Keller, T. C.; Arras, J.; Wershofen, S.; Perez-Ramirez, J. Design of Hierarchical Zeolite Catalysts for the Manufacture of Polyurethane Intermediates. *ACS Catal.* **2015**, *5* (2), 734–743.

(29) Tian, J.; An, H.; Cheng, X.; Zhao, X.; Wang, Y. Synthesis of 4,4′-Methylenedianiline Catalyzed by SO<inf>3</Inf>H-Functionalized Ionic Liquids. *Ind. Eng. Chem. Res.* **2015**, *54* (31), 7571–7579.

(30) Wang, C. Y.; Li, H. Q.; Wang, L. G.; Cao, Y.; Liu, H. T.; Zhang, Y. Insights on the Mechanism for Synthesis of Methylenedianiline from Aniline and Formaldehyde through HPLC-MS and Isotope Tracer Studies. *Chinese Chem. Lett.* **2012**, *23* (11), 1254–1258.

(31) Crescentini, T. M.; May, J. C.; Forsythe, J. G.; Stow, S. M.; Hercules, D. M.; McLean, J. A. Structural Characterization of Methylenedianiline Regioisomers by Ion Mobility-Mass Spectrometry, Tandem Mass Spectrometry, and Computational Strategies. 3. MALDI Spectra of 2-Ring Isomers. *Anal. Chem.* **2017**, *89* (18), 9900–9910.

(32) Benson, H. An Outer Approximation Algorithm for Generating All Efficient Extreme Points in the Outcome Set of a Multiple Objective Linear Programming Problem. *J. Glob. Optim.* **1998**, *13* (1), 1–24.

(33) Boros, R. Z.; Koós, T.; Wafaa, C.; Nehéz, K.; Farkas, L.; Viskolcz, B.; Szőri, M. A Theoretical Study on the Phosgenation of Methylene Diphenyl Diamine (MDA). *Chem. Phys. Lett.* **2018**, *706*, 568–576.

(34) Viskolcz, B.; Bérces, T. Enthalpy of Formation of Selected Carbonyl Radicals from Theory and Comparison with Experiment. *Phys. Chem. Chem. Phys* **2000**, *2*, 5430–5436.

(35) Marsi, I.; Viskolcz, B.; Seres, L. Application of the Group Additivity Method to Alkyl Radicals: An Ab Initio Study. *J. Phys. Chem. A* **2000**, *104* (19), 4497–4504.

(36) Merenov, A. S.; Jewell, D. W.; Gillis, P. A.; Jansma, G. I.; Breed, A. W.; Anderson, J. J.; Reed, D. J. Process for the Production of Methylene Diphenyl Diisocyanate Isomer Mixtures with Specific Isomer Distributions and New Products Derived. US20130172604 A1, 2013.

(37) Powers, E. L. Process for the Preparation of Halogenated Isoyanates. U.S.Patent 3,277,137A, 1966.

(38) *The Merck Index - An Encyclopedia of Chemicals, Drugs, and Biologicals*; O'Neil, M. J., Ed.; Merck and Co., Inc.: Whitehouse Station, NJ, 2006.

(39) Szycher, M. *Szycher's Handbook of Polyurethanes*, 2nd ed.; CRC Press Taylor & Francis Group, 2013.

(40) Wang, C.; Li, H.; Cao, Y.; Liu, H.; Hou, X.; Zhang, Y. Thermodynamic Analysis on Synthesis of 4,4-Methylenedianiline by Reaction of Aniline and Formaldehyde. *CIESC* **2012**, *63* (8), 2348–2355.

(41) Zhuravlev, E. Z.; Selivanov, V. D.; Mulyanov, P. V.; Konstantinov, I. I. Physicochemical Properties of 4,4-Diyclohexylmethane Diisocyanate. *Zhurnal Prikl. Khimii* **1975**, *48* (5), 1091–1094.

(42) Boros, R. Z.; Rágyanszki, A.; Csizmadia, I. G.; Fiser, B.; Guljas, A.; Farkas, L.; Viskolcz, B. Industrial Application of Molecular Computations on the Dimerization of Methylene Diphenyl Diisocyanate. *React. Kinet. Mech. Catal.* **2018**, *124*, 1–14.

(43) Babad, H.; Zeiler, A. G. Chemistry of Phosgene. *Chem. Rev.* **1973**, *73* (1), 75–91.

(44) Gibson, E. K. Amine Hydrochloride Salts: A Problem in Polyurethane Synthesis (PhD Thesis), University of Glasgow, 2007.

(45) Gibson, E. K.; Winfield, J. M.; Muir, K. W.; Carr, R. H.; Eaglesham, A.; Gavezzotti, A.; Lennon, D. A Structural and Spectroscopic Investigation of the Hydrochlorination of 4,4'-Methylenedianiline. *Phys. Chem. Chem. Phys.* **2010**, *12* (15), 3824–3833.

(46) Entelis, S. G.; Nesterov, O. V. Kinetics and Mechanism of the Reactions of Isocyanates with Compounds Containing Active Hydrogen. *Russ. Chem. Rev.* **1966**, *35* (12), 917–930.

(47) Sanders, J.; Brummer, H.; Laue, J.; Sojka, B.; Eichman, M.; Haverkamp, V. Gas Phase Phosgenation Process. U.S. Patent 2,007,004,323,3A1, 2007.

(48) Mattke, T.; Olbert, G.; Knoesche, C.; Schelling, H. Method for Producing Diisocyanates by Gas-Phase Phosgenation. U.S. Patent 8,716,517, B2, 2014.

(49) Wolfert, A.; Muller, C.; Strofer, E.; Weber, M.; Pfeffinger, J.; Knosche, C. Moderate-Pressure Gas Phase Phogenation. U.S. Patent 2,005,027,291,0A1, 2005.

(50) Knauf, T.; Wolfgang, L.; Friedhelm, S.; Rainer, B.; Wolfgang, T. Process for Operating a Gas Phase Phosgenation Plant. U.S.Patent 2,017,009,638,9A1, 2017.

(51) Fiser, B.; Cuerva, J. M.; Gómez-Bengoa, E. Baldwin-Type Rules for Metal-Controlled Intramolecular Migratory Insertions. A Computational Study of Ni, Pd, and Pt Case. *Organometallics* **2018**, *37* (3), 390–395.

(52) BASF Corporation. *Polyurethane MDI Handbook*; 2000.

(53) Schwarcz, A.; Brindell, G. D. Preparation of Diisocyanate Dimers in Aqueous Medium. US3489744 A, 1970.

(54) Edelmann, M.; Gedan-Smolka, M.; Heinrich, G.; Lehmann, D. Thermokinetic Analysis of Two-Step Curing Reactions in Melt. *Thermochim. Acta* **2006**, *452* (1), 59–64.

(55) Spyrou, E.; Metternich, H. J.; Franke, R. Isophorone Diisocyanate in Blocking Agent Free Polyurethane Powder Coating Hardeners: Analysis, Selectivity, Quantumchemical Calculations. *Prog. Org. Coatings* **2003**, *48* (2–4), 201–206.

(56) Schmitt, F.; Wenning, A.; Weiss, J. V. Dimeric Isocyanates in Polyurethane Powder Coatings. *Prog. Org. Coatings* **1997**, *34* (1–4), 227–235.

(57) Ahangari, M. G.; Fereidoon, A.; Ganji, M. D. Density Functional Theory Study of Epoxy Polymer Chains Adsorbing onto Single-Walled Carbon Nanotubes: Electronic and Mechanical Properties. *J. Mol. Model.* **2013**, *19* (8), 3127–3134.

(58) Shundalau, M. B.; Chybirai, P. S.; Komyak, A. I.; Zazhogin, A. P.; Ksenofontov, M. A.; Umreiko, D. S. Modeling of Structures and Calculation of IR Vibrational Spectra of N,N-Dimethylformamide Dimers by Density Functional Theory. *J. Appl. Spectrosc.* **2011**, *78* (3), 326–336.

(59) Leszczynski, J. *Computational Chemistry: Reviews of Current Trends*; Computational Chemistry: Reviews of Current Trends; WORLD SCIENTIFIC, 2001; Vol. 6.

(60) Errol G., L. *Computational Chemistry*, Third Edit.; Springer, 2016.

(61) Deglmann, P.; Schäfer, A.; Lennartz, C. Application of Quantum Calculations in the Chemical Industry - An Overview. *Int. J. Quantum Chem.* **2015**, *115* (3), 107–136.

(62) James B. Foresman and Aeleen Frisch. *Exploring Chemistry with Electronic Structure Methods*; Gaussian 09 Revision E.1, Ed.; 2015.

(63) IUPAC Gold Book http://goldbook.iupac.org.

(64) Hartree, D. The Wave Mechanics of an Atom with a Non-Coulomb Central Field. Part I. Theory and Methods. *Math. Proc. Cambridge Philos. Soc.* **1928**, *24* (01), 89–110.

(65) Hartree, D. The Wave Mechanics of an Atom with a Non-Coulomb Central Field. Part II. Some Results and Discussion. *Math. Proc. Cambridge Philos. Soc.* **1928**, *24* (01), 111–132.

(66) Roothaan C.C.J. New Developments in Molecular Orbital Theory. **1951**, *23* (2), 69–89.

(67) Møller, C.; Plesset, M. S. Note on an Approximation Treatment for Many-Electron Systems. **1934**, *46* (1), 618–622.

(68) Frisch, M. J.; Head-Gordon, M.; Pople, J. A. A Direct MP2 Gradient Method. *Chem. Phys. Lett.* **1990**, *166* (3), 275–280.

(69) Pople, J. A.; Head-Gordon, M.; Raghavachari, K. Quadratic Configuration Interaction. A General Technique for Determining Electron Correlation Energies. *J. Chem. Phys.* **1987**, *87* (10), 5968–5975.

(70) Bartlett, R. J.; Purvis, G. D. Many-body Perturbation Theory, Coupled-pair Many-electron Theory, and the Importance of Quadruple Excitations for the Correlation Problem. *Int. J. Quantum Chem.* **1978**, *14* (5), 561–581.

(71) Purvis, G. D.; Bartlett, R. J. A Full Coupled-Cluster Singles and Doubles Model: The Inclusion of Disconnected Triples. *J. Chem. Phys.* **1982**, *76* (4), 1910–1918.

(72) Kohn, W.; Becke, A. D.; Parr, R. G. Density Functional Theory of Electronic Structure. *J. Phys. Chem.* **1996**, *100* (31), 12974–12980.

(73) Equations, S.; Effects, C. Self-Consistent Equations Including Exchange and Correlation Effects*. *Phys. Rev.* **1965**, *385* (1951).

(74) Fekete, A. A Papain Enzimmechanikusának Elméleti Vizsgálata És a Humán Transzglutamázok Aktivációjának Korai Eseményei, Debreceni Egyetem, 2019.

(75) Zhao, Y.; Truhlar, D. G. The M06 Suite of Density Functionals for Main Group Thermochemistry, Thermochemical Kinetics, Noncovalent Interactions, Excited States, and Transition Elements: Two New Functionals and Systematic Testing of Four M06-Class Functionals and 12 Other Functionals. *Theor Chem Acc.* **2008**, *120* (1–3), 215–241.

(76) Rokob, T. A.; Hamza, A.; Pápai, I. Computing Reliable Energetics for Conjugate Addition Reactions. *Org. Lett.* **2007**, *9* (21), 4279–4282.

(77) Walker, M.; Harvey, A. J. A.; Sen, A.; Dessent, C. E. H. Performance of M06, M06-2X, and M06-HF Density Functionals for Conformationally Flexible Anionic Clusters: M06 Functionals Perform Better than B3LYP for a Model System with Dispersion and Ionic Hydrogen-Bonding Interactions. *J. Phys. Chem. A* **2013**, *117* (47), 12590–12600.

(78) Zhao, Y.; Truhlar, D. G. Density Functional Theory for Reaction Energies: Test of Meta and Hybrid Meta Functionals, Range-Separated Functionals, and Other High-Performance Functionals. *J. Chem. Theory Comput.* **2011**, *7* (3), 669–676.

(79) Johnson, B. G.; Gill, P. M. W.; Pople, J. A. The Performance of a Family of Density Functional Methods. *J. Chem. Phys.* **1993**, *98* (7), 5612–5626.

(80) Becke, A. D. Density-Functional Thermochemistry. III. The Role of Exact Exchange. *J. Chem. Phys.* **1993**, *98* (7), 5648–5652.

(81) Review, P. Density-Functional Exchange Approximation with Correct Asymptotic Behaviour. *Phys. Rev. A* **1988**, *38* (6), 3098–3100.

(82) Lee, C.; Hill, C.; Carolina, N. Into a Functional of the Electron Density f F. **1988**, *37* (2).

(83) Samuel, D. The Journal of Hepatology: An International Journal in a New Era. *J. Hepatol.* **2012**, *56* (1), 4.

(84) Becke, A. D. Perspective: Fifty Years of Density-Functional Theory in Chemical Physics. *J. Chem. Phys.* **2014**, *140* (18).

(85) Szőri, M. Telítetlen Szénhidrogének Gyökös Reakcióinak Elméleti Vizsgálata, 2008.

(86) Baboul, A. G.; Curtiss, L. A.; Redfern, P. C.; Raghavachari, K. Gaussian-3 Theory Using Density Functional Geometries and Zero-Point Energies. *J. Chem. Phys.* **1999**, *110* (16), 7650–7657.

(87) Curtiss, L. A.; Redfern, P. C.; Raghavachari, K.; Pople, J. A. Assessment of Gaussian-2 and Density Functional Theories for the Computation of Ionization Potentials and Electron Affinities. *J. Chem. Phys.* **1998**, *109* (1), 42–55.

(88) Curtiss, L. A.; Redfern, P. C.; Raghavachari, K. Gaussian-4 Theory Using Reduced Order Perturbation Theory. *J. Chem. Phys.* **2007**, *127* (12).

(89) Curtiss, L. A.; Redfern, P. C.; Raghavachari, K. Gaussian-4 Theory. *J. Chem. Phys.* **2007**, *126* (8).

(90) Montgomery, J. A.; Frisch, M. J.; Ochterski, J. W.; Petersson, G. A. A Complete Basis Set Model Chemistry. VI. Use of Density Functional Geometries and Frequencies. *J. Chem. Phys.* **2002**, *110* (6), 2822–2827.

(91) Ditchfield, R.; Hehre, W. J.; Pople, J. A. Self-Consistent Molecular-Orbital Methods. IX. An Extended Gaussian-Type Basis for Molecular-Orbital Studies of Organic Molecules. *J. Chem. Phys.* **1971**, *54* (2), 724–728.

(92) Rassolov, V. A.; Ratner, M. A.; Pople, J. A.; Redfern, P. C.; Curtiss, L. A. 6-31G* Basis Set for Third-Row Atoms. *J. Comput. Chem.* **2001**, *22* (9), 976–984.

(93) Marenich, A. V; Cramer, C. J.; Truhlar, D. G. Universal Solvation Model Based on Solute Electron Density and on a Continuum Model of the Solvent Defined by the Bulk Dielectric Constant and Atomic Surface Tensions. *J. Chem. Theory Comput.* **2009**, *5*, 2447–2464.

(94) Ochterski, J. W. Thermochemistry in Gaussian. *Gaussian Inc Pittsburgh PA* **2000**, *264* (1), 1–19.

(95) Vibration- Rotation Spectroscopy of HCl and DCl https://www.colby.edu/chemistry/PChem/lab/VibRotHClDCl.pdf.

(96) Schäfer, K. Statistical Thermodynamics. *Zeitschrift für Phys. Chemie* **2011**, *69* (5_6), 328–328.

(97) László Kiss, G. L. *Elektrokémia*; Semmelweis Kiadó, 2011.

(98) Atkins, P. .; Trapp, C. .; Cady, M. .; Giunta, C. *Atkins' Physical Chemistry*, 8th ed.; Oxford University Press, 2006.

(99) McQuarrie, D. .; Simon, J. D. *Physical Chemistry: A Molecular Approach*; University Science Books, 1997.

(100) Ruscic, B.; Bross, D. H. Active Thermochemical Tables (ATcT) values based on ver. 1.122 of the Thermochemical Network https://atct.anl.gov/ (accessed Dec 17, 2017).

(101) Goos, E.; Burcat, A.; Branko, R. Extended Third Millennium Ideal Gas and Condensed Phase Thermochemical Database for Combustion with Updates from Active Thermochemical Tables http://garfield.chem.elte.hu/ Burcat/hf.doc.

(102) Bennett, A.; Shirley, W. A.; Al-Laham, M. A.; Tensfeldt, T. G.; Petersson, G. A.; Mantzaris, J. A Complete Basis Set Model Chemistry. I. The Total Energies of Closed Shell Atoms and Hydrides of the First Row Elements. *J. Chem. Phys.* **2002**, *89* (4), 2193–2218.

(103) Curtiss, L. A.; Redfern, P. C.; Raghavachari, K.; Rassolov, V.; Pople, J. A. Gaussian-3 Theory Using Reduced Møller-Plesset Order. *J. Chem. Phys.* **1999**, *110* (10), 4703–4709.

(104) Montgomery, J. A.; Frisch, M. J.; Ochterski, J. W.; Petersson, G. A. A Complete Basis Set Model Chemistry. VII. Use of the Minimum Population Localization Method. *J. Chem. Phys.* **2000**, *112* (15), 6532–6542.

(105) Frisch, M. J.; Trucks, G. W.; Schlegel, H. B.; Scuseria, G. E.; Robb, M. A.; Cheeseman, J. R. .; Scalmani, G.; Barone, V.; Mennucci, B.; Petersson, G. A.; Nakatsuji, H.; Caricato, M.; Li, X. .; Hratchian, H. P.; Izmaylov, A. F.; Bloino, J.; Zheng, G.; Sonnenberg, J. L.; Hada, M.; Ehara, M. .; Toyota, K.; Fukuda, R.; Hasegawa, J.; Ishida, M.; Nakajima, T.; Honda, Y.; Kitao, O.; Nakai, H. ;1.; Vreven, T.; Montgomery, J. A., Jr.; Peralta, J. E.; Ogliaro, F.; Bearpark, M.; Heyd, J. J.; Brothers, E. .; Kudin, K. N.; Staroverov, V. N.; Kobayashi, R.; Normand, J.; Raghavachari, K.; Rendell, A. . B.; J. C.; Iyengar, S. S.; Tomasi, J.; Cossi, M.; Rega, N.; Millam, J. M.; Klene, M.; Knox, J. E.; Cross, J.; B.; Bakken, V.; Adamo, C.; Jaramillo, J.; Gomperts, R.; Stratmann, R. E.; Yazyev, O.; Austin, A. J. .; Cammi, R.; Pomelli, C.; Ochterski, J. W.; Martin, R. L.; Morokuma, K.; Zakrzewski, V. G.; Voth, G.; A.; Salvador, P.; Dannenberg, J. J.; Dapprich, S.; Daniels, A. D.; Farkas, O.; Foresman, J. B.; Ortiz, J.; et al. *Gaussian 09, Revision A.01*; Wallingford CT, 2009.

(106) https://www.chemeo.com/cid/59-283-3/Benzenamine%2C%204%2C4%27-methylenebis-.

(107) S.W. Benson. *Thermochemical Kinetics: Methods for the Estimation of Thermochemical Data and Rate Parameters*, 2nd ed.; John Wiley: New York, 1976.

(108) Santhanalakshmi, J. A Thermomechanical Kinetic Study Of Interconversion Reactions of Aniline-Formaldehyde Products. **1988**, *127*, 369–375.

(109) Katayama, M.; Ashiki, S.; Amakasu, T.; Ozutsumi, K. Liquid Structure of Benzene and Its Derivatives as Studied by Means of X-Ray Scattering. *Phys. Chem. Liq.* **2010**, *48* (6), 797–809.

(110) Griswold, J. Analysis of Aniline-Water Solutions. *Indsutrial Eng. Chem. Anal. Ed.* **1940**, *12* (2), 89–90.

(111) Technology, N. I. of S. and. NIST Computational Chemistry Comparison and Benchmark Database. NIST Standard Reference Database No. 101 https://cccbdb.nist.gov/exp1x.asp (accessed Nov 24, 2017).

(112) Boros, R. Z.; Farkas, L.; Nehéz, K.; Viskolcz, B.; Szőri, M. An Ab Initio Investigation of the 4,4′-Methlylene Diphenyl Diamine (4,4′-MDA) Formation from the Reaction of Aniline with Formaldehyde. *Polymers (Basel).* **2019**, *11* (398).

(113) Stephan R. Heller. Nist Structures and Properties Database and Estimation Program. *Med. Chem. Proj.* **1991**, *31* (3), 432–434.

(114) S.W. Benson. *Thermochemical Kinetics: Methods for the Estimation of Thermochemical Data and Rate Parameters*; 2nd ed. New York: John Wiley, 1976.

(115) National Institute of Standard and Technology, NIST Computational Chemistry Comparison and Benchmark Database. NIST Standard Reference Database No. 101 https://cccbdb.nist.gov/exp1x.asp (accessed Nov 24, 2017).

(116) National Institute of Standard and Technology. NIST Chemistry WebBook, SRD 69, Group Additivity Based Estimates http://webbook.nist.gov/chemistry/grp-add/. (accessed Nov 24, 2017).

(117) Zhang, J.; Sun, Y.; Mao, C.; Gao, H.; Zhou, W.; Zhou, Z. Theoretical Study of PKa for Perchloric Acid. *J. Mol. Struct. THEOCHEM* **2009**, *906* (1–3), 46–49.

(118) Muckerman, J. T.; Skone, J. H.; Ning, M.; Wasada-Tsutsui, Y. Toward the Accurate Calculation of PKa Values in Water and Acetonitrile. *Biochim. Biophys. Acta - Bioenerg.* **2013**, *1827* (8–9), 882–891.

(119) Ghalami-Choobar, B.; Ghiami-Shomami, A.; Nikparsa, P. Theoretical Calculation of PKb Values for Anilines and Sulfonamide Drugs in Aquous Solution. *J. Theor. Comput. Chem.* **2012**, *11* (02), 283–295.

(120) Behjatmanesh-Ardakani, R.; Safaeian, N. PKa Predictions of Some Aniline Derivatives by Ab Initio Calculations. *Iran. Chem. Commun.* **2014**, *2*, 147–156.

(121) Lu, H.; Chen, X.; Zhan, C. G. First-Principles Calculation of PKa for Cocaine, Nicotine, Neurotransmitters, and Anilines in Aqueous Solution. *J. Phys. Chem. B* **2007**, *111* (35), 10599–10605.

(122) Marenich, A. V.; Cramer, C. J.; Truhlar, D. G. Universal Solvation Model Based on the Generalized Born Approximation with Asymmetric Descreening. *J. Chem. Theory Comput.* **2009**, *5*, 2447–2464.

(123) Liptak, M. D.; Gross, K. C.; Seybold, P. G.; Feldgus, S.; Shields, G. C. Absolute PKa Determinations for Substituted Phenols. *J. Am. Chem. Soc.* **2002**, *124* (22), 6421–6427.

(124) Knjasev, V. , Universität Stuttgart. Beiträge Zur Reaktionskinetischen Untersuchung Der Säureinduzierten Anilin-Formaldehyd-Kondensation, 2007.

(125) Selivanov, V. D.; Konstantinov, I. I. Correction of the Heat of Combustion of Diphenylmethane-4,4'-Diisocyanate. *Zhurnal Prikl. Khimii* **1970**, *43*, 2565.

(126) Zalikin, A. A.; Strepikheev, Y. S. Some Physicochemical Constants of 4,4'-Diaminodiphenylmethane and 4,4'-Diphenylmethanediisocyanate. *Zhurnal Prikl. Khimii* **1966**, *39*, 2607.

(127) Handrick, G. R. Heats of Combustion of Organic Compounds. *Ind. Eng. Chem.* **1956**, *48* (8), 1366–1374.

(128) *MDI and TDI: Safety, Health and the Environment: A Source Book and Practical Guide*; Allport, D. C., Gillbert, D. S., Outterside, S. M., Eds.; John Wiley & Sons, Ltd., 2003.

(129) Rodziewicz, P.; Goclon, J. Structural Flexibility of 4,4'-Methylene Diphenyl Diisocyanate (4,4'-MDI): Evidence from First Principles Calculations. *J. Mol. Model.* **2014**, *20* (2), 2097.

(130) Montagu, J.; Configurations, M.; Deflection, B.; Technologies, S. United States Patent (19). **1993**, No. 19.

(131) Kaplan, A. Method for the Production of MDI Dimer. U.S. 2014/0135458 A1, 2013.